공학박사 학위논문

Prediction of the mechanical behavior of carbon fiber-reinforced plastic and steel laminate composites using a micromechanical approach

미소역학을 이용한 탄소섬유 복합재료-스틸 라미네이트 복합재료의 기계적 거동 예측

2020 년 2 월

서울대학교 대학원

재료공학부

성 민 창

Prediction of the mechanical behavior of carbon fiber-reinforced plastic and steel laminate composites using a micromechanical approach

Advisor: Woong-Ryeol Yu

by

Minchang Sung

2020

Department of Materials Science and Engineering Graduated School Seoul National University

Prediction of the mechanical behavior of carbon fiber-reinforced plastic and steel laminate composites using a micromechanical approach

미소역학을 이용한 탄소섬유 복합재료-스틸 라미네이트 복합재료의 기계적 거동 예측

지도 교수 유 웅 열

이 논문을 공학박사 학위논문으로 제출함

2019 년 12 월

서울대학교 대학원

재료공학부

성 민 창

성민창의 공학박사 학위논문을 인준함

2019 년 12 월

위 원 장 한 흥 남 (인)

부 위 원 장 유 웅 열 (인)

위 원 이 명 규 (인)

위 원 안 철 희 (인)

위 원 나 원 진 (인)

Abstract

Carbon fiber-reinforced plastics (CFRPs) have received great attention in the field of structural materials due to their high strength and light properties, but they have limitations in applications due to brittle fracture behavior. Metals have excellent mechanical properties such as ductility and impact resistance, while high density is a disadvantage. In order to obtain the advantages of both materials at the same time, researches have been conducted to produce a laminate composite by mixing the two materials. In this study, experimental and theoretical studies were conducted to predict the mechanical properties of CFRP and steel laminate composites.

Firstly, Synergistic effects of carbon fiber-reinforced plastic (CFRP) and steel hybrid laminate composites were investigated systematically by static and dynamic tensile testing. Various hybrid laminate composites were prepared by varying the adhesion between the CFRP and steel, the layup sequence, and the volume fraction of the CRFP. The fracture strain of the CFRP within the hybrid laminate composites increased, e.g., from 1.94% for pure CFRPs to 2.21% for the steel/CFRP/steel case. Finite element analysis

and fractography established that transverse compressive stress was the main source of the improvement. Different Poisson's ratios led to transverse compressive stress on the CFRP layer after yielding of the steel during the tensile test. This stress delayed the fiber-splitting behavior of the CFRP, leading to further deformation and thus increasing the breaking strain and tensile strength of the CFRP within the hybrid laminate composites. Our results provide insight into the design of ductile composites using CFRP and steel through optimization of the laminate structure.

Secondly, a micromechanical model was developed to explain the phenomenon and to predict the mechanical behavior of CFRP/steel hybrid laminate composites. First, the stress distributions on fibers and matrix material in a CFRP was calculated under multiaxial stress conditions using shear lag theory considering transverse compressive stress. Then, the deformation behavior of CFRP was predicted using average stress in the ineffective region and the Weibull distribution of carbon fibers. Finally, the mechanical properties of CFRP/steel hybrid laminate composites were predicted by considering the thermal residual stress generated during the manufacturing process. The micromechanical model revealed that increased transverse compressive stress decreases the ineffective lengths of partially broken fibers in the CFRP and results in increased fracture strain of the

CFRP, demonstrating the validity of the current micromechanical model.

Lastly, developed predictive model was applied to failure criterion of CFRP to analyze the behavior under multiaxial stress conditions. For this purpose, the effects of CFRP transverse stress on transverse fracture were analyzed. In addition, the transverse fracture of CFRP is affected by axial stress as well as transverse stress. To reflect this effect, criterion for transverse fracture was obtained by using the information on the ineffective region obtained from the predictive model. Finally, failure mode suitable for a given stress condition was analyzed and failure criterion based on micromechanical approach was developed and verified.

Keywords: fiber metal laminate, CFRP/steel hybrid, fracture strain, hybrid effect, multiaxial stress, failure criterion

Student number: 2014-21474

Contents

Abstract……i

Contents……iv

List of Tables……vii

List of Figures……vii

1. Introduction……...1

1.1. Carbon fiber reinforced plastic (CFRP)……..……..1

1.2. Fracture mechanism of CFRP ……6

1.3. CFRP and steel laminate composite ……11

1.4. Research objectives……...15

2. Experimental study of CFRP and steel laminate composites……17

2.1. Experimental……17

2.1.1. Materials and specimen……17

2.1.2. Single-lap shear test ……19

2.1.3. Uniaxial static and dynamic tensile tests ……20

2.1.4. Compressive test 24

2.2. Tensile behavior 26

2.2.1. Mechanical properties of the constituent materials 26

2.2.2. Increased breaking strain of CFRP within the laminate composites 28

2.2.3. Mechanism behind the increased breaking strain 36

2.2.4. Fractography 40

2.2.5. Effect of the laminate structure 47

2.3. Compressive behavior 52

2.4. Summary 55

3. Micromechanical model of CFRP and steel laminate composites 56

3.1. Modeling tensile behavior 56

3.1.1. Modeling approach 56

3.1.2. Transverse compressive stress in a CFRP layer 59

3.1.3. Predicting the tensile behavior 62

3.1.4. Residual stress of the laminate composites 71

3.2. Validation examples 73

3.2.1. Calculation procedure 73

3.2.2. Effect of matrix properties on stress distribution 74

3.2.3. Effect of carbon fiber properties 83

3.2.4. Prediction of the tensile behavior of the laminate composites 86

3.3. Analysis of compressive behavior 93

3.4. Summary.....97

4. New failure criterion of fiber-reinforced composites 98

4.1. Overview of failure criteria of the CFRP 98

4.2. Development of new failure criterion based on micromechanics 99

4.2.1. Effect of multiaxial stress on the CFRP fracture 99

4.2.2. Development of failure criterion based on the predictive model 100

4.2.3. Validation examples 107

4.2.4. Application to FEM analysis 109

4.3. Summary 113

5. Concluding remarks..... 114

Reference.....116

Korean abstract…….126

List of Tables

Table 2-1 Nomenclature for the static tensile test specimens.

Table 2-2 Mechanical properties of the CFRP/steel hybrid laminate composites subjected to finite element analysis.

Table 3-1 Mechanical properties of CFRP and steel lamina.

Table 3-2 Parameters for Mohr-Coulomb yield criterion and modified shear yield stress.

List of Figures

Figure 1-1 Differences in Tensile Behavior of Carbon Fiber Bundles and CFRP.

Figure 1-2 Shear deformation in the matrix around the point of partial fracture of the carbon fiber.

Figure 1-3 Tensile stress of carbon fiber and shear stress of matrix in ineffective region.

Figure 1-4 Observation of multiple fractures inside CFRP with increasing axial stress.

Figure 1-5 Various types of fiber metal laminate and their components.

Figure 2-1 Single-lap shear test specimens.

Figure 2-2 Static tensile test specimens.

Figure 2-3 Schematic diagram of the equipment used for the high-speed tensile test. In the high-pressure region (①), the bar was released at high pressure and generated a high strain rate by striking the fixture, with the specimen clamped in the impact region (②).

Figure 2-4 High-speed tensile test specimen. (a) Dimensions, (b) intermediate jig for fixing the specimen, and (c) test set-up.

Figure 2-5 Test jig and set-up for compressive testing of laminate composites.

Figure 2-6 Typical stress–strain curves of individual (a) carbon fiber-reinforced plastic (CFRP) and (b) electrogalvanized (EG) steel specimens.

Figure 2-7 Adhesion strength determined by the single-lap shear test. Three specimens were used to obtain the data. Note that S(EG) and S(GA) represent EG and GA steels, respectively.

Figure 2-8 Comparison of the stress–strain curves of the CFRP and steel hybrid laminate composites with and without general and enhanced adhesion.

Figure 2-9 Comparison of the stress–strain curves of the CFRP and steel hybrid laminate composites with different layer sequences, with and without interfacial adhesion. (a) Steel/CFRP/steel and (b) CFRP/steel/CFRP.

Figure 2-10 Dynamic tensile test results of the hybrid laminated composites. Comparison of the static and dynamic properties of (a) pure CFRP and (b) pure steel, and (c) dynamic mechanical properties of the hybrid laminated composites as a function of adhesion. The strain rate was about 50 s^{-1}.

Figure 2-11 Comparison of the fracture strain and tensile strength of the CFRP/steel hybrid laminate composites as a function of the adhesion between them. (a) and (c) Fracture strain and (b) and (d) tensile strength determined by static and dynamic tensile testing. At least four specimens were tested to obtain these results. In the static test, the adhesion determined by the single-lap shear test was 11 and 12.4 MPa for the general and enhanced adhesion cases, respectively, while the values were 10.6 and 13 MPa for specimens tested dynamically.

Figure 2-12 Distribution of the transverse compressive stress in the CFRP layer as a function of interfacial shear strength of (a) 1 MPa and (b) 11 MPa. Change in the average transverse compressive stress as a function of (c) interfacial shear strength and (d) layer sequence. All transverse compressive stresses were calculated when the axial strain of the hybrid laminate composite was 2%.

Figure 2-13 Optical microscope images showing the deformation process of pure CFRP. (a) From the start of deformation to failure (0.20% strain), (b) when partial splitting occurred at the edge of the CFRP (1.80% strain), and (c) at final fracture (1.82% strain).

Figure 2-14 Optical microscope images showing the deformation behavior of the hybrid laminate composite. a) From the start of deformation to failure (0.20% strain), (b) when partial splitting occurred at the edge of the CFRP (1.76% strain), and (c) at final fracture (2.00% strain). (a), (c), and (e) show the CFRP deformation behavior in the plan view, while (b), (d), and (f) show the CFRP and interface fracture behavior in the side view.

Figure 2-15 Optical microscope images of CFRP fragments remaining on the

surface of the steel after fracture of the hybrid laminate composites with adhesion of (a) 11 MPa (CS) and (b) 12.4 MPa (T_CS), and (c) the average width of 20 fragments.

Figure 2-16 Fracture strain of the CFRP within the hybrid laminated composites having (a) two and (b) four layers of CFRPs with one layer of steel. (c) Effect of layup sequence. (d) Comparison of the fracture strain and (e) the percentage increase thereof as a function of the CFRP volume fraction.

Figure 2-17 The results of compressive tests. (a) representative graphs and (b) fracture strains of the CFRP within the laminated composites.

Figure 2-18 Fracture morphology after compressive test of (a) pure CFRP, (b) CFRP/steel/CFRP, and (c) steel/CFRP/steel specimens.

Figure 3-1 The mechanical behavior of CFRP and steel hybrid laminates by axial tensile force: (a) no transverse compressive stress without interfacial bonding and (b) transverse compressive stress in the CFRP layer with interfacial bonding.

Figure 3-2 The general fracture mechanism of CFRP.

Figure 3-3 The transverse compressive stresses of CFRP layers within CFRP/steel hybrid laminates according to lay-up sequences (SCS: steel/CFRP/steel, CS: CFRP/steel, CSC: CFRP/steel/CFRP)

Figure 3-4 The relationships between (a) transverse and radial compressive stresses and (b) radial compressive stresses of the matrix surrounding a carbon fiber.

Figure 3-5 (a) Mohr-Coulomb yield criterion and (b) assumed stress-strain behavior of the polymer matrix.

Figure 3-6 The calculation procedure for predicting the mechanical properties of hybrid laminate composites.

Figure 3-7 The effects of the shear yield stress of the matrix in the ineffective region on the (a) shear stress distribution of the matrix and (b) tensile stress distribution of carbon fibers.

Figure 3-8 The effects of the shear fracture strain of the matrix in the ineffective region on the (a) shear stress distribution of the matrix and (b) tensile stress distribution of carbon fibers.

Figure 3-9 The effects of the frictional stress of the matrix in the ineffective region on the (a) shear stress distribution of the matrix and (b) tensile stress distribution of carbon fibers.

Figure 3-10 The mechanical behaviors of CFRPs as functions of (a) the scale

parameter and (b) the shape parameter of a Weibull distribution of carbon fibers.

Figure 3-11 Shear stress distributions within the matrix of CFRPs within various hybrid laminate composites for axial strains of (a) 0.2%, (b) 1%, and (c) 2%.

Figure 3-12 The tensile stress distributions of carbon fibers as a function of the structure of the hybrid composite for axial strains of (a) 0.2%, (b) 1%, and (c) 2%.

Figure 3-13 The predicted tensile behaviors of hybrid composites are compared with experimental results: (a) stress and strain curves and (b) breaking strain.

Figure 3-14 The transverse tensile stresses of CFRP layers within CFRP and steel laminates according to lay-up sequences.

Figure 3-15 Longitudinal shear behavior of pure CFRP in the presence of transverse tensile stress.

Figure 4-1 Relationship between axial strength and transverse strength, proposed in Puck's failure criterion.

Figure 4-2 Axial dominant fracture criterion of CFRP developed through micromechanical predictive model.

Figure 4-3 Ineffective region under critical axial strain assumed in transverse dominant fracture mode.

Figure 4-4 Fracture probability of carbon fiber depending on the defect factor to quantify the degree of fracture of matrix.

Figure 4-5 Transverse dominant fracture criterion of CFRP developed through micromechanical predictive model.

Figure 4-6 Combination of axial dominant criterion and transverse dominant criterion.

Figure 4-7 Comparison of developed criterion (micromechanical criterion) with experimental data from laminate composites.

Figure 4-8 Comparison of developed criterion (micromechanical criterion) with Gan’s experimental data.

Figure 4-9 Comparison of developed criterion (micromechanical criterion) with FEM calculation results.

Figure 4-10 Comparison of FEM calculation results of (a) steel/CFRP, (b) CFRP/steel/CFRP and (c) steel/CFRP/steel laminate composites with each experimental result.

Chapter 1. Introduction

1.1. Carbon fiber reinforced plastic (CFRP)

Carbon fiber-reinforced plastics (CFRPs) are structural materials in which carbon fibers are impregnated with a polymer matrix. Since its inception in the late 1800s, carbon fibers have been actively studied in various fields such as materials and processes to improve mechanical, thermal and electrical properties [1-4]. At present, the density of carbon fiber is about 1.8 g/cm^3, which is 4 times lighter than general electro-galvanized steel (7.8 g/cm^3), but the tensile strength is about 10 times stronger. Despite the superior specific strength of the carbon fibers, their high price is a limiting factor in their use [5]. Researches on mass production process to lower the price of carbon fiber and researches to improve mechanical properties of carbon fiber are continuously conducted [6, 7].

In spite of the enormous mechanical properties of carbon fiber, the fiber cannot itself be a structural material. The reason is that the fibers are connected only in the fiber axis direction and deform independently of nearby fibers. In order to overcome this, various methods of making a connection between fibers by impregnating a polymer material between carbon fibers are used [8, 9], and through this, it can be used as a structural material having excellent tensile strength and structural stability at the same time.

The role of the matrix is not only to connect the carbon fibers but also to localize the effects of partial breakdown of the carbon fibers. Before explaining this role of the matrix, it is necessary to understand the partial fracture of the carbon fiber. Materials such as metals and polymers undergo an elastic deformation in which the strain and the stress have a linear relationship at the initial stage of deformation, and plastic deformation in which the strain and the stress have a nonlinear relationship when the stress reaches the yield stress due to the deformation [10]. Such materials are called ductile materials. On the other hand, ceramic materials such as carbon fiber suddenly break during elastic deformation without plastic deformation, and these materials are called brittle materials [11]. The strength of the brittle material does not have a specific value and has a probabilistic distribution depending on the size and number of defects in the material [12]. In other words, even if the tensile test of the same type of carbon fiber, failure occurs at various stresses. Statistical methods such as Weibull distribution are used to characterize the stress distribution of these carbon fibers [1].

Figure 1-1 compares the tensile test results of carbon fiber bundles and CFRP. Since each carbon fiber in the carbon fiber bundle has a strength distribution, fiber fracture occurs sequentially from fibers having low strength as the tensile strain progresses. In this case, the load continuously decreases because the entire fiber cannot carry the load when the fiber fractures [13]. On the other hand, in the case of CFRP in which the matrix is impregnated with carbon fibers, even if partial fracture occurs, greater load can be applied by localizing the influence of fracture

with the help of the shear stress of the matrix.

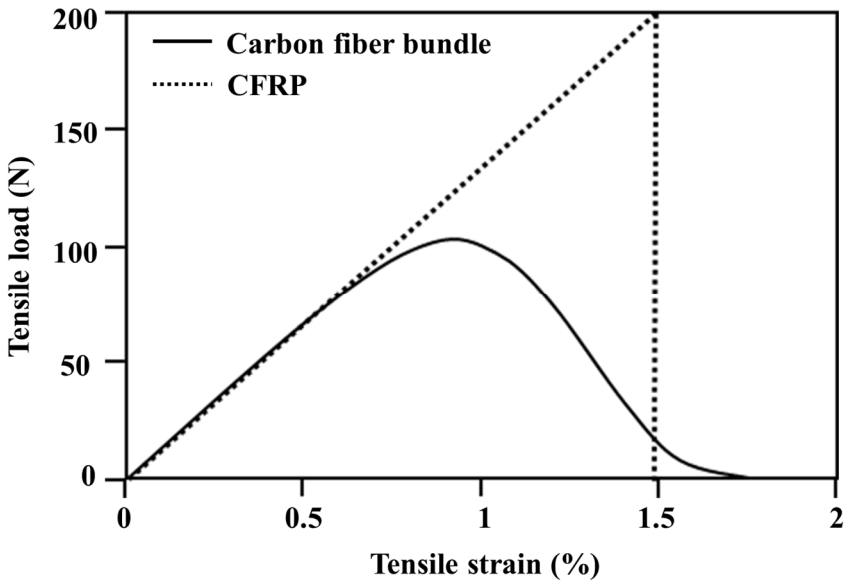

Figure 1-1 Differences in Tensile Behavior of Carbon Fiber Bundles and CFRP.

The most influential factor in the mechanical properties of CFRP is the properties of carbon fiber, but the properties of the matrix also play an important role. The reason why polymers are most widely used instead of metal or ceramic materials as matrix materials is due to the modulus and ductility of polymers, besides weight and productivity. As can be seen from the studies on fiber-reinforced composites, it is known that the closer the modulus between the reinforcing fibers and the matrix material is, the more prominent the stress concentration phenomenon is in the surrounding fibers [14]. In the case of metal or ceramic materials, the elastic

modulus is similar to that of carbon fiber, so when used as a matrix, the mechanical properties of the fiber-reinforced composites may deteriorate. On the contrary, if the modulus of the matrix is too small, it does not efficiently localize the effect of the partial fracture of the carbon fiber, which greatly reduces the role of the matrix [15]. Therefore, it is important to use a matrix with adequate modulus and ductility.

One important area of research in CFRP is the interface between carbon fibers and the matrix. In order for the matrix to play its role, there must be a strong bond between the carbon fiber and the matrix [16]. In the case of poor interfacial properties, interfacial separation occurs due to the shear stress generated in the matrix when partial fracture of the carbon fiber occurs. Separation of the interface reduces the shear strengthening effect of the matrix and can lead to the destruction of the entire CFRP, starting with longitudinal fracture of the matrix. Improving the interfacial strength between carbon fiber and matrix does not always improve the mechanical properties of CFRP. In some studies, mechanical properties have been found to decrease with increasing interfacial shear strength [17]. This is due to the increase in stress concentration factor with increasing interfacial shear strength, which will be explained further in the following section.

The study of CFRP is largely divided into the development of carbon fiber of excellent properties and the modification of matrix and interfacial properties accordingly. To date, CFRP has been widely used in aerospace construction because of its excellent mechanical properties, especially in the automotive field

with environmental issues. When replacing metal, which is the main material of automobiles, with CFRP, fuel efficiency is expected to increase dramatically due to weight reduction, and the use of CFRP is expected to increase further with the development of eco-friendly electric vehicles. In addition, carbon fiber can be applied to a variety of applications, such as sports, construction, it is necessary to make it easy to apply the material to an actual industrial field through various studies.

1.2. Fracture mechanism of CFRP

As mentioned above, the mechanical properties of CFRP are determined by the interaction between carbon fiber and matrix due to the statistical properties of carbon fiber. When CFRP deforms in the axial direction, in a strain smaller than the strain in which CFRP fractures, the internal carbon fibers already begin to break partially [18]. The broken carbon fiber shrinks relative to the surrounding carbon fibers to return to the zero stress state. When the carbon fiber shrinks, the surrounding matrix catches the fiber through shear deformation, to prevent fiber shrinkage, as shown in Figure 1-2. This role of the matrix causes the carbon fibers to recover their tensile stress after a certain distance from the point of failure. In contrast, the matrix receives the greatest shear stress at the point of failure and the shear stress decreases as the distance from the point of failure increases (see Figure 1-3). The relationship between the tensile stress of the carbon fiber and the shear stress of the matrix can be calculated by the force equilibrium, which is known as the shear lag theory [19]. The shear lag theory provides information about regions where carbon fibers cannot apply tensile stress, and the region is called an ineffective region, which plays an important role in the fracture behavior of CFRP.

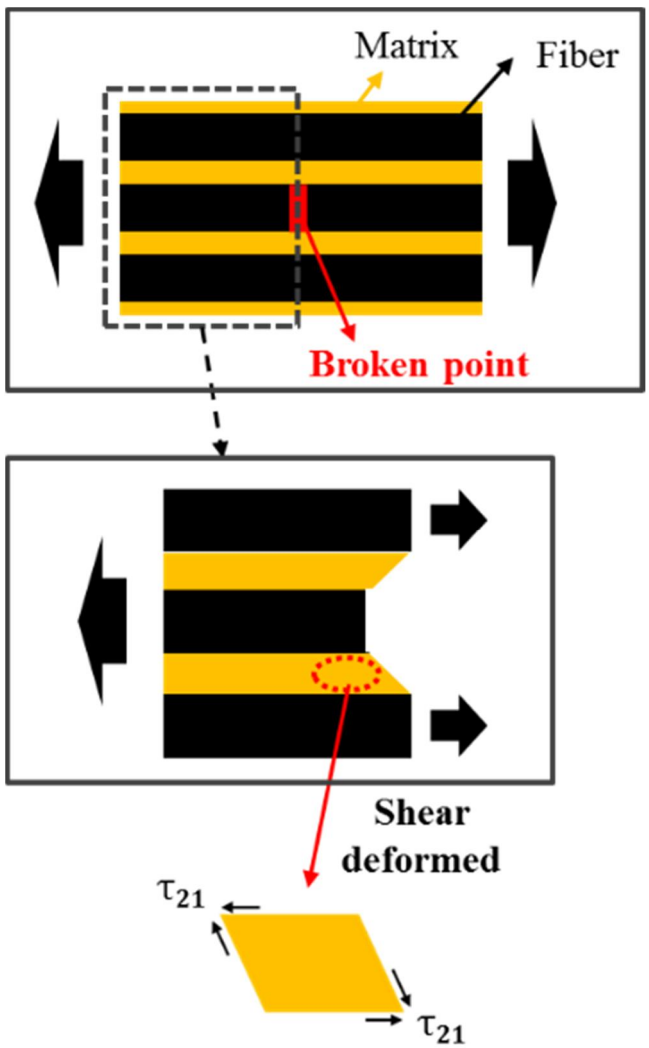

Figure 1-2 Shear deformation in the matrix around the point of partial fracture of the carbon fiber.

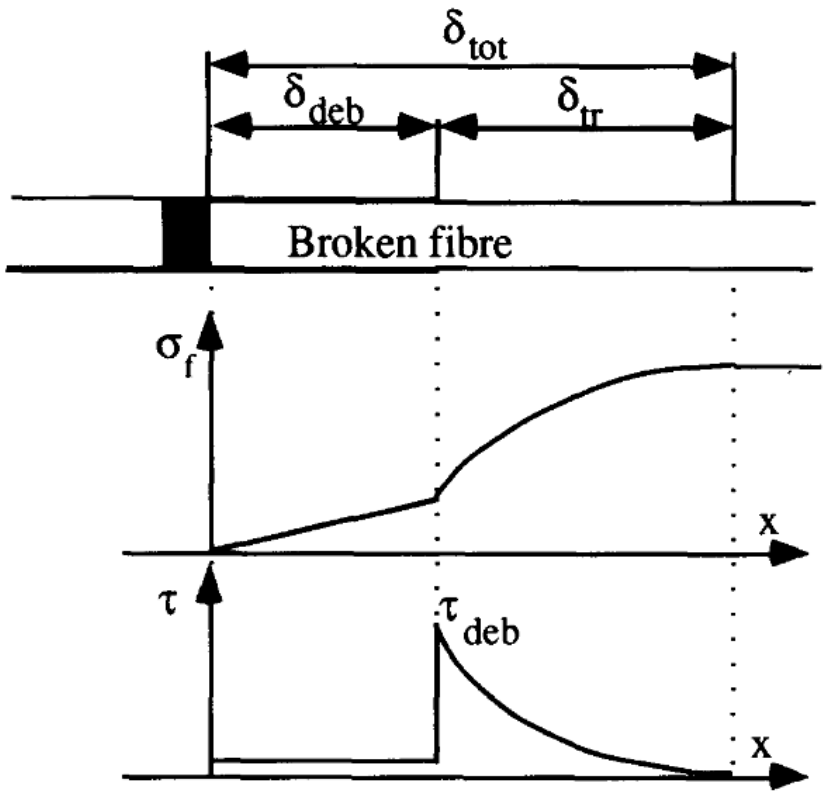

Figure 1-3 Tensile stress of carbon fiber and shear stress of matrix in ineffective region [20].

There are two major phenomena that can occur in ineffective regions. Firstly, because the carbon fiber in the ineffective region does not apply stress properly, the ineffective region is considered to be a crack from the point of view of CFRP. If cracks are present inside the material, stress is concentrated around the cracks, causing continuous failure. In the case of CFRP, partial fracture of carbon fibers results in stress concentration in the fibers surrounding the ineffective region,

which increases the probability of fracture of the surrounding fibers and causes multiple fractures in which continuous fracture occurs. Multiple fracture phenomenon was observed by x-ray computed tomography (see Figure 1-4). The magnitude of the stress concentration is known to increase as the interfacial shear strength increases. In general, as the interfacial shear strength increases, the mechanical properties of CFRP improve, but when the interfacial shear strength exceeds the threshold, the multiple fracture phenomenon due to stress concentration becomes dominant and the mechanical properties decrease.

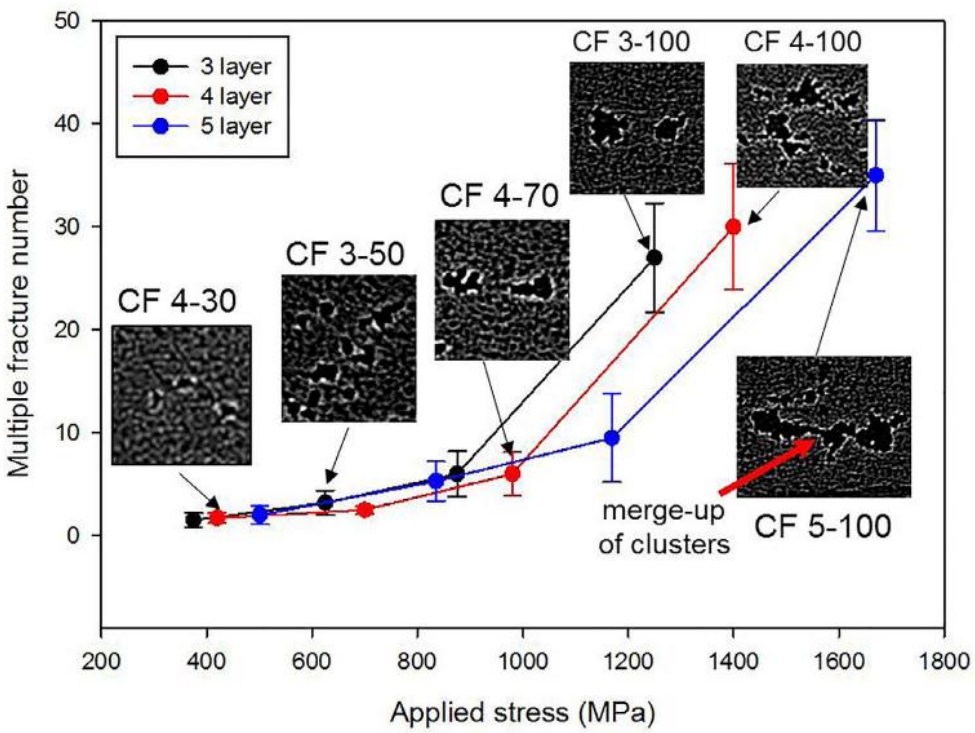

Figure 1-4 Observation of multiple fractures inside CFRP with increasing axial

stress [21].

The second phenomenon that occurs in ineffective regions is the fracture of the matrix around the fractured fibers. The matrix around the fractured fiber undergoes shear deformation for the purpose of preventing shrinkage of the fractured fiber [20]. When the shear strain of this matrix exceeds the failure strain, shear failure occurs, which is called longitudinal splitting. When splitting occurs, the ineffective region begins to expand rapidly, and the properties of CFRP are greatly reduced. Longitudinal splitting and multiple fracture phenomena are crack propagation phenomena in the direction of fiber axis and perpendicular to fiber axis, respectively. These phenomena accumulate internal damage, and if the defects exceed the threshold, the final failure of CFRP occurs.

1.3. CFRP and steel laminate composite

CFRPs exhibit high specific strength because of their high tensile strength and light weight [22-24]. However, the fracture strain of CFRPs is lower than that of other materials, such as metals and polymers, and shows brittle fracture behavior [5, 25]. A simple way to overcome this limitation is to hybridize CFRPs with metals, to leverage the high ductility and strength of metals.

Hybridization of CFRPs and metal can be done by 1) manufacturing hybrid fiber composites by mixing carbon and metal fibers [26-28], 2) fabricating carbon fiber-reinforced metal matrix composites [29, 30], and 3) making laminated composite materials using CFRP plates and metal plates [31-35]. Hybrid fiber composites have been studied in attempts to increase the fracture toughness and bearing strength [36], while carbon fiber-reinforced metal matrix composites have been used to overcome the brittleness of CFRPs [29]. Laminated composites manufactured by laminating CFRP and steel plates have been studied because of their simple fabrication methods and load-bearing properties after fracture of the CFRP [35].

A fiber-metal laminate (FML) is a hybrid composite of fiber-reinforced plastic (FRP) and metal, generally demonstrating high specific strength and excellent fatigue properties due to the presence of the FRP [22-24] and high fracture strain and impact resistance due to the presence of the metal [31-35]. FML has been developed in various structures (see Figure 1-5). ARALL, a laminate composite of

aramid fiber and aluminum, was first introduced in 1978 [37]. Since then, a variety of FMLs have been developed, including CARALL [38], carbon fiber/metal composites, and GLARE [39], glass-fiber/metal composites. In addition to aluminum, magnesium and titanium alloys have also been used in FMLs [40, 41]. Due to their mechanical stability and light weight, applications of FMLs have broadened from the construction industry into the automobile and aerospace fields.

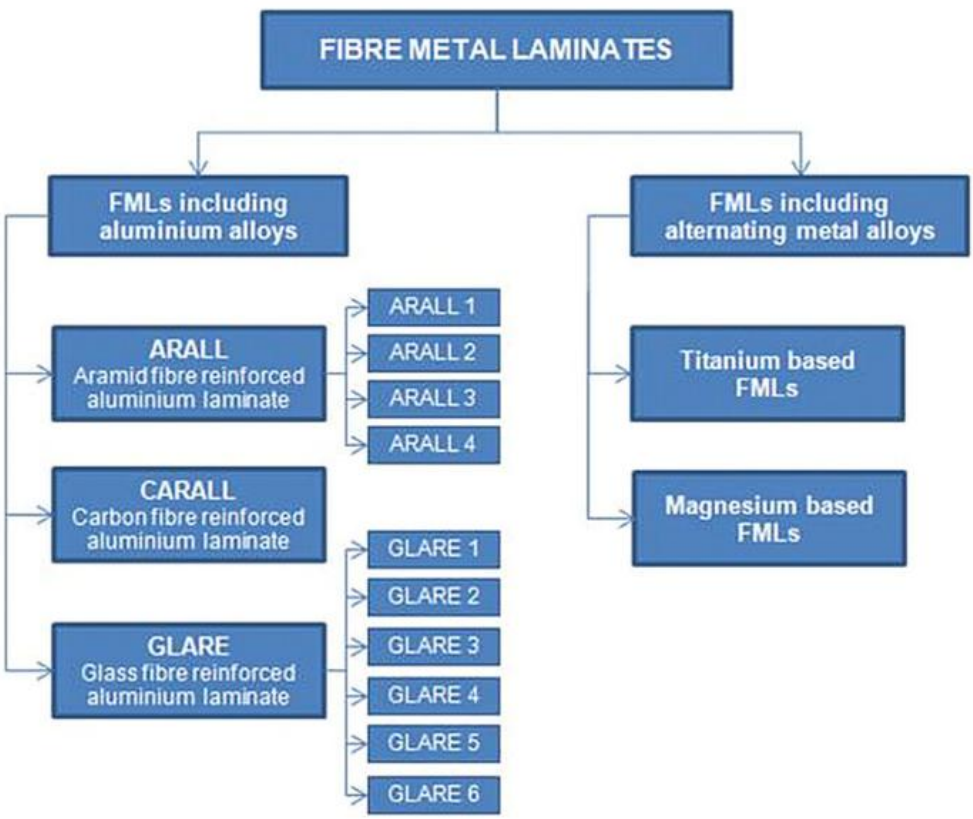

Figure 1-5 Various types of fiber metal laminate and their components [42].

The primary interest in FMLs is their mechanical properties such as tensile and bearing strength, impact resistance, fatigue property, and corrosion characteristics [43-45]. As such, the tensile strength of an FML has traditionally been predicted using the rule of mixture, where the overall mechanical properties of the composite are calculated based on the properties and volume fraction of each constituent material [46, 47]. In addition, several properties have been shown to be dependent on the fabrication process and interface properties [48-51]. Other studies have taken into account the thermal residual stress that occurs in the manufacture of FRPs. When an FRP and a metal are bonded at high temperature and then cooled to room temperature, thermal residual stress occurs due to their different coefficients of thermal expansion (CTEs). Accordingly, thermal residual stress can be used to predict the yield stress of an FML, and the yield strain of an FML can be less than that of the pure metal [52]. It has also been confirmed that a thermal residual strain of about 0.1 ~ 0.2% occurs along the axial compressive direction in CFRPs due to CTE differences [53].

In some researches on the prediction of mechanical properties based on the rule of mixture [46, 47], predictions of the mechanical behavior of these composites based on the fracture strain of the CFRPs did not agree with experimental results, where the tensile strength of the laminate composites occurred at a greater strain than the fracture strain of the pure CFRP [54-56]. This implies that synergistic

effects were involved in the hybridization of the CFRP and steel laminate, although the authors did not discuss this possibility. The synergistic effects may occur due to the thermal residual stress present during the manufacturing process, which arises due to the different coefficients of thermal expansion (CTEs) of the two materials. In addition, it may be caused by the axial compressive stress generated when the FRP and metal are bonded at high temperature and then cooled to room temperature [53, 57, 58]. Few studies have been dedicated to addressing this issue in detail. It is important to analyze the causes of these phenomena and to accurately predict the mechanical properties.

1.4. Research objectives

In this study, experimental and theoretical studies were conducted to predict the mechanical properties of CFRP and steel laminate composites. In addition, the failure criterion of CFRP in multiaxial stress situations was developed based on the predictive model of mechanical properties.

In chapter 2, we systematically investigated the synergistic effects involved in the hybridization of CFRP and steel plates to form laminate composites, focusing on the interfacial shear strength between the CFRP and steel, the layup sequence, and the CFRP volume fraction. The tensile strength of the hybrid laminate composite should be determined according to the fracture strain of the CFRP constituent if there is no synergistic effect, i.e., when the fracture strains of the pure CFRP and the CFRP within the composite are identical. Both static and dynamic tensile tests were performed and fractography was used to determine the tensile strength (and strain at this point) of the hybrid laminate composites. Finite element analysis (FEA) was performed to calculate the stress exerted on the CFRP and steel within the hybrid laminate composites, and to analyze the experimental results.

In chapter 3, CFRP/steel hybrid laminate composites were analyzed under multiaxial stress. First, the transverse compressive stress developed in a CFRP during axial deformation of a hybrid laminate composite was calculated using a finite element method. To analyze the effects of multiaxial stress on the fracture behavior of the CFRP given the fracture mechanism, the shear lag theory was

invoked to calculate the internal stress distribution of the CFRP in the presence of transverse compressive stress. The tensile deformation behavior of the CFRP was then predicted by considering the internal stress distribution and fracture probability of the carbon fibers. Finally, the mechanical behavior of the hybrid laminate composite was predicted through the rule of mixture using the individual properties of the CFRP and steel. The developed model was validated by comparing predicted and experimental results.

In chapter 4, the developed predictive model was applied to the failure criteria of CFRP to predict the failure of CFRP under multiaxial stress conditions. The developed predictive model includes only the positive effects of transverse compressive stress on the axial properties of CFRP, but the negative effects that occur as the magnitude of transverse compressive stress increases. The failure modes of CFRP suitable for given stress conditions were analyzed and failure criteria developed and validated based on micromechanical approaches.

Chapter 2. Experimental study of CFRP and steel laminate composites

2.1. Experimental

2.1.1. Materials and specimen

Unidirectional CFRP prepregs (USN150Y; SK Chemical, Korea) were used in this study. The prepregs consisted of reinforced carbon fiber (TRW40; Mitsubishi Rayon, Japan) and an epoxy resin (K51; SK Chemical, Korea) matrix. The fiber volume fraction of the prepregs was about 55%. Electrogalvanized (EG) and galvannealed (GA) steels, the surfaces of which were coated with zinc by electroplating and hot-dip galvanization processes, respectively, were obtained from a company in Korea. The steel surfaces were cleaned with ethanol before use, and silane was additionally applied for enhanced adhesion to the polymers [59, 60].

B-stage prepregs of CFRP, having a matrix of uncured resin with a latent (low-reactivity) curing agent, were first prepared and then stacked with the steels in a metal mold. The metal mold was then transferred to a hot-press machine (Samdoo, Korea) and cured at a pressure of 0.2 MPa. The curing temperature and time were 160°C and 3 min, respectively. Note that the epoxy resin in the prepreg underwent curing and adhesion to the steel surface simultaneously. After curing, the mold was detached from the hot-press equipment and cooled to room temperature.

Various kinds of specimens were fabricated to analyze the mechanical properties of the hybrid laminate composites. To investigate the effect of adhesion between the CFRP and steel on the mechanical properties, specimens were prepared with and without general adhesion. Under the 'without adhesion' condition, the CFRP layers were fully cured and stacked with steels without any adhesive, while under the 'with general adhesion' condition, the specimens were prepared by co-curing the B-state prepregs of the CFRP and steels. Some specimens for enhanced adhesion were prepared by co-curing the B-state prepregs of the CFRP with silane-treated steels. The volume fraction of the CFRP in the hybrid laminate composites was controlled according to the number of CFRP layers (i.e., one, two, or four layers) and steel layers (one or two layers). The static tensile test specimen nomenclature is given in Table 2-1. The first character of the specimen code is 'N' or 'T', which represent no adhesion and enhanced adhesion, respectively. For the general adhesion case, those letters are omitted. The next character is C or S, which refers to one layer of CFRP and one layer of steel, respectively; the number before this character denotes the number of layers. For example, N_SCS represents a hybrid laminate composite consisting of steel, CFRP, and steel layers without adhesion, while 2CS2C represents two layers of CFRP, one layer of steel, and two layers of CFRP with general adhesion. The specimens were also subjected to dynamic tensile tests.

Table 2-1 Nomenclature for the static tensile test specimens.

Specimen code	Layer sequence	V_{CFRP}	Adhesion
C	1 layer of CFRP	-	-
N_SCS	Steel/CFRP/steel	12.3	X
SCS	Steel/CFRP/steel	12.3	O
N_CS	CFRP/steel	21.9	X
CS	CFRP/steel	21.9	O
T_CS	CFRP/steel	21.9	O (enhanced)
2C	2 layers of CFRP	-	-
2CS	2 layers of CFRP/steel	36.0	O
N_CSC	CFRP/steel/CFRP	36.0	X
CSC	CFRP/steel/CFRP	36.0	O
4C	4 layers of CFRP	-	-
4CS	4 layers of CFRP/steel	52.9	O
2CS2C	2 layers of CFRP/steel/2 layers of CFRP	52.9	O

Thickness: CFRP (0.16 mm), steel (0.57 mm)

2.1.2. Single-lap shear test

Single-lap shear testing was conducted according to the standard ASTM D1002, to evaluate adhesion according to the steel surface treatment used [61]. Figure 2-1 shows the specimens. A steel support was used to maintain the shape of each specimen during the pressing process, and was subsequently removed. A release film (Teflon sheet) was used to prevent adhesion between the steel support and specimen. The interface area of the specimens for the test was 25.4 × 12.7 mm2.

The lap shear strength was calculated by dividing the load at the interface boundary by the interface area.

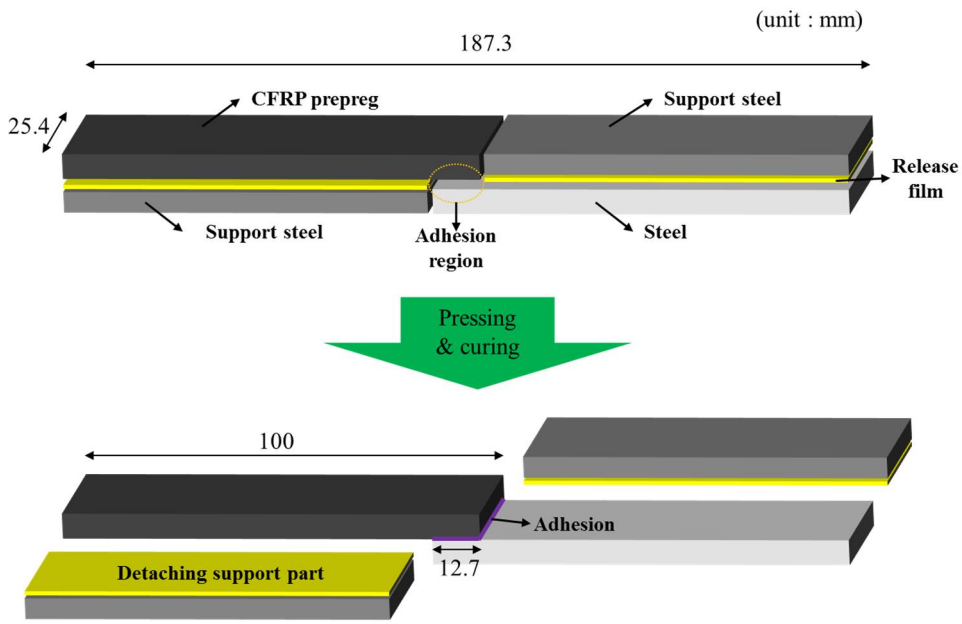

Figure 2-1 Single-lap shear test specimens.

2.1.3. Uniaxial static and dynamic tensile tests

The shape of the specimens used for the tensile test in a static environment is shown in Figure 2-2. The tensile properties of the CFRP, steel, and hybrid laminated composites were measured using a universal testing machine (Model 5584; Instron, USA). Strains were measured using an extensometer (Epsilon, USA)

and the gauge length was 25 mm. The mechanical properties of the CFRP were measured according to ASTM standard 3039 [62]. The properties of the steel and hybrid laminated composites were also evaluated using this standard, because we were interested in the properties of the CFRP within the hybrid laminate composite.

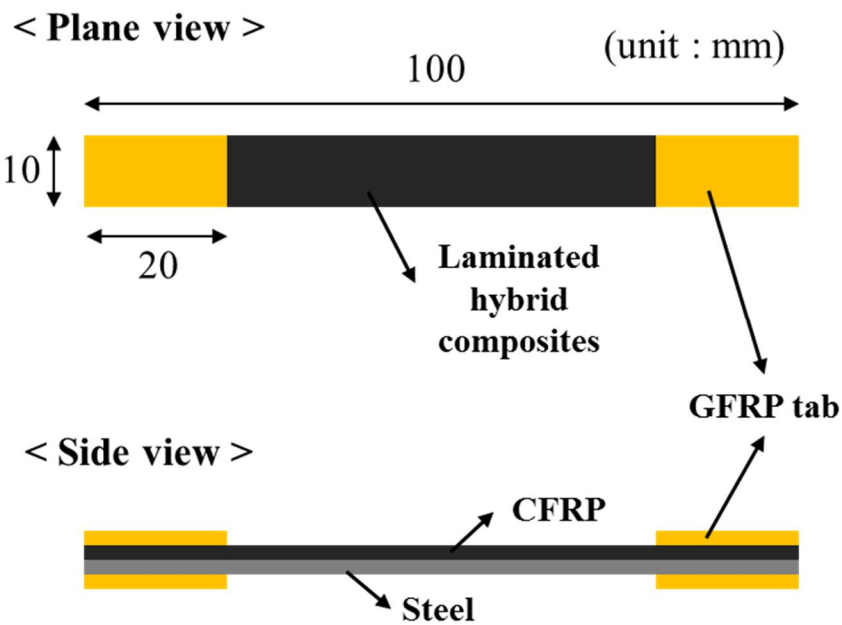

Figure 2-2 Static tensile test specimens.

Dynamic tensile testing was carried out to determine whether the findings were similar between the static and dynamic conditions. The equipment used for the dynamic tensile test consisted of a nitrogen gas-pressurized gun, a force-transmitting bar, and a specimen-clamping fixture [63]. Figure 2-3 schematically

illustrates the dynamic tensile test. The acceleration plate connected to the transmitting bar could move at high speed because of the gas gun. As the acceleration plate collided with the specimen fixture, the specimen was pulled at high speed. A constant deformation rate could be maintained because of the low friction of the linear bearing. Figure 2-4 shows the shape of the specimens used for the dynamic tensile test. A strain gauge (Tokyo Sokki Kenkyujo, Japan) was attached to the center of the specimen, and the strain was measured using a dynamic analyzer (System 6000; Vishay Precision Group, USA) by collecting 10,000 images per second at an excitation voltage of 0.5 V. A load cell installed in the test rig was used to measure the load at 10,000 units per second. The nitrogen gas pressure was 4 bar, and the strain rate was about 50 s–1. Because data acquisition rates of were identical between the strain and load, the stress–strain curves were derived by combining the data from each analyzer. The mechanical properties of the 2CS specimens were determined by the dynamic tensile test and the results were compared with those of the static tensile test.

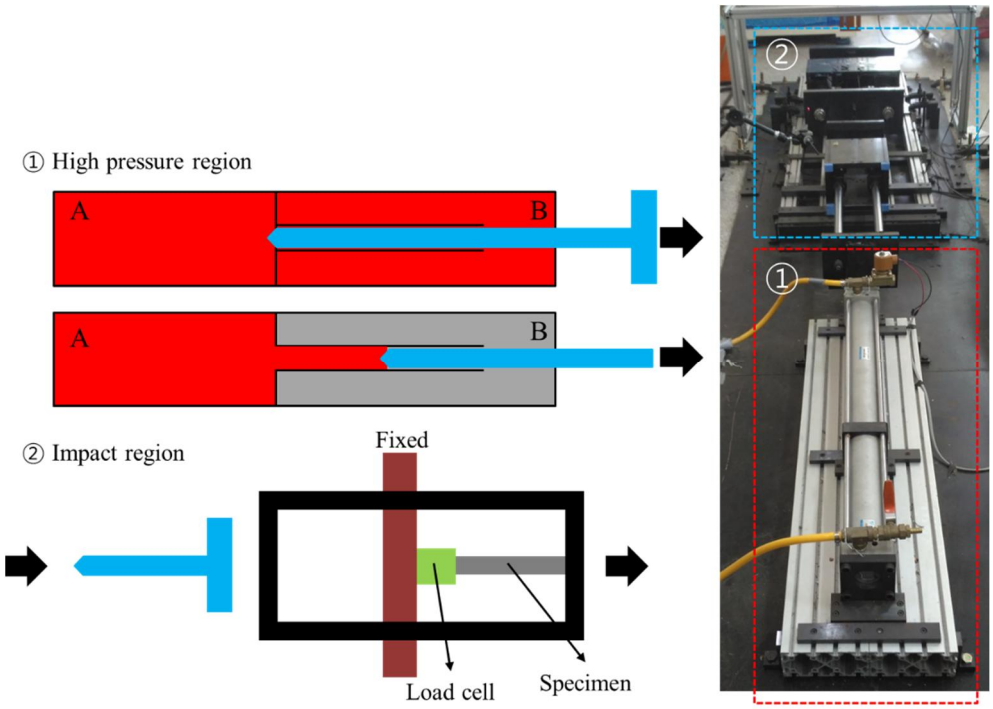

Figure 2-3 Schematic diagram of the equipment used for the high-speed tensile test. In the high-pressure region (①), the bar was released at high pressure and generated a high strain rate by striking the fixture, with the specimen clamped in the impact region (②).

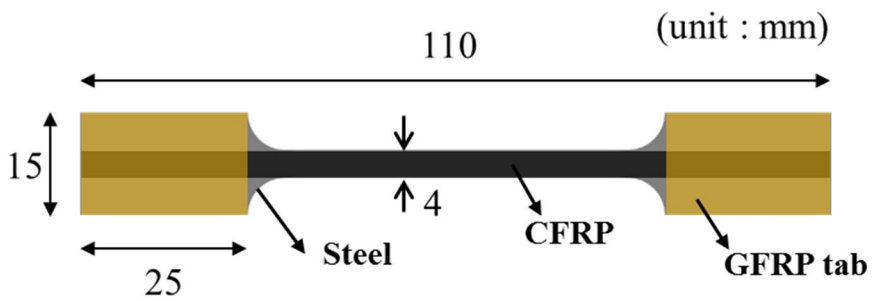

(a)

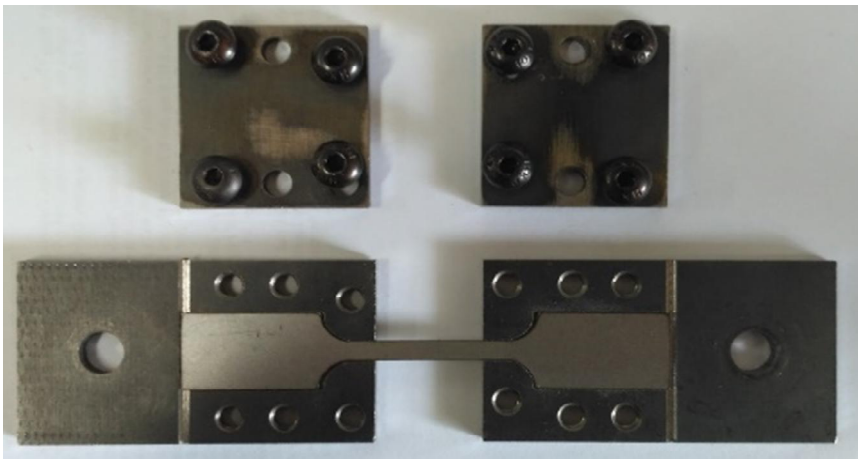

(b)

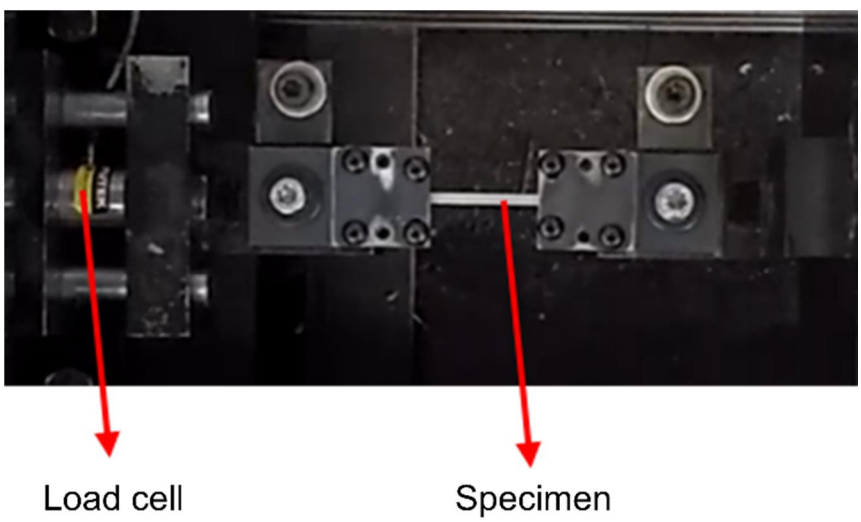

(c)

Figure 2-4 High-speed tensile test specimen. (a) Dimensions, (b) intermediate jig for fixing the specimen, and (c) test set-up.

2.1.4. Compressive test

The compressive test was conducted according to ASTM D6641 [64]. Figure 2-5

shows a schematic drawing of the test. The total length of the specimen is 140 mm, the width is 13 mm, and the gauge length is 13 mm. Strain gauges were attached to both sides of the gauge section for the measurement of the strain, and the average value of the two strains was used. The stress was measured while compressing with a universal testing machine (Model 5582; Instron, USA), and the crosshead stroke speed was 1.3 mm/min.

Figure 2-5 Test jig and set-up for compressive testing of laminate composites.

2.2. Tensile behavior

2.2.1. Mechanical properties of the constituent materials

The mechanical behavior of the CFRP and steel hybrid laminate composites was first studied by characterizing each constituent, but with a focus on any synergistic effects. The mechanical behavior of CFRPs prepared with different numbers of prepreg layers was investigated as a function of thickness (Figure 2-6 (a)). The modulus of the three types of CFRPs was about 126 GPa and catastrophic fracture was observed during elastic deformation. However, the fracture strains of the CFRPs decreased with increasing thickness, i.e., 1.94%, 1.82%, and 1.71% for CFRPs prepared with one, two, and four layers of prepregs, respectively. The strength of the CFRP also decreased with increasing CFRP thickness (i.e., with an increasing number of CFRP layers). These changes are attributed to the size effect reported for uniaxial fiber-reinforced plastics (FRPs), which is related to the volume (and probability) of critical defects, and the microstructure and processing method [65]. As the volume occupied by the CFRP increases, the probability of critical defects in the interior increases [66, 67]. Additionally, a CFRP fabricated using multiple layers of prepregs is more likely to contain microdefects such as residual strains, fiber misalignment and waviness, porosity, and fiber clusters [68, 69]. Such microdefects explain the failure strain and tensile strength behavior of the CFRPs prepared in this study. The EG steel that we used exhibited the typical stress–strain behavior of ductile materials; it had an elastic modulus and yield

strength of 194 GPa and 176 MPa, respectively (Figure 2-6(b)). After yielding, the stress increased due to hardening behavior. The ultimate tensile stress and fracture strain were 330 MPa and 26%, respectively. Even if the CFRP in the hybrid laminate composite was destroyed, mechanical stability was expected because the load would be carried by the steel.

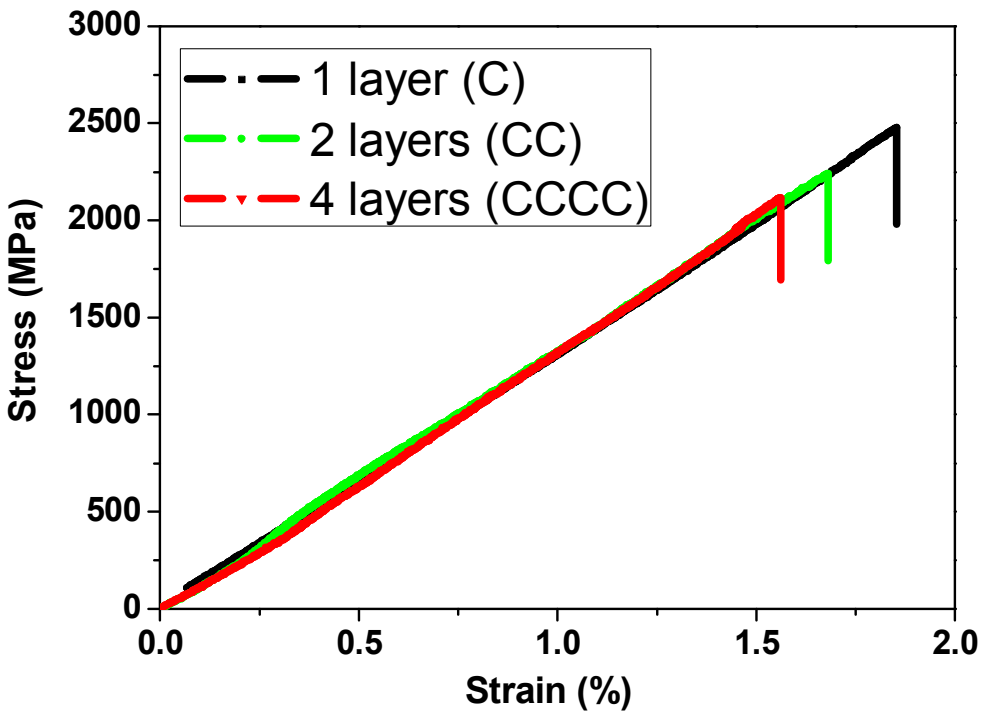

(a)

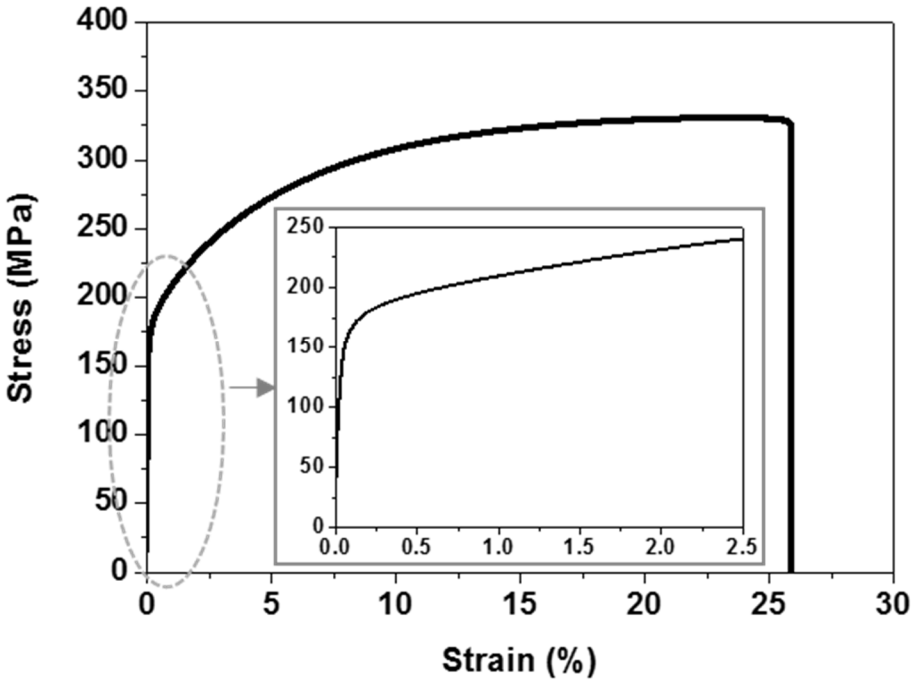

(b)

Figure 2-6 Typical stress–strain curves of individual (a) carbon fiber-reinforced plastic (CFRP) and (b) electrogalvanized (EG) steel specimens.

2.2.2. Increased breaking strain of CFRP within the laminate composites

First, the tensile behavior of the hybrid laminate composites with and without adhesion between the CFRP and steel was investigated. Silane treatment of the steel surface increased the interfacial shear strength determined by the single-lap shear test; the values were 13% and 23% for the EG and GA steels, respectively (Figure 2-7).

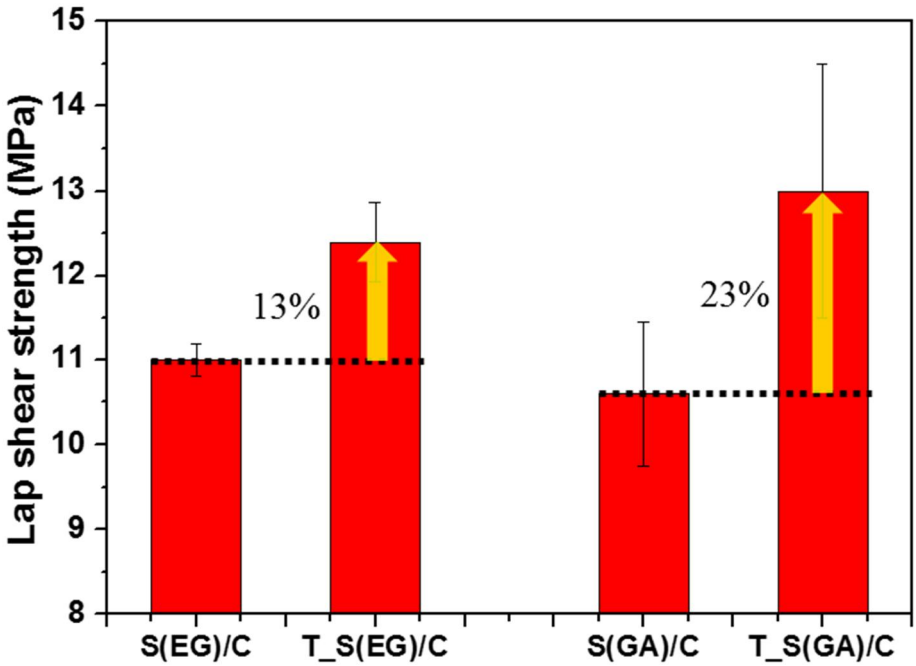

Figure 2-7 Adhesion strength determined by the single-lap shear test. Three specimens were used to obtain the data. Note that S(EG) and S(GA) represent EG and GA steels, respectively.

The deformation behavior of the hybrid laminate composites proceeded according to three stages: elastic deformation, which occurred in both the CFRP and the steel; CFRP failure after yielding of the steel; and carrying of the load by the steel only after CFRP failure. Based on this sequence, the mechanical behavior of the hybrid laminate composites was predicted using the rule of mixtures (Figure 2-8). The experimental results were in good agreement with the predictions. The extensometer used to measure the strain slipped markedly immediately after the CFRP failed, which made it difficult to collect reliable data; thus, the third stage of

the behavior is not plotted in Figure 2-8. Nevertheless, the load–displacement curve, which is based on the crosshead movement, suggests that the behavior after CFRP failure was similar to that predicted by the rule of mixtures.

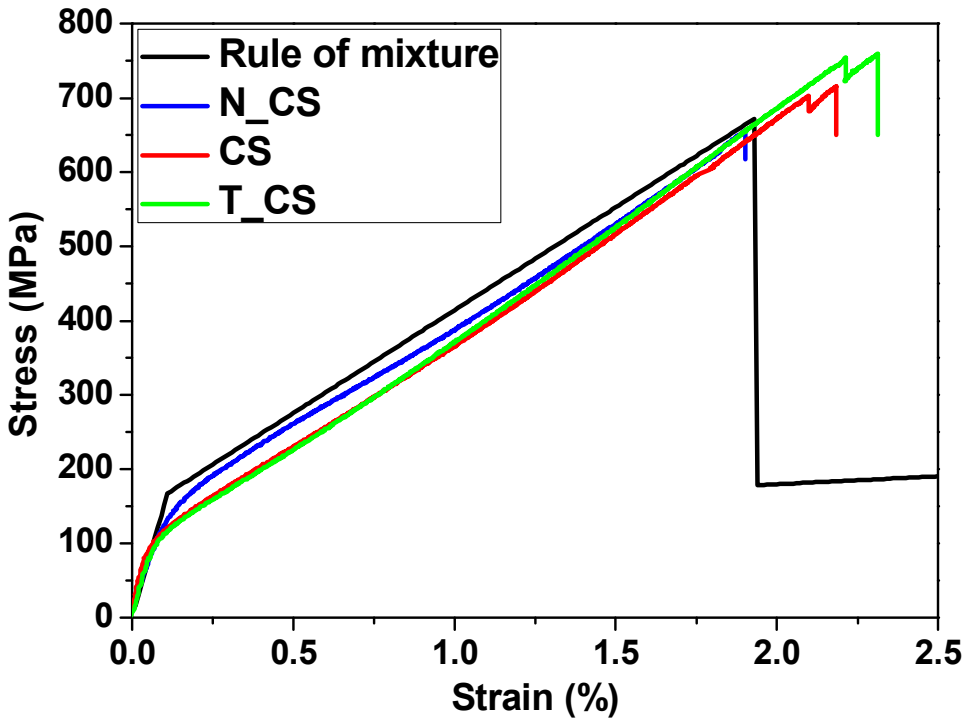

Figure 2-8 Comparison of the stress–strain curves of the CFRP and steel hybrid laminate composites with and without general and enhanced adhesion.

Two interesting results are evident in Figure 2-8. The mechanical behavior of the hybrid laminate composites without adhesion between the CFRP and steel was similar to that predicted by the rule of mixtures, which implied that the constituents deformed without any interaction. In contrast, in the composites with adhesion

between the CFRP and steel, yielding of the steel occurred at lower strains than for the adhesion case. This phenomenon was more evident with increasing volume fraction of the CFRP in the hybrid laminate composites (Figure 2-9). Notably, the fracture strain of the CFRP in the hybrid laminate composites increased in the case of adhesion between the CFRP and steel. The fracture strain with adhesion was larger than that of pure CFRP (Figure 2-8). Note that partial fracture occurred before the final fracture in case of the adhesion between the CFRP and steel, which will be discussed further using fractography in section 2.2.4. The fracture strain of the CFRP inside the composites increased by 14%, 11%, and 15% for the SCS, CS, and CSC specimens. Note, however, that the calculated improvements were based on the properties of one layer of CFRP for the SCS and CS cases, but two layers for the CSC case. Nevertheless, it is clear that the fracture strain of the CFRP was higher for the hybrid laminate composites with adhesion between the CFRP and steel. This observation is discussed in detail in the following section. The dynamic behavior of the composites was also characterized to establish whether the increased failure strain of the CFRPs was also evident under a high strain rate.

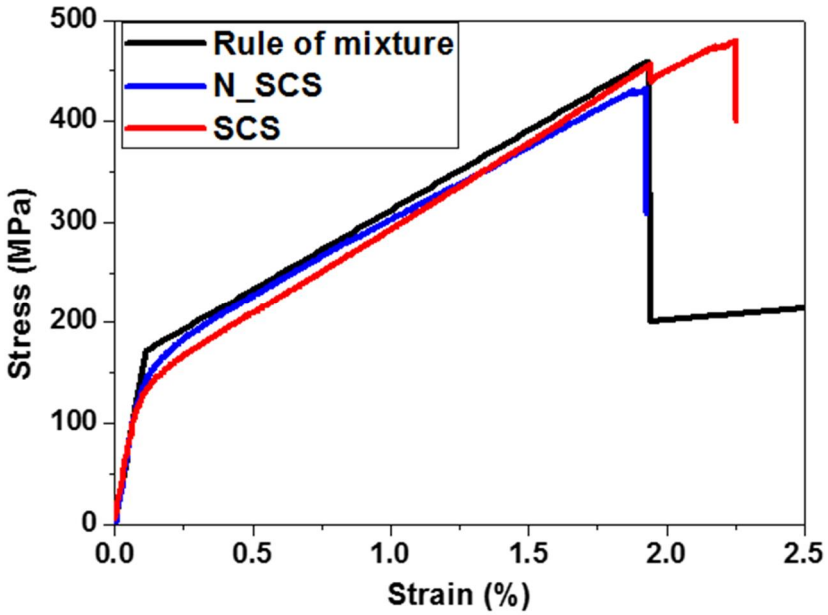

(a)

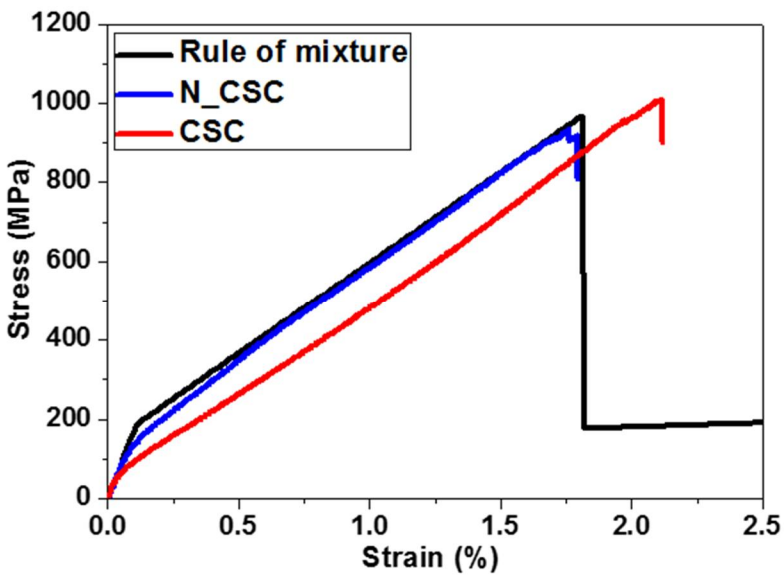

(b)

Figure 2-9 Comparison of the stress–strain curves of the CFRP and steel hybrid laminate composites with different layer sequences, with and without interfacial adhesion. (a) Steel/CFRP/steel and (b) CFRP/steel/CFRP.

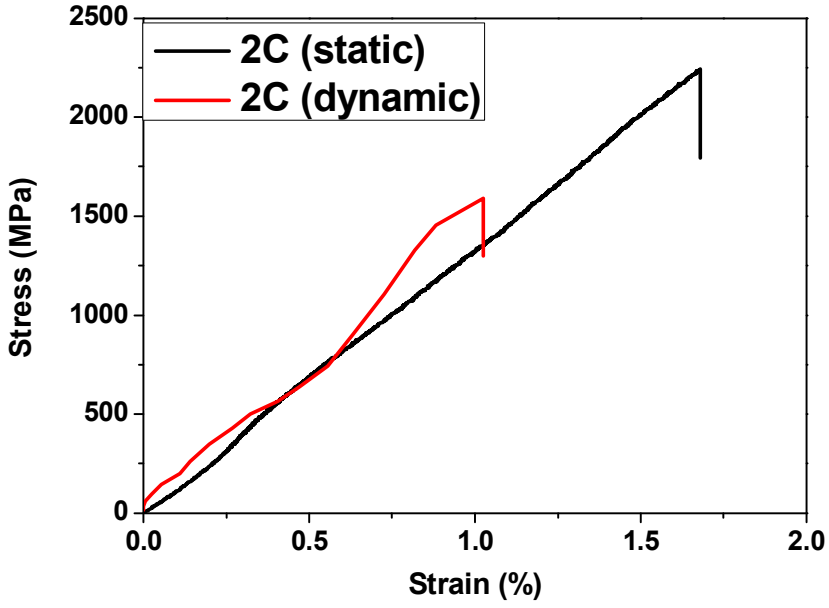
2C (static)
2C (dynamic)
Stress (MPa)
Strain (%)
0
500
1000
1500
2000
2500
0.0
0.5
1.0
1.5
2.0

(a)

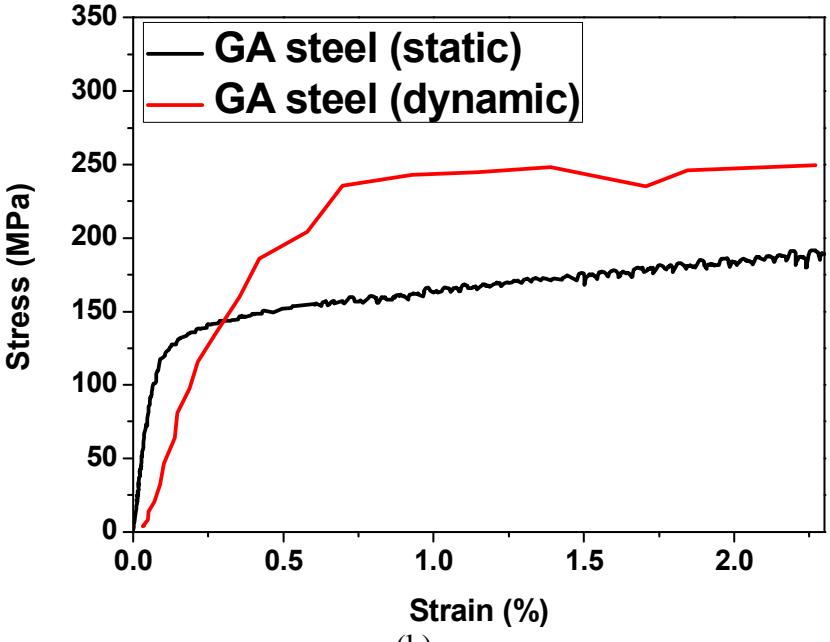
GA steel (static)
GA steel (dynamic)
Stress (MPa)
Strain (%)
0
50
100
150
200
250
300
350
0.0
0.5
1.0
1.5
2.0

(b)

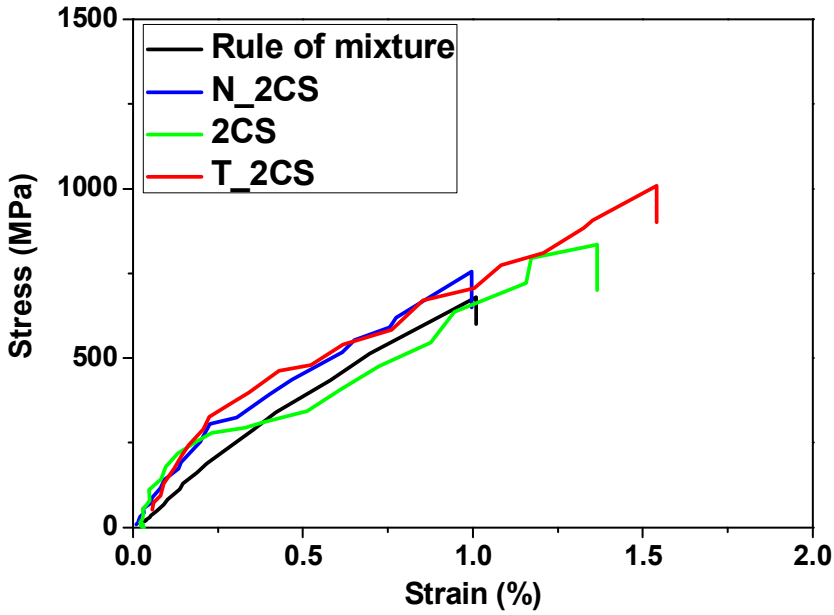

(c)

Figure 2-10 Dynamic tensile test results of the hybrid laminated composites. Comparison of the static and dynamic properties of (a) pure CFRP and (b) pure steel, and (c) dynamic mechanical properties of the hybrid laminated composites as a function of adhesion. The strain rate was about 50 s^{-1}.

Figure 9 shows the dynamic tensile behavior of the hybrid laminate composites. The deformation time in this test was very short due to the high deformation rate; fewer data points were acquired than during the static test. The dynamic tensile behavior of the 2C specimens was nonlinear (Figure 9(a)), but linear fitting of the data provided a modulus of 140 GPa, which is slightly greater than that obtained from the static test (126 GPa). The mechanical properties of uniaxial carbon fiber composites do not depend significantly on the deformation rate [70]. The fracture strain was smaller in the dynamic tensile test than in the static test. Figure 9(b)

compares the static and dynamic tensile behavior of the GA steel, which displayed increased yield strength but decreased modulus. This behavior is inconsistent with the usual behavior of metals, i.e., increasing modulus and yield strength, and decreasing strain at fracture, with increasing strain rate [71]. Figure 9(c) shows the deformation behavior of the 2CS specimens with adhesion between the CFRP layers and steel. Here, the predicted results were obtained using the rule of mixtures based on dynamic test results of pure CFRP and steel and the volume fractions of each material. The predictions were similar to those for the case without adhesion. The fracture strain and tensile strength of the hybrid laminate composites under a high strain rate increased with increasing adhesion, as also observed in the static tensile test. This confirmed that the phenomenon was independent of strain rate (Figure 10). In the figure, the increase in the maximum stresses was generally smaller than the increase in the fracture strain. This is because the increase in the axial fracture strain of CFRP was not only caused by the transverse compressive stress in CFRP but also affected by the axial thermal residual stress in CFRP generated during the manufacturing process. The transverse compressive stress affected both the fracture strain and the maximum stress, while the axial thermal residual stress affected only the fracture strain. Therefore, the increase in the fracture strain was generally larger than the increase in the maximum stress.

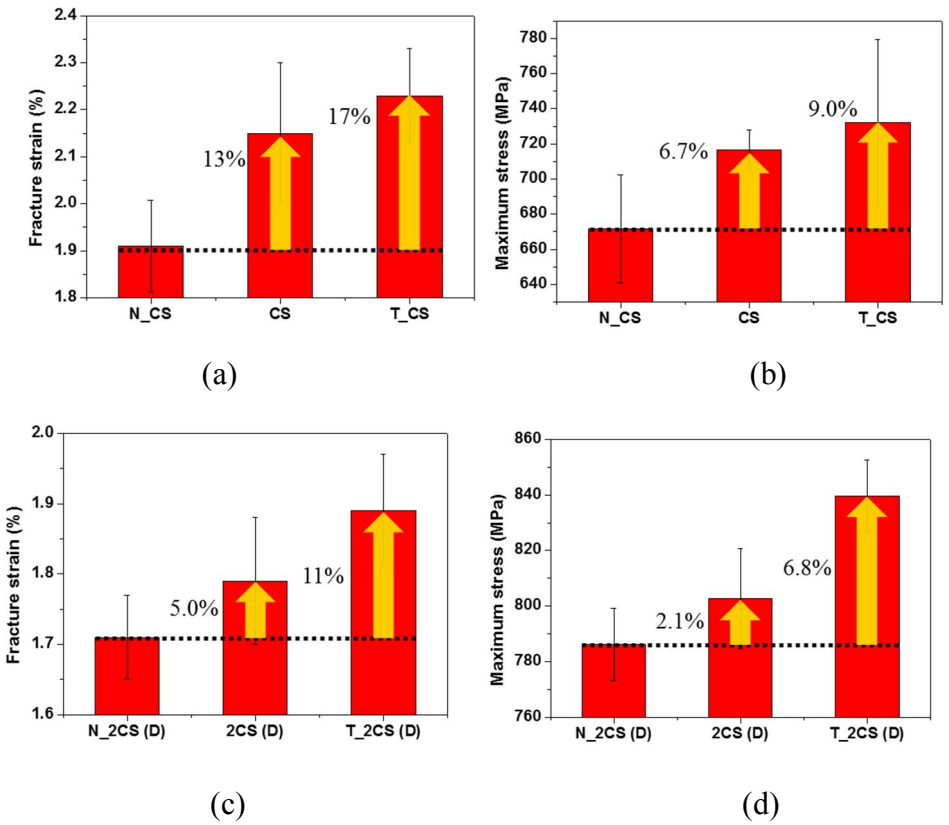

Figure 2-11 Comparison of the fracture strain and tensile strength of the CFRP/steel hybrid laminate composites as a function of the adhesion between them. (a) and (c) Fracture strain and (b) and (d) tensile strength determined by static and dynamic tensile testing. At least four specimens were tested to obtain these results. In the static test, the adhesion determined by the single-lap shear test was 11 and 12.4 MPa for the general and enhanced adhesion cases, respectively, while the values were 10.6 and 13 MPa for specimens tested dynamically.

2.2.3. Mechanism behind the increased breaking strain

The hybrid laminate composites with adhesion between the CFRP and steel displayed increased failure strain and tensile strength in the static and dynamic tensile tests. This implied that the underlying mechanism in the tensile test delayed

the failure of CFRP within the composite. Commercial finite element software (ABAQUS; Simulia, USA) was used to better understand the mechanical properties of these composites under tension.

Table 2-2 Mechanical properties of the CFRP/steel hybrid laminate composites subjected to finite element analysis.

CFRP	
Young's modulus in axial direction $\boldsymbol{E_{11}}$ (GPa)	126
Young's modulus in transverse direction $\boldsymbol{E_{22}}$, $\boldsymbol{E_{33}}$ (GPa)	7.40
longitudinal shear modulus $\boldsymbol{G_{12}}$, $\boldsymbol{G_{13}}$ (GPa)	3.89
In-plane shear modulus $\boldsymbol{G_{23}}$ (GPa)	3.50

Steel	
Young's modulus $\boldsymbol{E_{s,elastic}}$ (GPa)	194
Hardening modulus $\boldsymbol{E_{s,hard}}$ (GPa)	4
Yield stress $\boldsymbol{\sigma_{s,y}}$ (MPa)	176
Failure strain $\boldsymbol{\gamma_{s,f}}$ (%)	25

The mechanical properties of each constituent material in the hybrid laminate composites are provided in Table 2-2. The CS specimens having a CFRP volume fraction of 21.9% were analyzed first. The cohesive zone model was used to model the adhesion between the CFRP and steel. The stiffness coefficient and maximum normal stress of the cohesive zone model were assumed to be 106 N mm^{-3} and 15 MPa, respectively, while the interfacial shear strength was used as the maximum shear stress in the model.

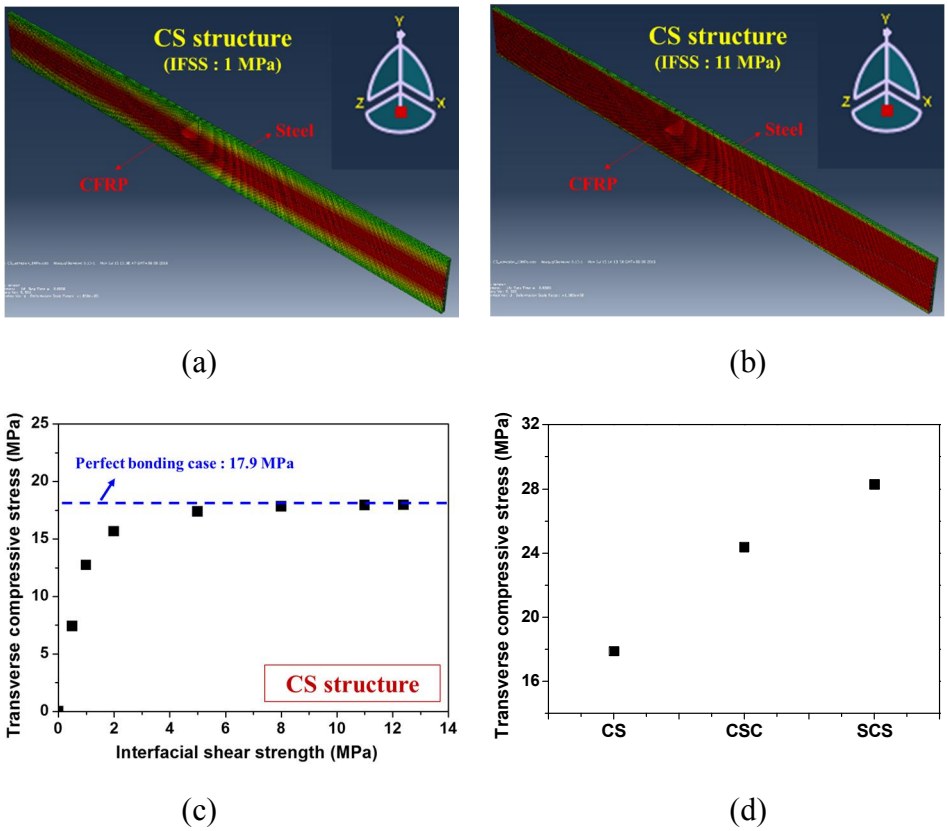

Figure 2-12 Distribution of the transverse compressive stress in the CFRP layer as a function of interfacial shear strength of (a) 1 MPa and (b) 11 MPa. Change in the average transverse compressive stress as a function of (c) interfacial shear strength and (d) layer sequence. All transverse compressive stresses were calculated when the axial strain of the hybrid laminate composite was 2%.

Figure 2-12 (a) and (b) show the transverse (y-direction) compressive stress developed in the CFRP during the tensile testing for weak (1 MPa) and strong (11 MPa) interfacial shear strengths. These results were obtained under 2% axial strain.

When the interfacial shear strength was weak, interfacial separation occurred at the side of the specimen during the tensile test, which kept the transverse compressive stress at the center of the specimen. Under high interfacial shear strength, the transverse compressive stress was uniformly distributed throughout the CFRP, except at the edges. The transverse compressive stress in the CFRP increased with increasing interfacial shear strength and became saturated at a constant value (Figure 2-12 (c)). Figure 2-12 (d) shows the transverse compressive stresses in the case of perfect interfacial adhesion as a function of layer sequence. The transverse compressive stress of CFRP increased with increasing steel volume fraction. The transverse compressive stress was highest in the SCS specimens (28.3 MPa) because bending of specimens having an asymmetric layer sequence, such as the CS specimens, decreases the transverse compressive stress. The FEA established that transverse compressive stress developed in the CFRP layer. This is intuitive considering the mismatch in material properties between the steel and CFRP layers. It is reasonable to assume a Poisson's ratio of 0.3 for both CFRP and steel over the range of elastic deformation. When the steel exceeded the yield strain, plastic deformation occurred within it and the Poisson's ratio increased to 0.5. Because of this mismatch in the Poisson's ratio, the CFRP underwent transverse compressive stress, while the steel experienced tensile stress. This transverse compressive stress strengthened the longitudinal shear properties [72, 73], resulting in increased axial fracture strain and strength [74].

The axial compressive stress that developed in the composite was thermally

induced [53, 57, 58]. Bonding of CFRP and steel was done at high temperature (160°C) to cure the adhesive material, which resulted in thermal expansion of the CFRP and steel according to their CTEs. The CTE of steel is about 10 × 10–6 K–1 [75], while that of CFRP is close to zero in the fiber-axis direction [76]. Steel tends to shrink more than CFRP at room temperature after bonding at high temperature because of its higher CTE. Strong bonding of steel to CFRP leads to tensile and compressive residual stress in the steel and CFRP, respectively [58]. As such, the CFRP was subjected to the axial compressive stress, resulting in higher tensile strain at the fracture of the CFRP component. This phenomenon, together with the transverse compressive stress, resulted in increased axial fracture strain of the CFRP within the hybrid laminate composites.

2.2.4. Fractography

The fracture behavior of pure CFRP was observed in situ under an optical microscope. Figure 2-13 (a) shows the specimen at the beginning of the tensile deformation. This macroscopic deformation remained constant up to the initiation of fracture of the CFRP. As the axial tensile strain approached the fracture strain, local splitting and partial fracture occurred at the side of the CFRP (see the dashed box in Figure 2-13 (b)). As the axial tensile strain increased further, final fracture occurred, revealing split fibers between the cracked CFRPs (Figure 2-13 (c)). Pure CFRP was completely broken once the damage had accumulated up to the stage

where fiber splitting occurred and the load could no longer be carried.

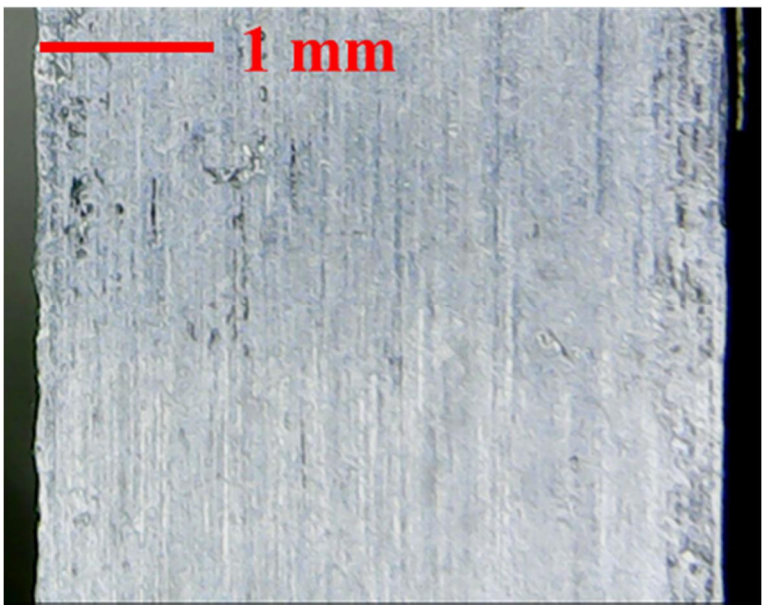

(a)

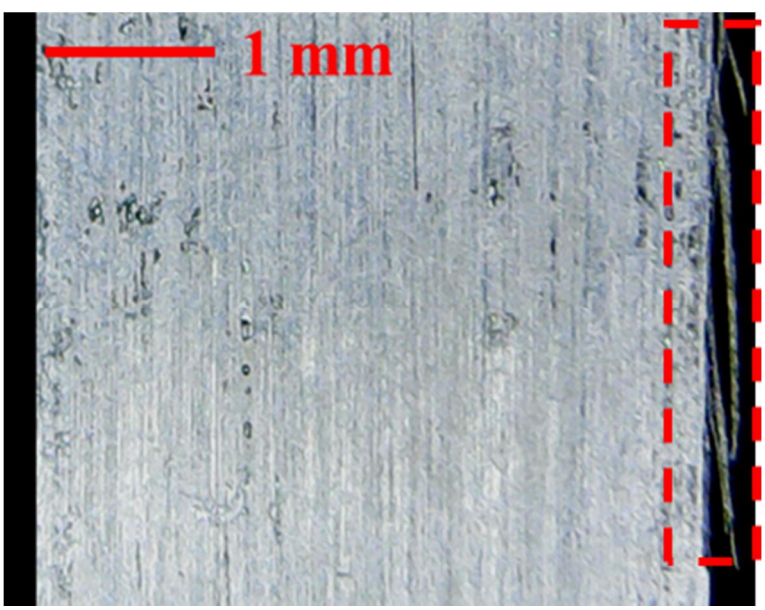

(b)

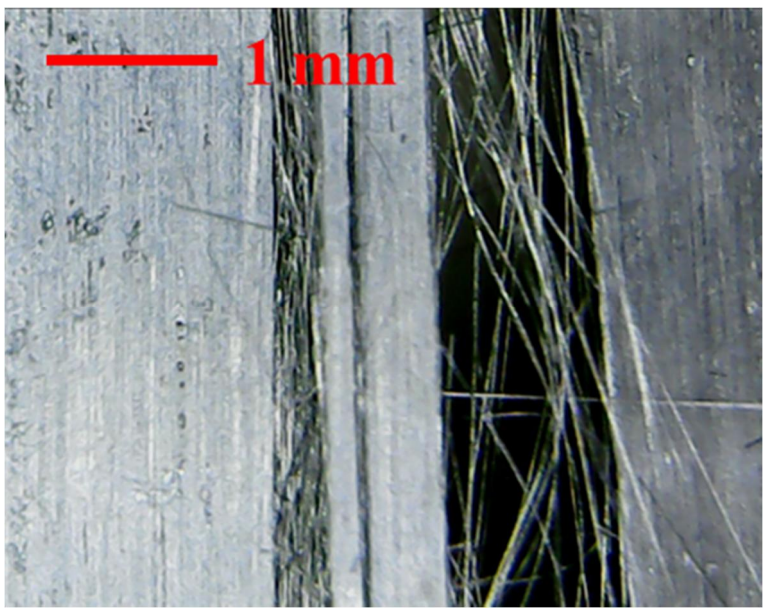

(c)

Figure 2-13 Optical microscope images showing the deformation process of pure CFRP. (a) From the start of deformation to failure (0.20% strain), (b) when partial splitting occurred at the edge of the CFRP (1.80% strain), and (c) at final fracture (1.82% strain).

The fracture behavior of the hybrid laminate composites was similar in situ. The macroscopically deformed shape of the CFRP (Figure 2-14 (a), (c), and (e)) and the interface (Figure 2-14 (b), (d), and (f)) were clearly evident. As also observed for pure CFRP, partial splitting occurred at the edge of the CFRP as the composite approached its fracture strain (Figure 2-14 (c)). This was explained by the FEA results discussed in Section 2.2.3, i.e., the transverse compressive stress around the edges of the specimen was small and the splitting was not effectively suppressed at

the edges. Therefore, the partial splitting of the CFRP occurred at the edge, resulting in the stress loss of the hybrid laminate composite before the final fracture (Figure 2-8). Such splitting was also observed in the CFRP, and at the interface between the CFRP and steel (Figure 2-14 (d)). The splitting at the interface indicated partial separation of the interface.

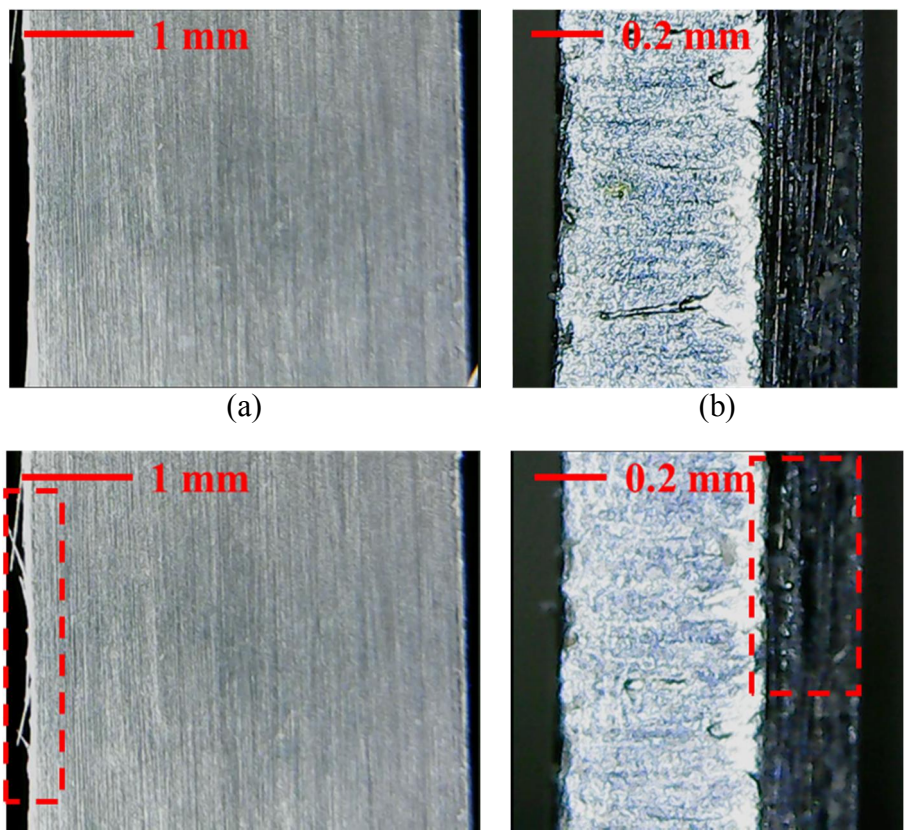

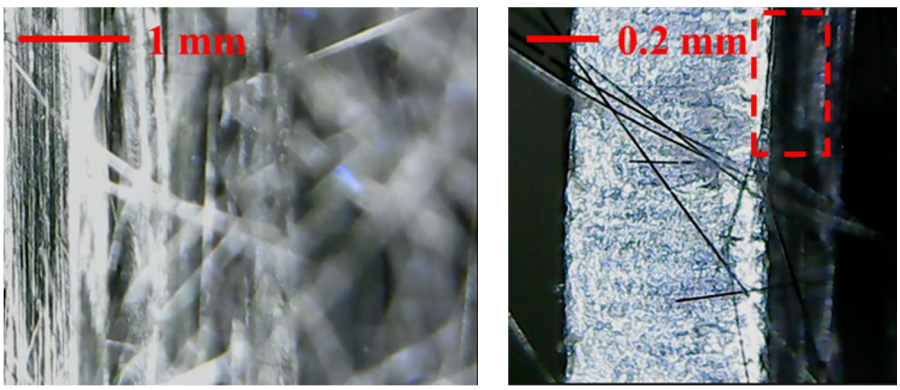

(e) (f)

Figure 2-14 Optical microscope images showing the deformation behavior of the hybrid laminate composite. a) From the start of deformation to failure (0.20% strain), (b) when partial splitting occurred at the edge of the CFRP (1.76% strain), and (c) at final fracture (2.00% strain). (a), (c), and (e) show the CFRP deformation behavior in the plan view, while (b), (d), and (f) show the CFRP and interface fracture behavior in the side view.

Unlike pure CFRP, the partial fracture and splitting of the CFRP were not directly related to the final fracture. The partial fracture occurred due to low transverse compressive stress at the edge of CFRP, but did not lead to severe fractures sufficient for interface separation and new edge creation. In other words, axial tensile deformation continued after partial fracture at the edges of CFRP, and damages accumulated throughout the specimen, resulting in final fracture. This is because the longitudinal shear strength of the CFRP increased due to the transverse compressive stress that developed therein [72, 73]. Since the longitudinal splitting of the CFRP was caused by the shear stress of the matrix, the splitting behavior of the CFRP was expected to be inhibited by increasing longitudinal shear strength.

The completely ruptured hybrid laminate composite had a brush-like form with interfacial separation (Figure 2-14(e) and (f)). While pure CFRP fractured in regions of partial splitting, the mechanical properties of the hybrid laminate composites were improved via suppression of such partial splitting by the transverse compressive stress.

The fragments of CFRP remaining on the surface of the steel after fracture of the hybrid laminate composites were investigated by optical microscopy. The more longitudinal splitting occurred in CFRP, the more the inter-fiber fracture occurred within the unit width, reducing the width of each fragment. When the CFRP was destroyed, some fragments were separated from the steel, while the other fragments remained attached to the steel. It was observed that the widths of these two types of fragments were similar. Therefore, the width of fragments remaining on the surface of steel after fracture was investigated. The average size of the 20 CRFP fragments shown in Figure 2-15 (a) and (b) was calculated (Figure 2-15 (c)), and was about 62 μm for the general adhesion case and 80 μm for the enhanced adhesion case, which suggested delayed splitting. The delay in splitting with increasing interfacial shear strength was due to the transverse compressive stress, which reduced the partial separation at the interface.

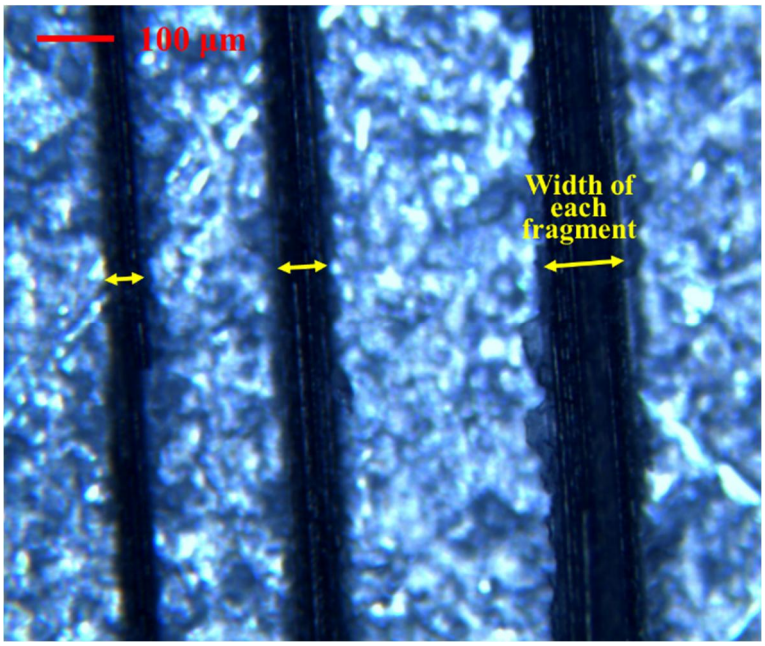

(a)

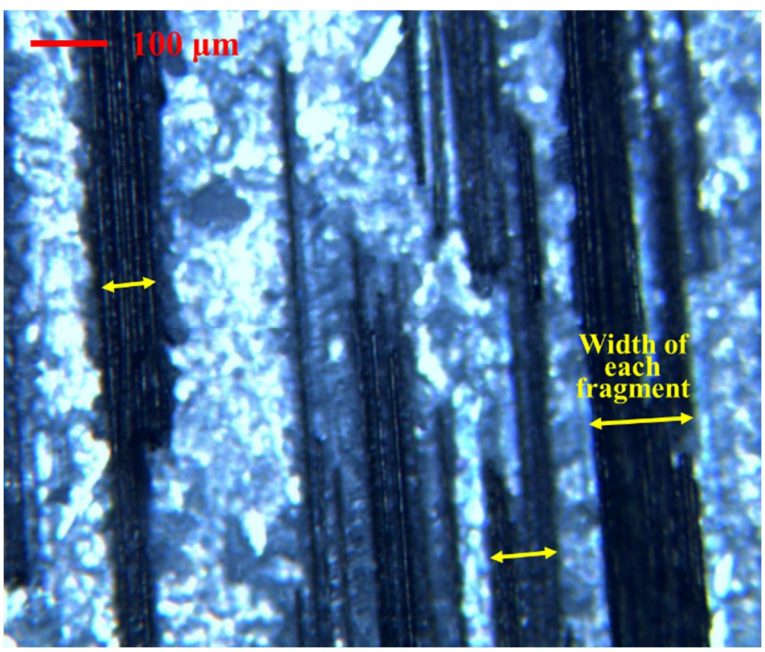

(b)

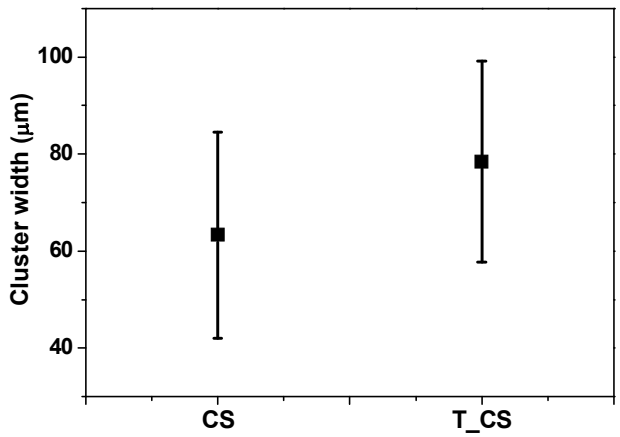

(c)

Figure 2-15 Optical microscope images of CFRP fragments remaining on the surface of the steel after fracture of the hybrid laminate composites with adhesion of (a) 11 MPa (CS) and (b) 12.4 MPa (T_CS), and (c) the average width of 20 fragments.

2.2.5. Effect of the laminate structure

The effect of the layup sequence on the fracture strain of the CFRP within the hybrid laminate composites was investigated using specimens comprising two or four CFRPs layers with one layer of steel. Higher fracture strain was observed for the symmetric CSC (sandwich) composites compared with the asymmetric 2CS case (Figure 2-16 (a)). This was also observed for the composites comprising four CFRP layers and one layer of steel (Figure 2-16 (b)). The increase was 7.2% and 4.9% for the 2CS2C and 4CS cases, respectively (Figure 2-16 (c)). This behavior was due to the bending of the asymmetric structure being less effective in transferring the transverse stress from the steel to the CFRP, and thus less effective

in increasing the fracture strain of the CFRP within the hybrid laminate composite. The fracture strains of the CFRP within the hybrid laminate composites were again compared with those of pure CFRP, with a focus on the increased volume fraction of CFRP in the former (Figure 2-16 (d)). There was clearly a synergistic effect, i.e., increased fracture strain of CFRP within the hybrid laminate composites irrespective of the volume fraction of the CFRPs. However, the percentage increase in fracture strain decreased with increasing CFRP volume fraction. This was investigated in detail by considering the fracture strains of the SCS, CS, 2C, and 4CS composites (Figure 2-16 (e)). The CFRP volume fractions of these composites were 12.3%, 21.9%, 36.0%, and 52.9%, respectively. The percentage increase in the fracture strain decreased with increasing CFRP volume fraction, which was again attributed to the transverse compressive stress. The effect of steel on the transverse compressive stress on the CFRP layer diminished with increasing CFRP volume fraction; the FEA discussed in Section 2.2.3 supported this notion. Decreased transverse compressive stress was less effective in suppressing the splitting and increasing the fracture strain of the CFRP. This observation also supports the mechanism proposed for the observed increase in fracture strain of the CFRP within the hybrid laminate composites.

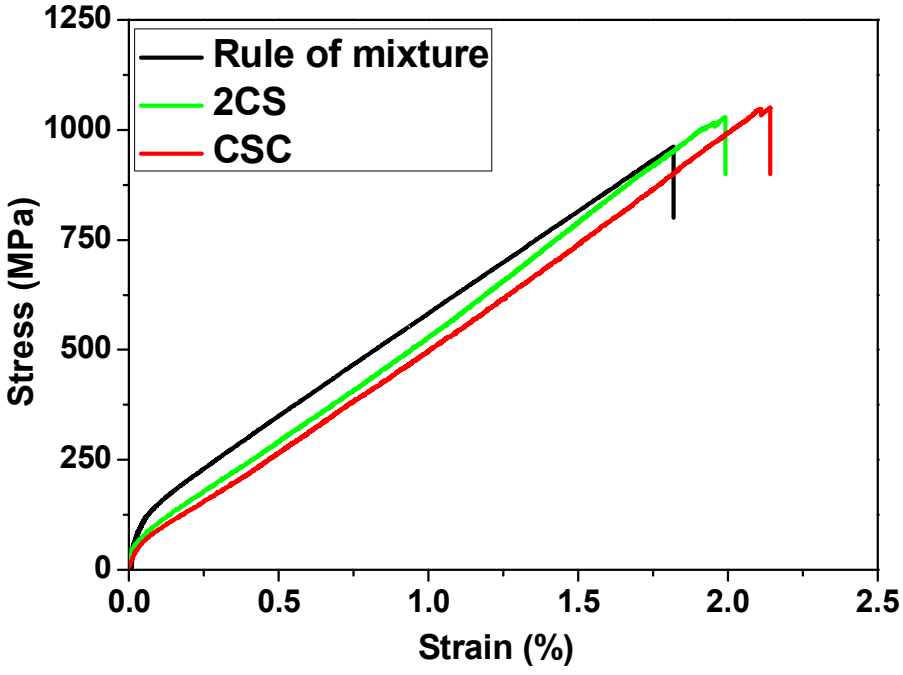
Rule of mixture
2CS
CSC
Stress (MPa)
Strain (%)
0
250
500
750
1000
1250
0.0
0.5
1.0
1.5
2.0
2.5

(a)

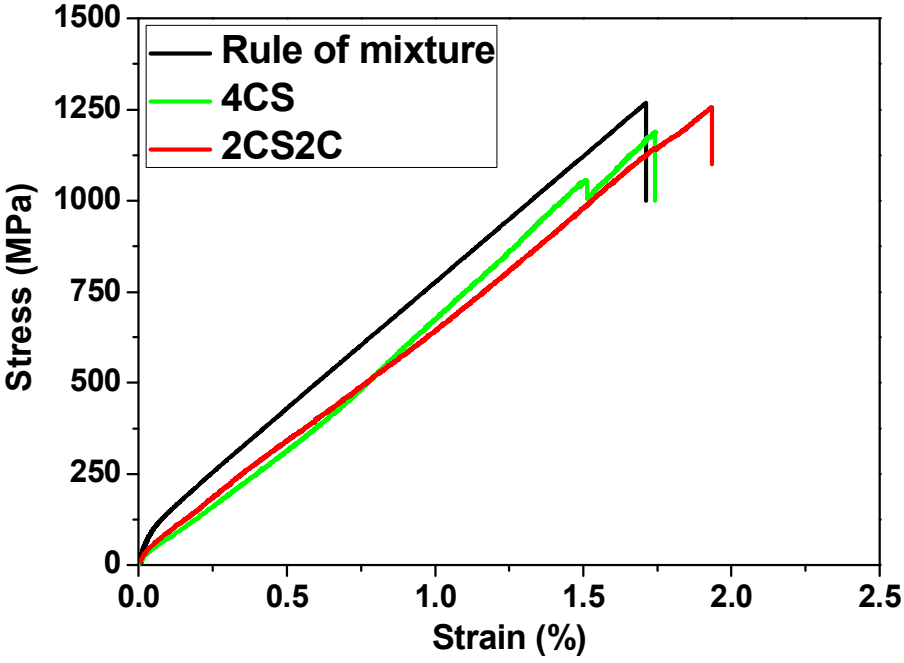
Rule of mixture
4CS
2CS2C
Stress (MPa)
Strain (%)
0
250
500
750
1000
1250
1500
0.0
0.5
1.0
1.5
2.0
2.5

(b)

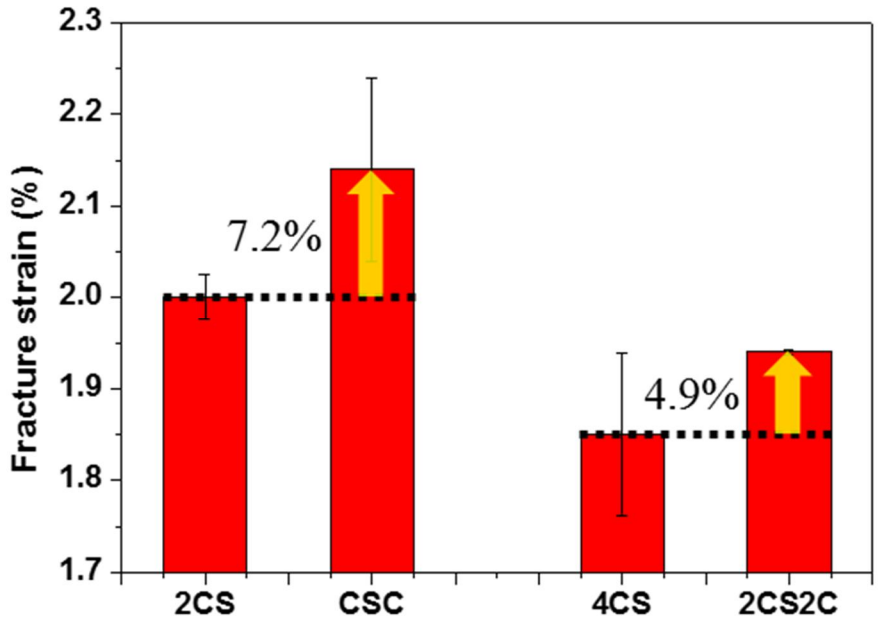
Fracture strain (%)
2.3
2.2
2.1
2.0
1.9
1.8
1.7
7.2%
4.9%
2CS
CSC
4CS
2CS2C

(c)

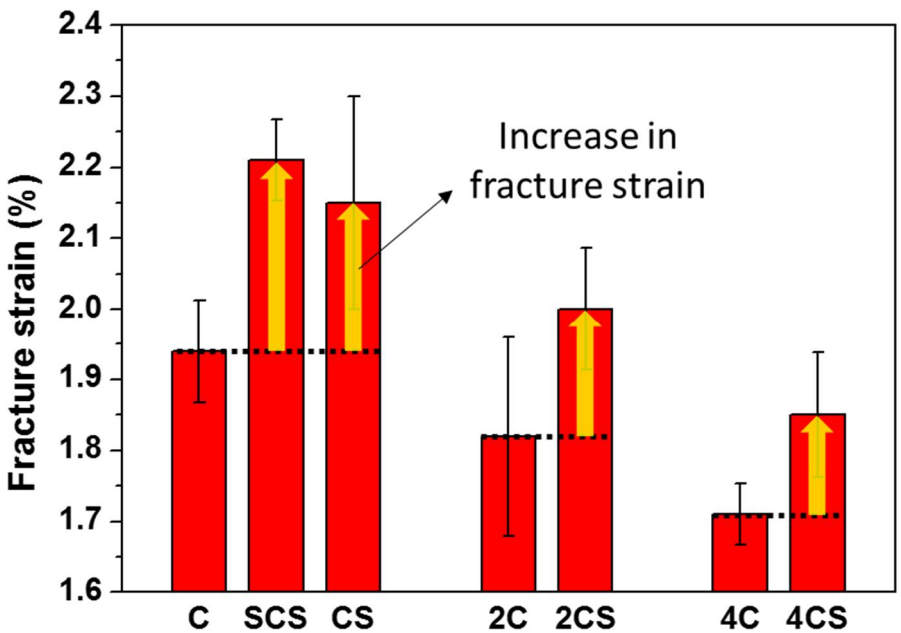
Fracture strain (%)
2.4
2.3
2.2
2.1
2.0
1.9
1.8
1.7
1.6
Increase in
fracture strain
C
SCS
CS
2C
2CS
4C
4CS

(d)

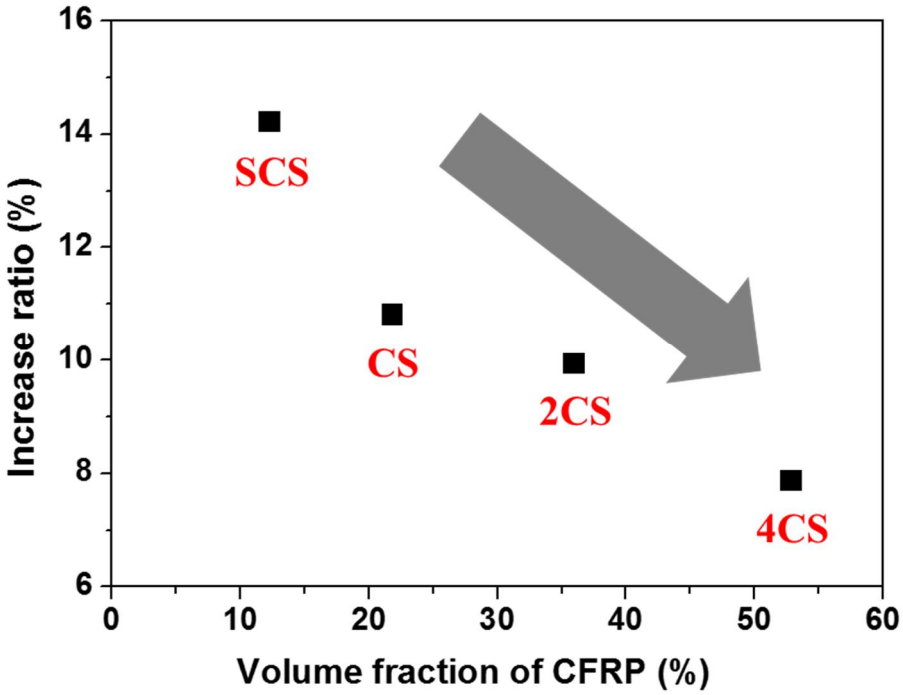

(e)

Figure 2-16 Fracture strain of the CFRP within the hybrid laminated composites having (a) two and (b) four layers of CFRPs with one layer of steel. (c) Effect of layup sequence. (d) Comparison of the fracture strain and (e) the percentage increase thereof as a function of the CFRP volume fraction.

2.3. Compressive behavior

Figure 2-17 shows representative compression behavior for each specimen type. As in the tensile test, in the case of compressive deformation, pure CFRP exhibits elastic deformation behavior, and the laminate composite undergoes plastic deformation after the yield strain of steel after the initial elastic deformation behavior. In general, the compressive strength of CFRP is known to be weak compared to the tensile strength. This is because the compression failure behavior is different from the tensile failure behavior. Compressive strength is known as about 40~60 % of tensile strength, and in this study, compressive strength is measured as about 40% of tensile strength.

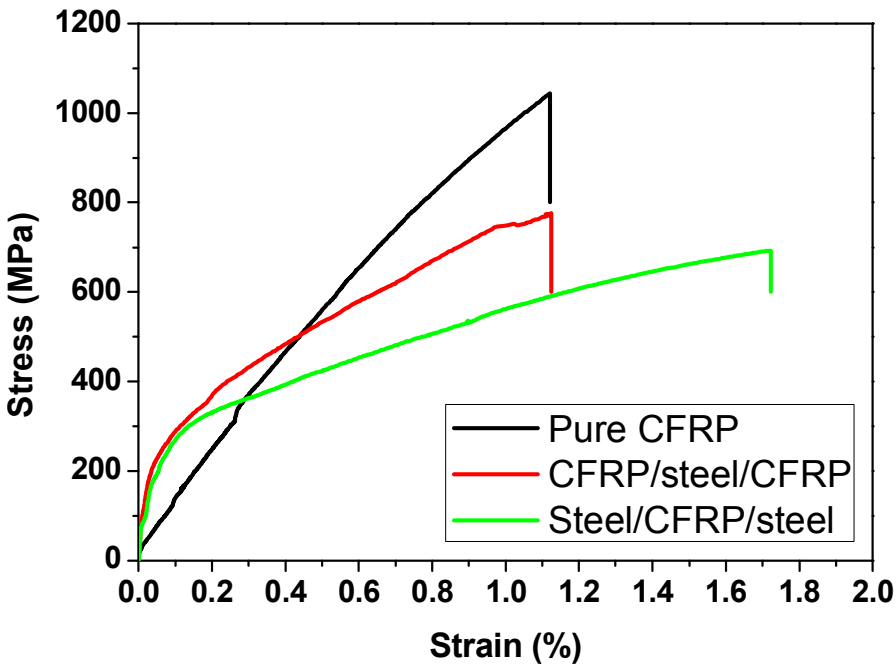

(a)

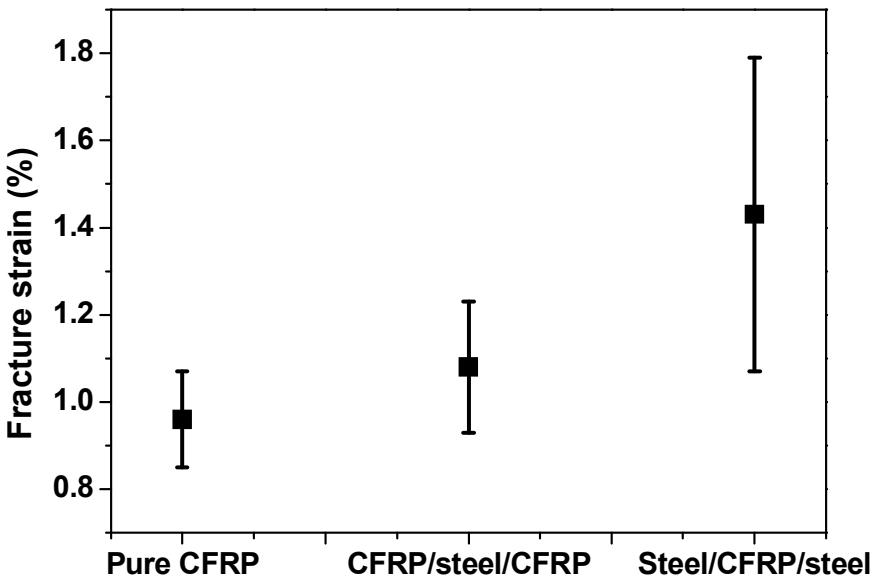

(b)

Figure 2-17 The results of compressive tests. (a) representative graphs and (b) fracture strains of the CFRP within the laminated composites.

A notable feature is that in compressive fracture strain, the CFRP within the laminate composite is larger than pure CFRP. The magnitude of increase in fracture strain increases as the volume fraction of the steel constituting the laminate composite increases. This result is similar to the tensile test result, and it was confirmed that when the steel is attached to CFRP, not only the tensile property but also the compression property of the CFRP can be improved.

Figure 2-18 shows the specimen after compression fracture of pure CFRP and the laminate composites. Compression failure of CFRP is generally known to be caused by microbuckling and kinking. From Figure 2-18 (a), it can be seen that the

compression failure of pure CFRP was broken at a certain angle by kinking. Compressive fracture of the laminate composites, like tensile fracture, is accompanied by separation of the interface. Therefore, improving interfacial properties is considered to be important for improving mechanical properties of the laminate composites.

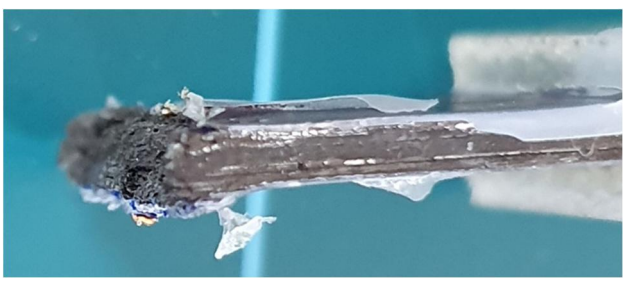

(a)

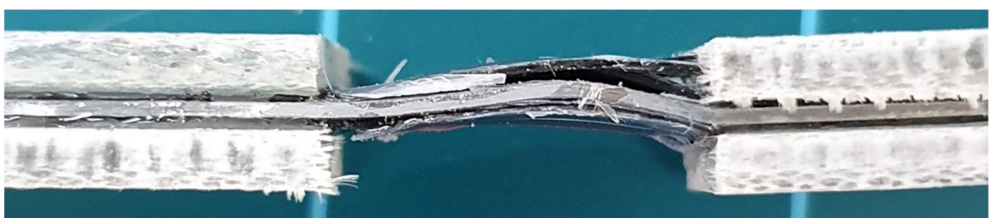

(b)

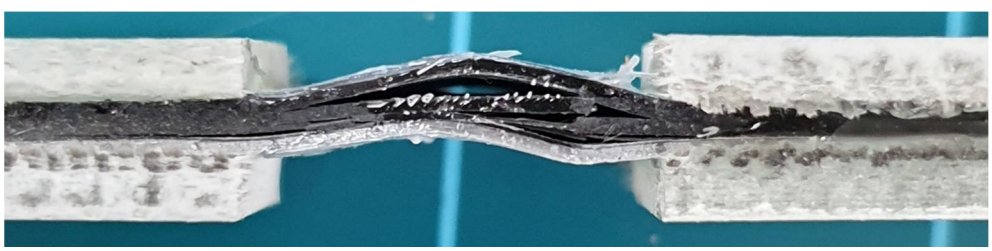

(c)

Figure 2-18 Fracture morphology after compressive test of (a) pure CFRP, (b) CFRP/steel/CFRP, and (c) steel/CFRP/steel specimens.

2.4. Summary

Static and dynamic tensile testing of the CFRP/steel hybrid laminate composites revealed increased (by up to 20%) fracture strain of their CFRP constituent. This became more pronounced with increasing interfacial shear strength between the CFRP and the steel, increased volume fraction of the steel, and a more symmetric layup sequence. These improvements were attributed to the transverse compressive stress that resulted from the high Poisson's ratio of steel; FEA confirmed this mechanism. Micromechanical theory was used to explain the effect of this transverse compressive stress on the mechanical properties of the hybrid laminate composites, and thereby identify the optimal design thereof.

Chapter 3. Micromechanical model of CFRP and steel laminate composites

3.1. Modeling tensile behavior

In this study, the mechanical properties of hybrid laminate composites were predicted by analyzing interactions between CFRP and steel. In Section 3.1.1, the transverse compressive stress occurring in a CFRP during axial deformation of the hybrid laminate composite is analyzed as an interaction between the CFRP and the steel. The effects of this interaction on the longitudinal splitting of the CFRP are discussed. In Section 3.1.2, actual transverse compressive stress is quantitatively calculated using a finite element method. The shear lag theory is then used to calculate the stress distribution around broken fibers inside the CFRP under transverse compressive stress. Based on these calculations, the mechanical properties of the CFRP are predicted in Section 3.1.3 according to a global load sharing model. Finally, the mechanical behavior of the hybrid laminate composite is predicted by considering the thermal residual stresses that occur during its manufacture.

3.1.1. Modeling approach

Consider a CFRP and steel hybrid laminate under iso-strain conditions. Without interfacial bonding between the lamina, each material deforms, extending along the

tensile direction with transverse contraction according to their Poisson's ratios (Figure 3-1 (a)). With interfacial bonding, this situation changes such that the amount of contraction of the two layers is the same. This develops tensile and compressive stresses inside the steel and CFRP layers, respectively, due to the relatively high Poisson's ratio of steel (0.3 and 0.5 for elastic and plastic deformation cases, respectively) compared to that of the CFRP (Figure 3-1 (b)). This compressive stress can affect the fracture behavior of the CFRP.

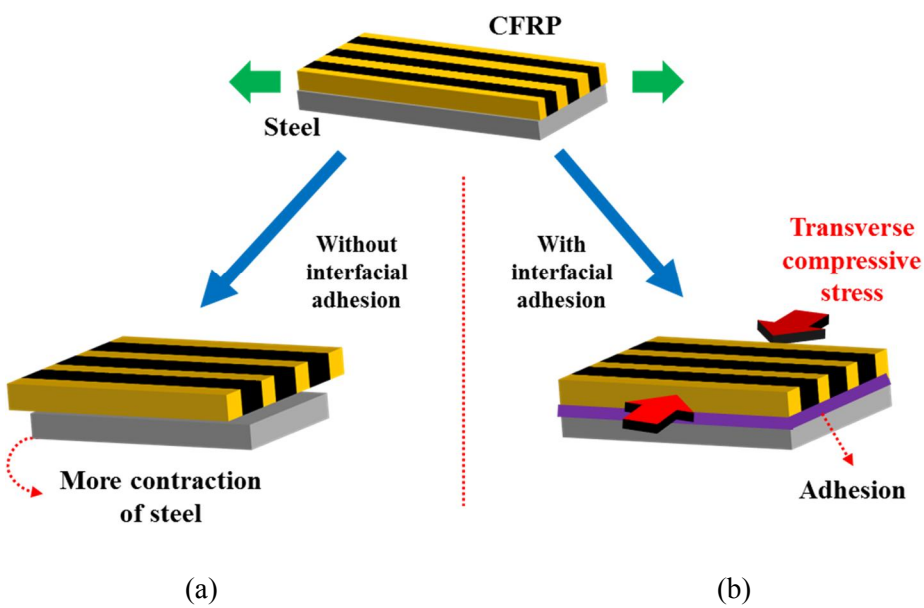

Figure 3-1 The mechanical behavior of CFRP and steel hybrid laminates by axial tensile force: (a) no transverse compressive stress without interfacial bonding and (b) transverse compressive stress in the CFRP layer with interfacial bonding.

Longitudinal splitting is a phenomenon in which the matrix is destroyed by shear stress during CFRP deformation. When a CFRP is partially fractured, i.e., some of the carbon fibers fracture, the matrix can remain bonded to the broken fiber through interfacial interactions. In this way, the matrix localizes the effects of partial fracture of the carbon fiber. However, if the shear stress exceeds the failure stress of the matrix, the matrix is destroyed, resulting in longitudinal splitting. Figure 3-2 shows the fracture behavior of a CFRP [77]. As CFRPs undergo tensile deformation, the first step in material failure is the partial fracture of internal carbon fibers. At this point, the partial fracture is affected only by the strength distribution of the carbon fiber itself. In the second step, stress is redistributed via longitudinal splitting or the occurrence of multiple fractures around the partially broken fibers [78]. Longitudinal splitting can be affected by transverse compressive stress that develops in the CFRP layer. In the third step, isolated, multiple carbon fiber fractures and longitudinal splitting events connect, resulting in final fracture of the CFRP in the fourth step [17, 79]. Thus, transverse compressive stress can influence the fracture behavior of a CFRP. Transverse compressive stress is calculated in the following section to predict the mechanical behavior of CFRP/steel hybrid laminates.

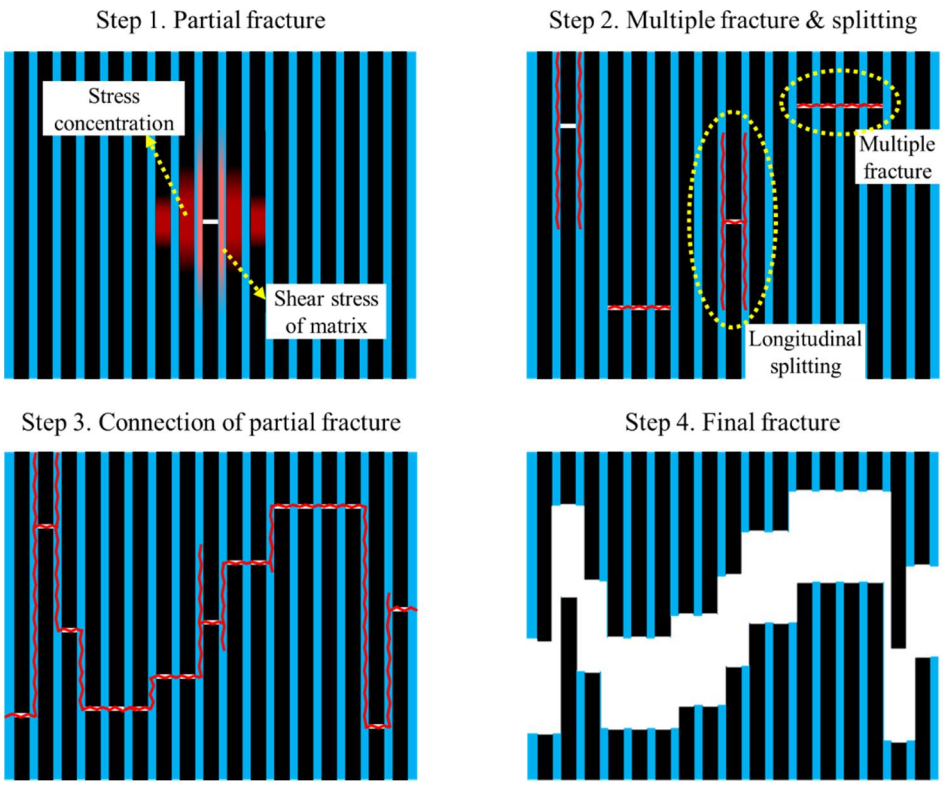

Figure 3-2 The general fracture mechanism of CFRP [77].

3.1.2. Transverse compressive stress in a CFRP layer

Transverse compressive stresses were calculated using a finite element software (ABAQUS, Simulia, USA). The mechanical properties of CFRP and steel lamina, and their lay-up sequence in the hybrid laminate, are listed in Table 3-1. The perfect bonding was assumed at the interface between the CFRP and steel. This assumption was validated in a previous study [80], in which calculations of transverse compressive stress in a system featuring interfacial shear strength of

more than 5 MPa were similar to those of a system featuring perfect bonding.

Table 3-1 Mechanical properties of CFRP and steel lamina.

CFRP		Steel	
E_{11} (GPa)	126	$E_{s,elastic}$ (GPa)	194
E_{22}, E_{33} (GPa)	7.40	$E_{s,hard}$ (GPa)	2.7
G_{12}, G_{13} (GPa)	3.89	$\sigma_{s,y}$ (MPa)	176
G_{23} (GPa)	3.50	$\gamma_{s,f}$ (%)	25

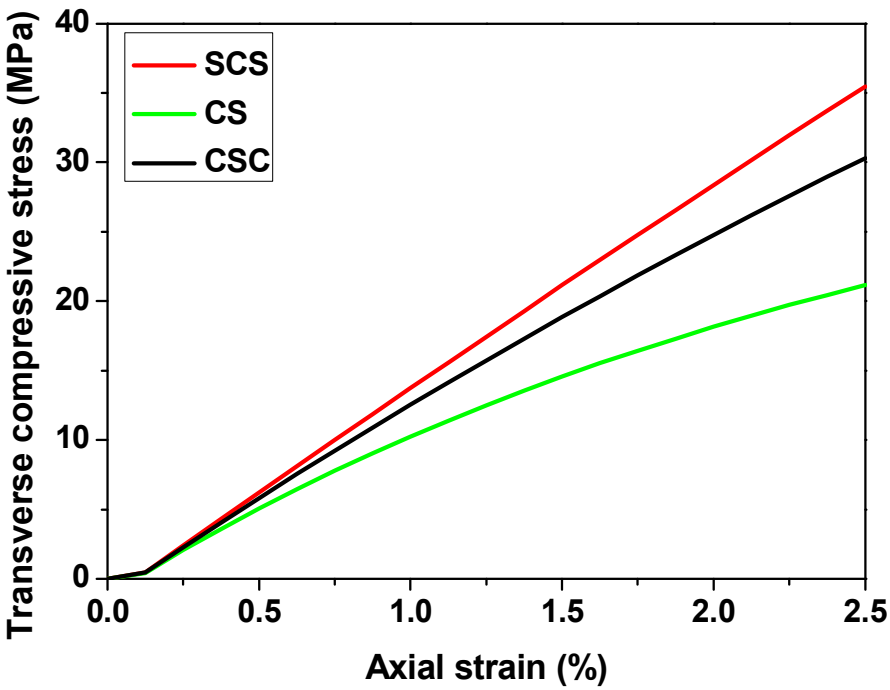

Figure 3-3 The transverse compressive stresses of CFRP layers within CFRP/steel hybrid laminates according to lay-up sequences (SCS: steel/CFRP/steel, CS: CFRP/steel, CSC: CFRP/steel/CFRP)

The calculation results show that the compressive stress increased with axial deformation after the initial yielding of the steel (Figure 3-3). In general, the transverse compressive stress depends on the CFRP volume fraction and the lay-up sequence of the hybrid laminate. Steel/CFRP/steel (SCS) laminate shows the highest transverse compressive stress of CFRP. Since the transverse stresses are caused by the force balance between CFRP and steel, the larger the volume fraction of steel, the greater the transverse compressive stress in CFRP. On the other hand, CFRP/steel (CS) laminate sample shows a lower transverse compressive stress than the CSC sample, although the CS sample has a higher volume fraction of steel than CFRP/steel/CFRP (CSC) laminate. This is due to the lay-up sequence of laminate composites, i.e. the symmetry in the thickness direction. In the asymmetric sample (CS), the transverse bending can partially relieve transverse compressive stress along the material thickness.

To simplify the calculations, a transverse compressive stress at an axial tensile strain of 2% was used as the compressive stress in each sample. It was assumed that the transverse compressive stress of the CFRP was equal to that of the epoxy matrix. With a broken carbon fiber, the surrounding matrix was assumed to experience the shear deformation along the radial direction of the carbon fiber. Therefore, to accurately reflect its effects on matrix deformation, the transverse compressive stress had to be converted to a radial compressive stress, as shown in

Figure 3-4 (a). Radial compressive stress can be calculated by multiplying the transverse compressive stress by 2/π as shown in Figure 3-4 (b).

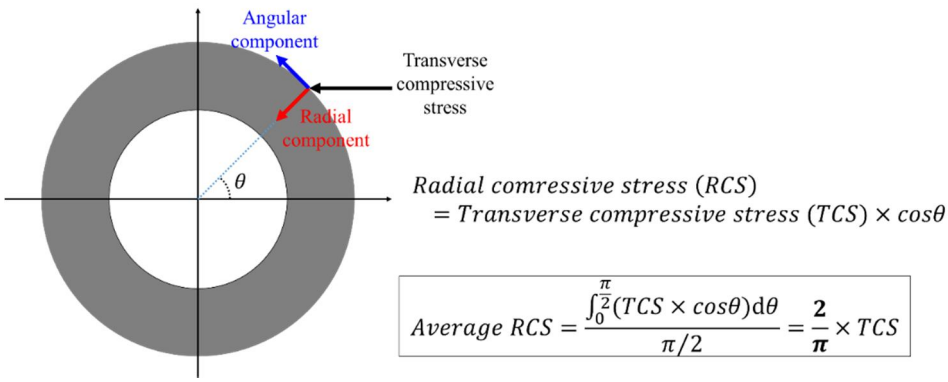

(a)

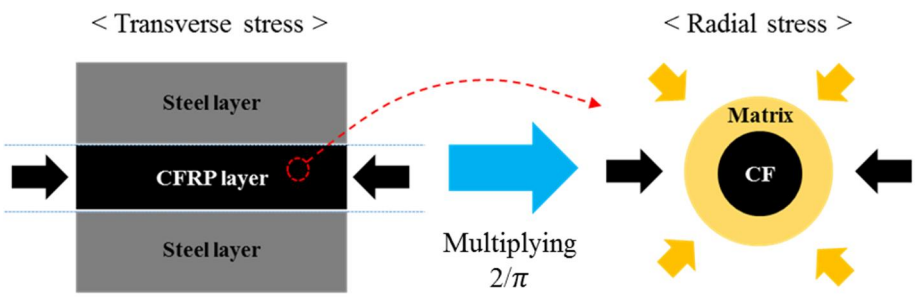

(b)

Figure 3-4 The relationships between (a) transverse and radial compressive stresses and (b) radial compressive stresses of the matrix surrounding a carbon fiber.

3.1.3. Predicting the tensile behavior

The tensile stress of a CFRP/steel hybrid laminate composite can be calculated using the rule of mixtures as follows.

$$\sigma_{hybrid} = V_{CFRP}\sigma_{CFRP} + V_{STEEL}\sigma_{STEEL} \quad (1)$$

where V and σ are the volume fraction and stress of each component in the hybrid laminate. The subscripts 'CFRP' and 'STEEL' represent CFRP and steel lamina, respectively. Here, the stress of the steel lamina was simply obtained from a stress and strain curve obtained via tensile tests. The stress of the CFRP lamina cannot be calculated in such a simple manner because, as explained in Sections 3.1.1 and 3.1.2, the mechanical behavior of a CFRP lamina is influenced by transverse compressive stress induced by the steel lamina. Here, the stress of each CFRP lamina was calculated using the probability of the carbon fiber breaking and the stress distribution around fractured fiber in the presence of the transverse compressive stress, as explained below.

The global load sharing (GLS) model is often used to predict the mechanical properties of CFRPs [81]. This model assumes that stress loss due to the partial fracture of internal carbon fibers affects the overall mechanical behavior of the CFRP lamina. The stress of the CFRP can be calculated by considering the failure probability of the carbon fiber (P_f) and the average stress around broken fiber as follows,

$$\sigma_{CFRP} = V_{CF}\left\{\sigma_{CF,intact}\left(1 - P_f\right) + \sigma_{CF,ineffective}P_f\right\} \quad (2)$$

where V_{CF} is the volume fraction of carbon fiber in the CFRP lamina. The failure probability of the carbon fiber (P_f) is a Weibull distribution [82],

$$P_f(\sigma, 2\delta) = 1 - exp\left\{-\frac{2\delta}{L_0}\left(\frac{\sigma}{\sigma_0}\right)^m\right\} \cong \frac{2\delta}{L_0}\left(\frac{\sigma}{\sigma_0}\right)^m \qquad (3)$$

where δ is the length of the ineffective region, m is the shape parameter, σ_0 is the scale parameter, and L_0 is the reference length. $\sigma_{CF,intact}$ is the stress of the fiber not influenced by the partial fracture and can be calculated as the Young's modulus times the axial strain of the fiber. In contrast, $\sigma_{CF,ineffective}$ is the average stress in the ineffective region, which is the stress recovery zone of the fiber near the failure point due to interfacial shear stress.

To obtain the average stress on fibers in the ineffective region, fiber stress distribution needs to be calculated along the distance from the fracture point. Once the stress distribution is known, up to 90% recovery of fiber stress can be defined as the ineffective region and the average stress of the corresponding region can be calculated. In this study, the shear lag theory [83] was used to calculate stress. Equation (4) shows the relationship between the tensile stress of a fiber and the shear stress of the matrix around the broken fiber,

$$\frac{dF}{dx} - 2r\pi\tau = 0 \qquad (4)$$

where x is the distance from the fracture point along the fiber direction, F is the axial load of the carbon fiber, r is the radius of the carbon fiber, and τ is the shear stress of the matrix. This equation can be also expressed as a function of

displacement (u) as follows,

$$\pi r^2 \frac{d\sigma_{CF}(u(x))}{dx} - 2\pi r\tau\big(u(x)\big) = 0 \qquad (5)$$

where σ_{CF} is the tensile stress of the carbon fiber. To solve Equation (5), it is necessary to know the relationship between the displacement ($u(x)$), the tensile stress of the carbon fiber (σ_{CF}), and the shear stress of the matrix (τ). Since the carbon fiber can be assumed to be elastically deformed, the tensile stress of the carbon fiber is calculated according to the elastic modulus (E) of carbon fiber times the axial strain (ε) of the CFRP as follows.

$$\sigma_{CF}\big(u(x)\big) = E\varepsilon\big(u(x)\big) = E\frac{du(x)}{dx} \qquad (6)$$

In contrast, the shear stress of the matrix should be calculated differently depending on its deformation state, *e.g.*, elastic deformation (Section 3.1.3.1), plastic deformation (Section 3.1.3.2), or fracture (Section 3.1.3.3). For these cases, Equation (4) can be modified as follows.

$$\sigma_{CF}(x) = \frac{2}{r}\int_0^x \tau dx \qquad (7)$$

Note that as x becomes large, σ_{CF} converges to the tensile stress of the intact fiber ($\sigma_{CF,intact}$) as shown below.

$$\sigma_{CF}(\infty) = \frac{2}{r}\int_0^\infty \tau dx = E\varepsilon \qquad (8)$$

Equation (8) is used as the boundary condition for calculating the shear stress distribution of the matrix.

3.1.3.1. Elastic deformation of the matrix

In this case, the matrix around the broken fiber undergoes only elastic deformation under low axial strain of CFRP and its shear stress can be calculated by the shear modulus (G) and the shear strain (γ) as shown in Equation (9),

$$\tau_{low}\big(u(x)\big) = G\gamma\big(u(x)\big) = G\frac{u(x)}{h} \qquad (9)$$

where h is the average distance between the carbon fibers. By substituting Equation (6) and (9) into (5), the differential equation in terms of displacement is obtained and can be solved as

$$\tau_{low}(\varepsilon, x) = \sqrt{\frac{rEG}{2h}}\ \varepsilon\, e^{-\sqrt{\frac{2G}{rEh}}x} \qquad (10)$$

where τ_{low} is the shear stress when the matrix around the broken fiber is elastically deformed. Since τ_{low} cannot exceed the shear yield stress (τ_y) of the matrix, the maximum value of the low axial strain ($\varepsilon_{low,max}$) is given by

$$\varepsilon_{low,max} = \sqrt{\frac{2h}{rEG}}\ \tau_y \qquad (11)$$

3.1.3.2. Inelastic (plastic) deformation of the matrix

In this case, the matrix around the broken fiber undergoes plastic deformation in response to intermediate axial strain of the CFRP and Equation (5) is modified by replacing τ with τ_y as follows

$$\frac{d^2u(x)}{dx^2} - \frac{2}{rE}\tau_y = 0 \qquad (12)$$

The solution of Equation (12) can be calculated as a quadratic equation for the distance from the fracture point (x). To obtain the boundary conditions, it is assumed that the maximum displacement within the elastic deformation zone is equal to the minimum displacement within the inelastic deformation zone. Thus, the displacement (u_{inter}) and shear strain (γ_{inter}) of the matrix undergoing inelastic deformation are given by

$$u_{inter}(x,\varepsilon) = \frac{\tau_y}{rE}(x - a(\varepsilon))^2 + \frac{h\tau_y}{G} \qquad (13)$$

$$\gamma_{inter}(x,\varepsilon) = \frac{\tau_y}{rhE}(x - a(\varepsilon))^2 + \frac{\tau_y}{G} \qquad (14)$$

where $a(\varepsilon)$ is the length of the inelastic deformation zone and is expressed as a function of the axial strain of the CFRP. To obtain $a(\varepsilon)$, the shear stress distribution for the intermediate axial strain case is applied to Equation (8) as follows

$$\frac{2}{r}[\tau_y a(\varepsilon) + \int_{a(\varepsilon)}^{\infty} \tau_{low}\left(\left(x - a(\varepsilon)\right), \varepsilon_{low,max}\right) dx] = E\varepsilon \qquad (15)$$

$$a(\varepsilon) = \frac{r}{2\tau_y}[E\left(\varepsilon - \varepsilon_{low,max}\right)] \qquad (16)$$

$$\gamma_{inter}(x,\varepsilon) = \frac{\tau_y}{rEh}[x - \frac{r}{2\tau_y}\left(E\left(\varepsilon - \varepsilon_{low,max}\right)\right)]^2 + \frac{\tau_y}{G} \qquad (17)$$

Since the shear strain of the matrix cannot exceed the shear fracture strain (γ_f), the maximum value of the intermediate axial strain ($\varepsilon_{inter,max}$) can be obtained as follows

$$\gamma_{inter}(0,\varepsilon) = \frac{\tau_y}{rEh}[\frac{r}{2\tau_y}\left(E\left(\varepsilon - \varepsilon_{low,max}\right)\right)]^2 + \frac{\tau_y}{G} < \gamma_f \qquad (18)$$

$$\varepsilon_{inter,max} = \frac{1}{E}[\sqrt{\frac{2Eh\tau_y}{r}(\gamma_f - \frac{\tau_y}{G})}] + \sqrt{\frac{2h}{rEG}}\,\tau_y \qquad (19)$$

$$\sqrt{\frac{2h}{rEG}}\,\tau_y < \varepsilon_{inter} < \frac{1}{E}[\sqrt{\frac{2Eh\tau_y}{r}(\gamma_f - \frac{\tau_y}{G})}] + \sqrt{\frac{2h}{rEG}}\,\tau_y \qquad (20)$$

The yielding behavior of metallic materials is generally independent of hydrostatic stress [84, 85]. However, since hydrostatic stress affects the yielding behavior of polymeric materials [86], the Mohr-Coulomb yield criterion shown in Figure 3-5 (a) can be used to calculate the mechanical behavior of the polymer

matrix under multiaxial stress [87]. According to this criterion, shear yield strength increases with the compressive stress applied to the polymeric material in the transverse direction. To simplify this calculation, the stress-strain curve of the matrix is assumed to be elastic and exhibit perfectly plastic behavior with increasing yield strength, as shown in Figure 3-5 (b). The parameters of the Mohr-Coulomb yield criterion and the modified shear yield stresses used in this study are given in Table 3-2.

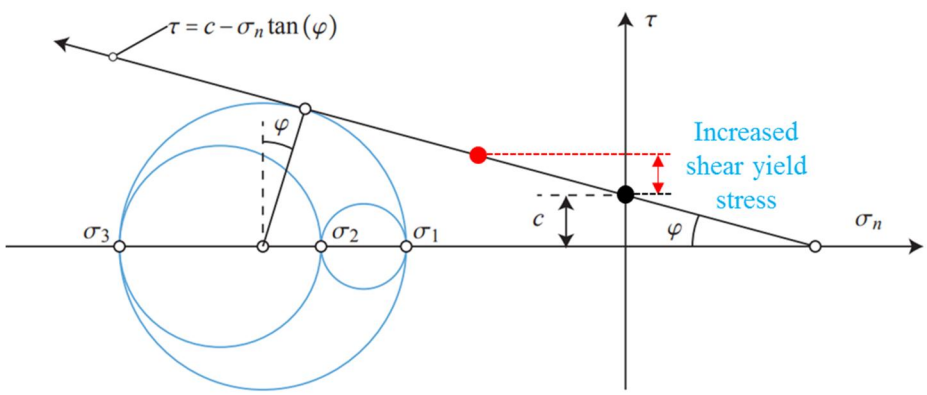

(a)

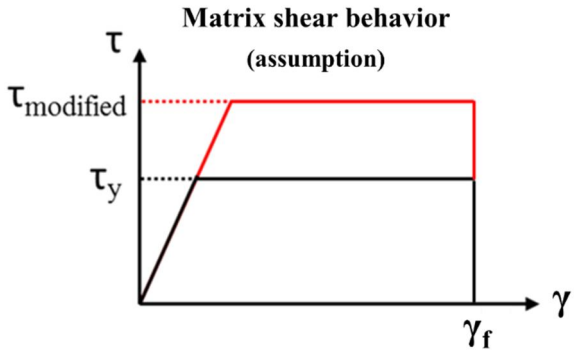

(b)

Figure 3-5 (a) Mohr-Coulomb yield criterion [87] and (b) assumed stress-strain behavior of the polymer matrix.

Table 3-2 Parameters for Mohr-Coulomb yield criterion and modified shear yield stress.

Mohr-Coulomb Parameters [88]		Modified shear yield stress (MPa)			
C	*tan(φ)*	Pure CFRP	CS	CSC	SCS
88.5	1.48	88.5	105.3	111.5	115.2

3.1.3.3. Fracture of the matrix

Under high axial strain of the CFRP, the matrix around the broken fiber is partially fractured. In this fracture zone, the shear stress of the matrix is still maintained by frictional stress and can be increased as the transverse compressive stress increases. In this study, frictional stress is calculated by multiplying the

radial compressive stress ($\sigma_{radial,compressive}$) by the friction coefficient (μ) and then adding the frictional stress in the absence of the normal stress ($\tau_{friction,0}$) as follows

$$\tau_{friction} = \tau_{friction,0} + \mu\sigma_{radial,compressive} \qquad (21)$$

where $\tau_{friction,0}$ and μ are assumed to be 10 MPa [88] and 0.5, respectively. The length of the fracture zone ($b(\varepsilon)$) can be calculated using the same method as in Section 3.1.3.2 as follows

$$b(\varepsilon) = \frac{r}{2\tau_{friction}}[E(\varepsilon - \varepsilon_{inter,max})] \qquad (22)$$

Now, the shear stress distribution of the matrix around the broken fiber can be obtained for a given axial strain of the CFRP. When the axial strain is smaller than $\varepsilon_{low,max}$, only the elastic behavior of the matrix needs to be considered. If the axial strain is larger than $\varepsilon_{inter,max}$, then the elastic, inelastic, and friction behaviors of the matrix also need to be taken into account. In particular, the effects of transverse compressive stress on the yield stress and friction stress of the matrix should be considered when the matrix exhibits both inelastic and friction behaviors. The shear stress distribution of the matrix is used to obtain the tensile stress distribution of the carbon fiber in Equation (7). The length of the ineffective region is defined as the length from the fiber fracture point to the region that exhibits 90% of the

intact fiber stress and can be calculated from the tensile stress distribution. Finally, the average stress in the ineffective region ($\sigma_{CF,ineffective}$) can be obtained from the tensile stress distribution of the carbon fibers. The average stress in the ineffective region can be used in Equation (2) to calculate the stress of the CFRP with a given axial strain.

3.1.4. Residual stress of the laminate composites

Thermal residual stresses are generated during the manufacture of hybrid laminate composites and can affect their deformation behavior. These stresses are caused by the differential coefficients of thermal expansion (CTEs) of steel ($10 \times 10^{-6}\,K^{-1}$) and the CFRP (approximately zero). In this study, the CFRP prepregs were bonded to steel at 160°C and cured. The layered CFRP and steel composite was then cooled to room temperature, inducing differential thermal shrinkage. Note that differences in thermal expansion mean that the steel layers shrink more than the CFRP layers. Consequently, the CFRP and steel are subjected to thermally residual compressive and tensile stresses along the fiber direction, respectively, due to the force equilibrium. The axial residual stress of each material is then calculated as follows

$$\sigma_{residual,CFRP} = \frac{E_s V_s + E_c V_c}{\left(V_c + V_s \frac{E_s}{E_c} \frac{(\alpha_c \Delta T + 1)}{(\alpha_s \Delta T + 1)}\right)} - E_c \tag{23}$$

$$\sigma_{residual,STEEL} = \frac{E_s V_s + E_c V_c}{\left(V_s + V_c \frac{E_c}{E_s} \frac{(\alpha_s \Delta T + 1)}{(\alpha_c \Delta T + 1)}\right)} - E_s \tag{24}$$

where $\sigma_{residual,CFRP}$ and $\sigma_{residual,STEEL}$ represent the residual stresses of CFRP and steel, respectively. E, V, and α are the Young's modulus, volume fraction, and CTE, respectively, of each material in the hybrid laminate composite. Note that the subscripts 'C' and 'S' represent CFRP and steel lamina, respectively, and ΔT is the temperature difference between the fabrication temperature and room temperature. Finally, Equation (1) is modified to include these thermal residual stresses.

$$\sigma_{hybrid} = V_{CFRP}\left(\sigma_{CFRP} + \sigma_{residual,CFRP}\right) + V_{STEEL}\left(\sigma_{STEEL} + \sigma_{residual,STEEL}\right) \quad (25)$$

3.2. Validation examples

3.2.1. Calculation procedure

The calculation procedure for predicting the mechanical properties of hybrid laminate composites is described step-by-step in Figure 3-6. First, the transverse compressive stress is calculated using FEM software (Section 3.1.2). This transverse compressive stress is used to calculate the modified yield stress (Section 3.1.3.2) and the frictional stress (Section 3.1.3.3) of the matrix in the vicinity of broken fibers. Then, Equation (7) and the shear stress distribution of the matrix are used to calculate the tensile stress distribution of the carbon fiber near the fracture point. The tensile stress distribution of the carbon fiber contains information on the ineffective region and the average stress in the region. The fracture probability of the carbon fiber in the ineffective region can then be calculated using Equation (3) and the Weibull parameters of the carbon fiber. Equation (2) can be used to calculate the tensile stress of the CFRP. Finally, the tensile stress of the hybrid laminate composite is calculated using Equation (25), considering the thermal residual stress that occurs during fabrication. A stress-strain curve can be obtained by repeating the calculations for each axial strain in the hybrid laminate composite. The CFRP is assumed to be fractured when the stress loss due to internal fiber breakage exceeds 5% of the total stress.

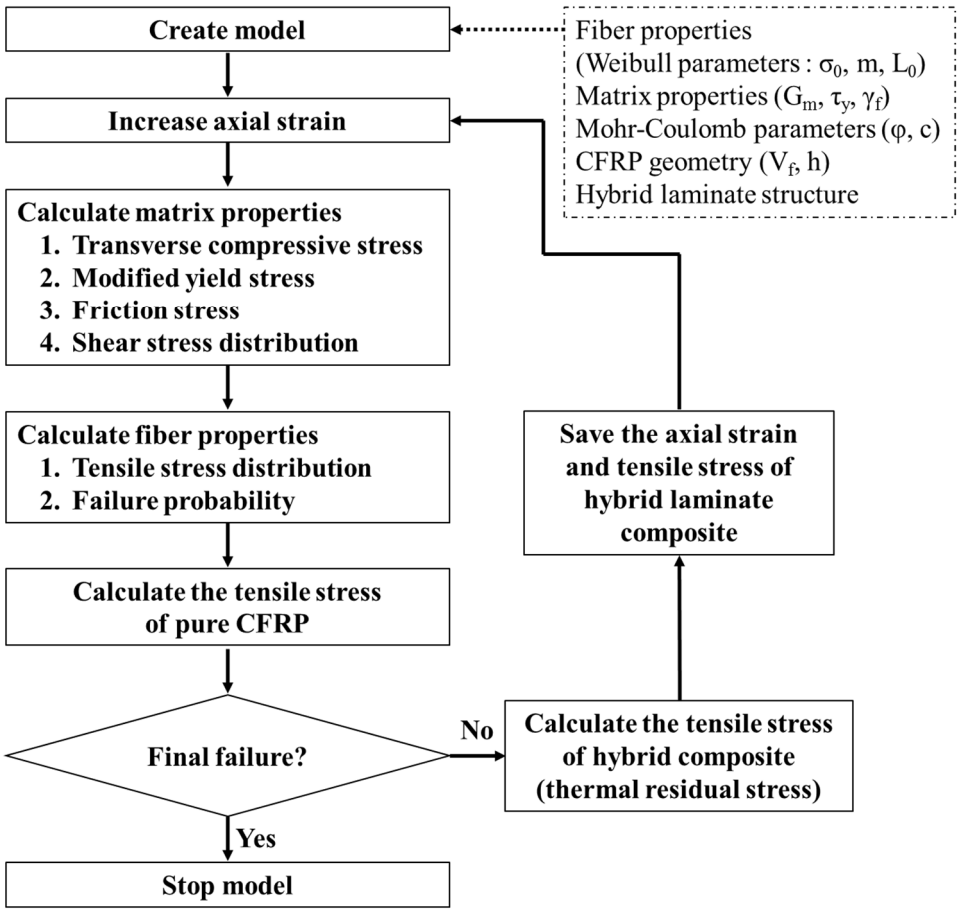

Figure 3-6 The calculation procedure for predicting the mechanical properties of hybrid laminate composites.

3.2.2. Effect of matrix properties on stress distribution

Figure 3-7 shows the stress distribution of the ineffective region near the broken fibers as a function of the yield stress of the matrix. Note that the axial strain of pure CFRP is 1.8%. Here, the fracture strain and the frictional stress of the matrix were assumed to be 25% and 10 MPa, respectively. At high axial strain, the data in Figure 3-7 (a) show that the shear stress distribution of the matrix was divided into

three zones: elastic deformation, inelastic deformation, and fracture. Note that the shear stress in the inelastic deformation zone corresponds to the yield stress of the matrix. The effects of yield stress on the Mohr-Coulomb criterion regarding stress distribution around fractured fibers in the CFRP were investigated with a transverse compressive stress in the matrix. When the yield stress is 110 MPa (red line), the fracture zone (debonded region) is relatively narrow (70 μm), while a yield stress of 70 MPa (black line) results in a relatively wide fracture zone (220 μm). This is because, according to Equation (7), the value obtained by integrating the shear stress with respect to the distance from the broken fiber should be the same when the axial strain of the CFRP is the same. Therefore, higher yield stresses within the inelastic deformation zone result in narrower fracture zones while lower yield stresses result in wider fracture zones. Figure 3-7 (b) shows the tensile stress distribution of carbon fibers around broken fibers calculated by Equation (7). At the fracture point, the tensile stress of a carbon fiber is zero. As the distance from the fracture point increases, the tensile stress increases due to the shear stress of the surrounding matrix, converging to the stress of an intact fiber. The lengths of the ineffective region are 285, 212, and 135 μm when the yield stresses of the matrix are 70, 88.5, and 110 MPa, respectively. The length of the ineffective region decreases with increasing yield stress of the matrix, implying that the effects of carbon fiber fracture are limited to small areas. As the length of the ineffective region decreases, the fracture probability for carbon fibers decreases according to Equation (3) and the average stress on carbon fibers in the ineffective region

increases, resulting in an increase in the tensile stress of pure CFRP, as indicated by Equation (2). Therefore, the mechanical properties of the CFRP can be improved by increasing the yield stress of the matrix.

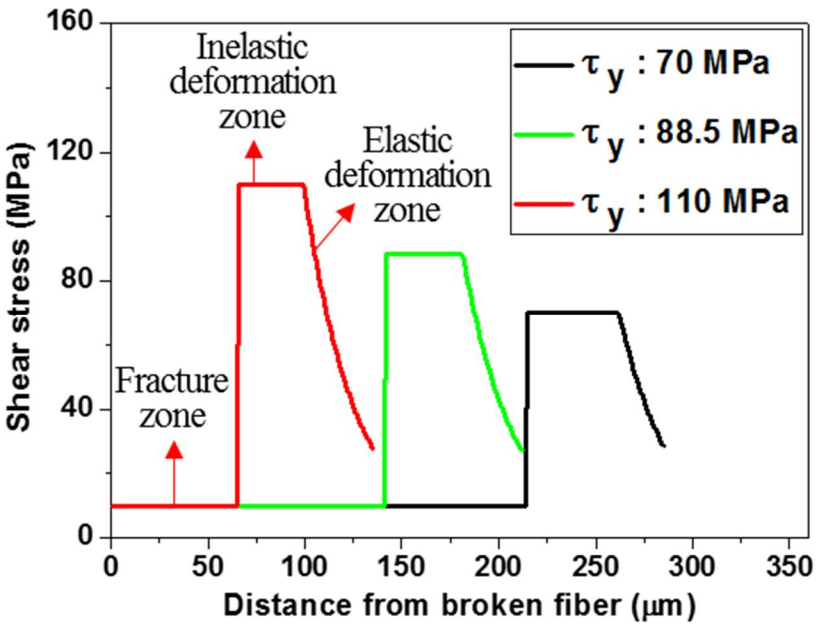

(a)

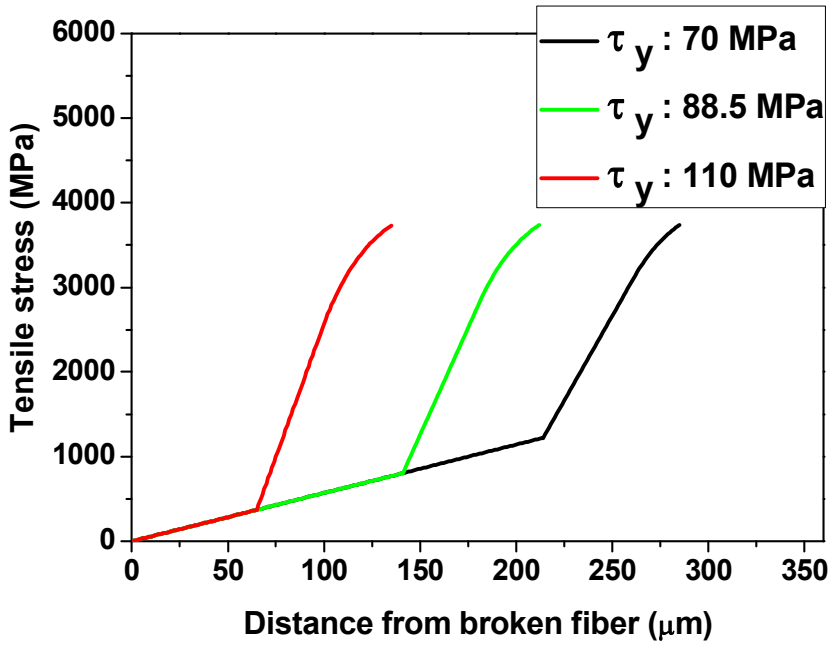

(b)

Figure 3-7 The effects of the shear yield stress of the matrix in the ineffective region on the (a) shear stress distribution of the matrix and (b) tensile stress distribution of carbon fibers.

The effects of matrix failure strain on the mechanical properties of CFRP were investigated using the predictive model. Figure 3-8 shows the stress distribution around the fracture point as a function of the fracture strain of the matrix. Here, the yield stress and the frictional stress of the matrix were assumed to be 88.5 and 10 MPa, respectively. Figure 3-8 (a) shows that the inelastic deformation zone was 26, 40, and 50 μm when the fracture strain of the matrix was 15, 25, and 35%, respectively. Figure 3-8 (b) shows the tensile stress distribution of the carbon fiber around the fracture point. When the fracture strain of the polymer matrix increases

from 15% to 25% and 35%, the lengths of the ineffective regions are reduced from 319 μm to 212 and 133 μm, respectively. Thus, the length of the fracture zone decreases as the fracture strain of the matrix increases, thereby decreasing the length of the ineffective region and increasing the tensile stress of pure CFRP according to Equations (2) and (3).

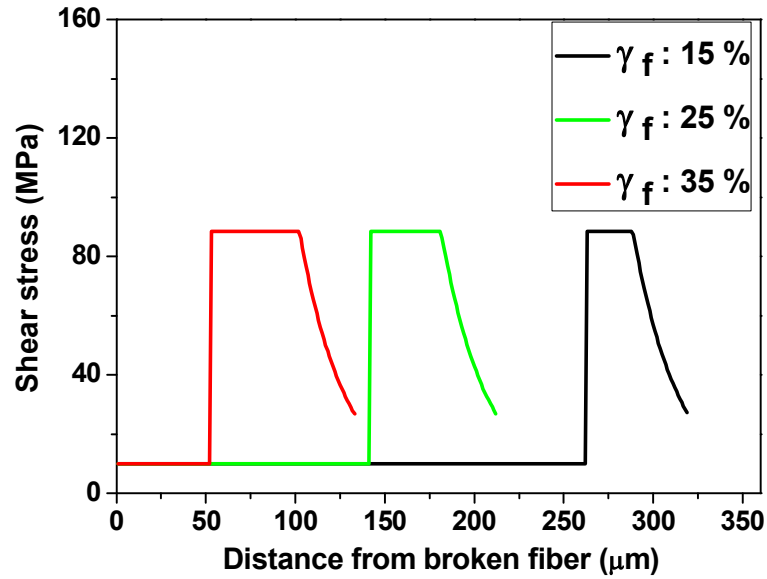

(a)

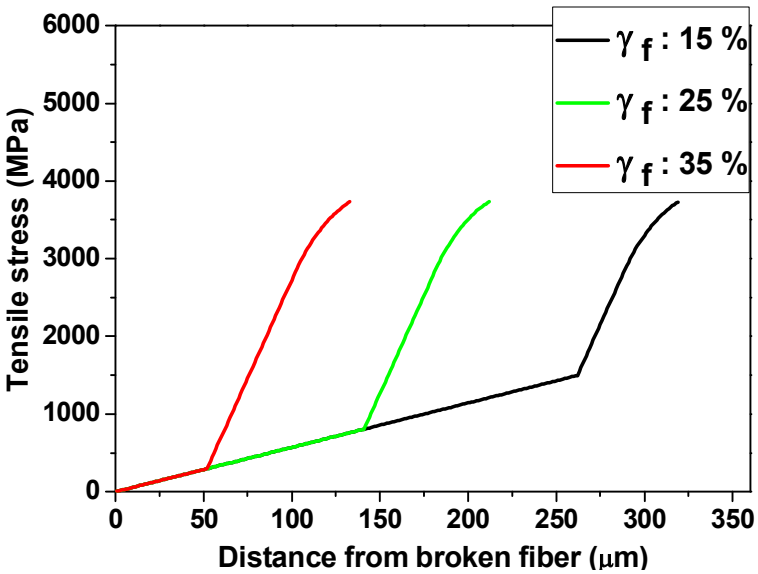

(b)

Figure 3-8 The effects of the shear fracture strain of the matrix in the ineffective region on the (a) shear stress distribution of the matrix and (b) tensile stress distribution of carbon fibers.

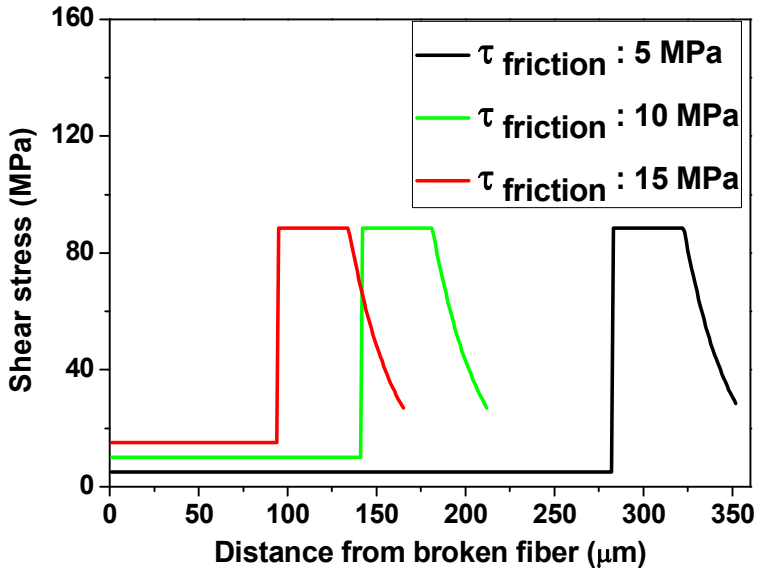

(a)

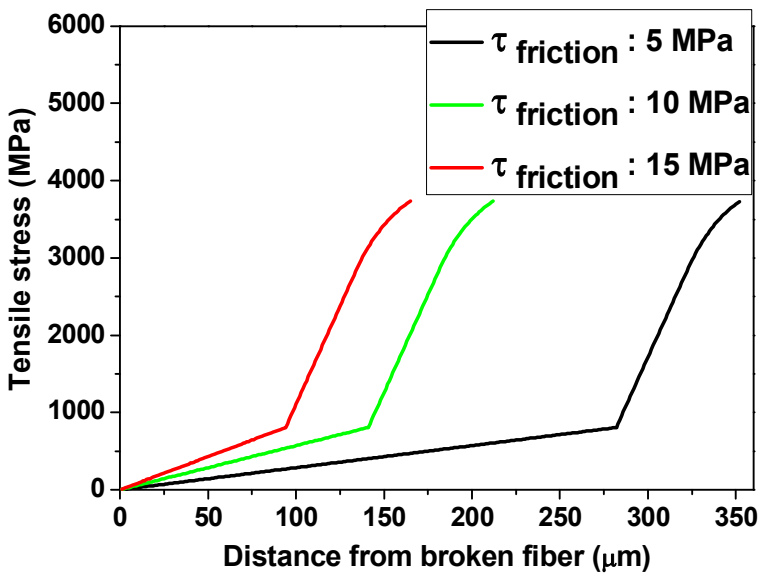

(b)

Figure 3-9 The effects of the frictional stress of the matrix in the ineffective region on the (a) shear stress distribution of the matrix and (b) tensile stress distribution of carbon fibers.

In addition to the inherent mechanical properties of the matrix, frictional forces play an important role in the stress distribution around a fractured fiber [20]. This was investigated using the predictive model developed herein. Figure 3-9 shows the stress distribution around the fracture point as the frictional stress of the matrix increases. Here, the yield stress and the fracture strain of the matrix were assumed to be 88.5 MPa and 25%, respectively. The frictional stress increases as the normal stress acting along the vertical direction of the friction surface increases. In Figure 3-9 (a), only the fracture zone is affected by changes in the frictional stress of the matrix, and there are no changes in the stress distributions in other zones. The frictional stress of the polymer matrix was inversely proportional to the length of the fracture zone. When the former was changed from 5 MPa to 10 MPa and 15 MPa, the latter changed from 282 μm to 141 μm and 94 μm, respectively. As mentioned above, according to Equation (7), the value obtained by integrating the shear stress with respect to the distance from broken fibers should be the same when the axial strain of the CFRP is the same. Therefore, when a high stress is applied within the fracture zone, the length of the fracture zone narrows. Figure 3-9 (b) shows the tensile stress distribution of carbon fibers around the fracture point. The frictional stress of the polymer matrix determines the recovery length of tensile stress for a broken carbon fiber. The initial stress recovery slope of the graph in Figure 3-9 (b) is larger when a frictional stress of 15 MPa (red line) is applied compared to when a 5 MPa stress is applied (black line). This implies that the carbon fiber can recover the stress over a shorter distance from the break point.

When the frictional stresses of the matrix were 5, 10, and 15 MPa, the lengths of the ineffective region were 352, 212, and 165 μm, respectively. Thus, the effects of partial fiber fracture within the CFRP are reduced as the frictional stress of the matrix increases, thereby enhancing the mechanical properties of the laminate composite.

There have been few studies that aimed to improve the frictional stress of the matrix directly to improve the mechanical properties of a CFRP. Instead, the effects of frictional stress on the mechanical properties of FRPs have been indirectly considered when fillers are added to the matrix [89]. The addition of CNTs to a polymer matrix increases both the mode II fracture initiation energy and the crack propagation energy [90, 91]. The CNT acts as a filler to increase the fracture strength of the matrix and also improves the frictional stress after fracture. Similarly, the transverse compressive stress in this study is regarded as a normal stress that can enhance the frictional stress and thereby improve the mechanical properties of the CFRP. In a CFRP composite, the polymer matrix serves to localize the effects of partial fiber fracture. The matrix helps to accommodate the strain energy of the CFRP. As the yield stress and fracture strain of the matrix increase, the length of the ineffective region near the fracture fiber decreases, strengthening the CFRP. When a CFRP lamina is hybridized with steel, the transverse compressive stress in the CFRP improves the yield stress of the matrix. In addition, even after the matrix is fractured, the friction stress of the matrix, which is enhanced by transverse compressive stress, helps to improve the properties of the

CFRP by reducing the length of the ineffective region.

3.2.3. Effect of carbon fiber properties

The mechanical strength of brittle materials such as carbon fiber is determined by the size and number of defects in the material. Unlike ductile materials, the strength of a brittle material can be described by a Weibull distribution (see Equation (3)) where the scale parameter, σ_0,, is related to the average strength and the shape parameter, m, represents the degree of dispersion. Large values of m correspond to small standard deviations in strength. The reference length (L_0) of the Weibull distribution is the gauge length used to determine the shape and scale parameters and was assumed to be 5 mm in this study.

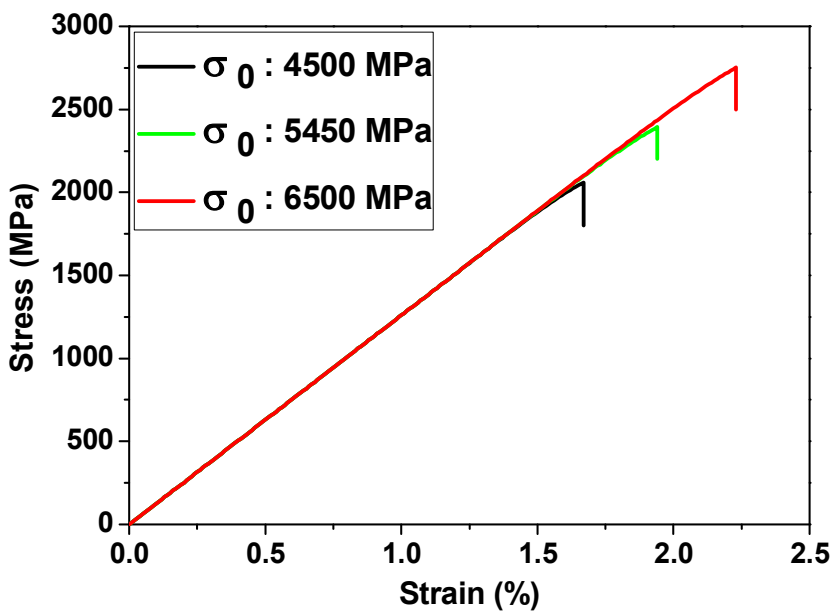

(a)

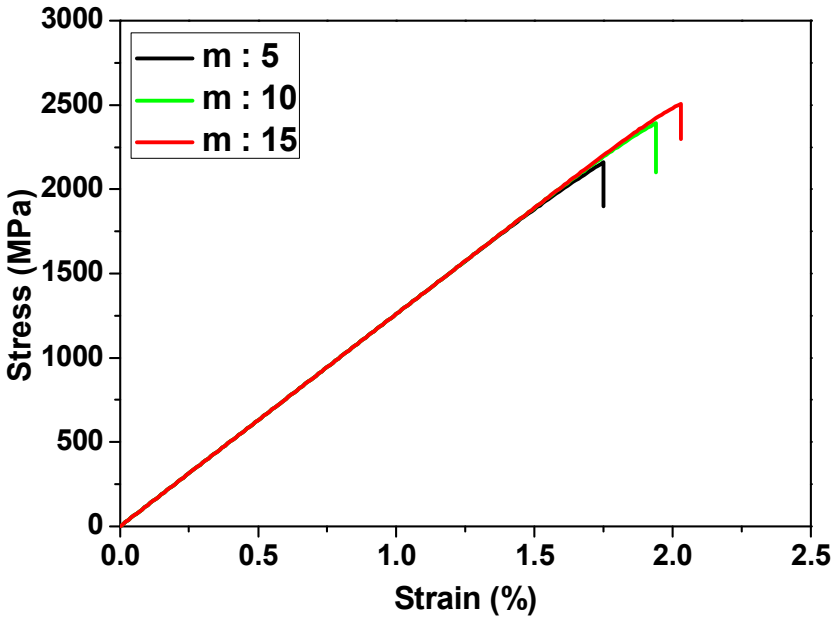

(b)

Figure 3-10 The mechanical behaviors of CFRPs as functions of (a) the scale parameter and (b) the shape parameter of a Weibull distribution of carbon fibers.

Figure 3-10 (a) shows stress-strain curves of pure CFRP according to the scale parameters of the carbon fibers. The shape parameter of the carbon fiber was assumed to be 10 and the yield stress, fracture strain, and frictional stress of the matrix were assumed to be 88.5 MPa, 25%, and 10 MPa, respectively. As the scale parameter of the carbon fiber was increased from 4,500 to 5,450 and 6,500 MPa, the tensile strength of the corresponding CFRPs increased from 2,061 to 2,394 and 2,752 MPa, respectively. CFRPs made with carbon fibers boasting large scale parameters exhibited better mechanical properties. This result indicates that the

effects of the scale parameter on the mechanical properties of a CFRP are more influential than the properties of the matrix material (see Section 3.2.2). As a result, the most important factor in determining the mechanical strength of a CFRP is the strength of the carbon fiber itself. Therefore, using high-quality carbon fiber is the easiest way to improve the mechanical properties of a CFRP. However, the high cost of quality carbon fibers often limits their widespread use. Note that, in the current study, the tensile strength of a CFRP increased by 16% and 34% as the scale parameter increased by 21% and 44%, respectively. Increases in the mechanical properties of the carbon fiber were not proportional to the mechanical properties of the CFRP. This was due to the matrix properties used for these calculations. As demonstrated Section 3.1.3, the mechanical properties of a CFRP depend strongly on the length of the ineffective region and the average stress in regions near partially broken fibers. Therefore, the strength of the carbon fiber itself should be considered together with the mechanical properties of the polymer matrix when trying to improve the mechanical properties of CFRP.

The effects of the shape parameter of carbon fibers on the stress-strain curve of pure CFRP are shown in Figure 3-10 (b). Here, the scale parameter of the carbon fiber was assumed to be 5,450 MPa, and the yield stress, fracture strain, and frictional stress of the matrix were assumed to be 88.5 MPa, 25%, and 10 MPa, respectively. When the shape parameter was increased from 5 to 10 and 15, the maximum stresses of the CFRP increased from 2,160 to 2,394 and 2,506 MPa, respectively. As discussed above, larger shape parameters correspond to narrower

fiber strength distributions. Even if a CFRP is made with carbon fibers having the same average strength, a large standard deviation in strength can result in a high number of partially broken carbon fibers at a particular axial strain. The mechanical properties of a CFRP are generally determined by its weakest components. Therefore, a small standard deviation in strength is considered advantageous.

3.2.4. Prediction of the tensile behavior of the laminate composites

In this study, the mechanical properties of a CFRP were obtained from tensile tests on a single layer of pure CFRP. The scale parameter, shape parameter, and reference length of carbon fibers in the CFRP were assumed to be 5,450 MPa, 10, and 5 mm, respectively [26, 92]. The tensile strength of the carbon fiber used in this study was 4,100 MPa [50], which is between the tensile strengths of T300 (3,500 MPa, Toray, Japan) and T700 (4,900 MPa, Toray, Japan) [51, 52]. The yield stress and frictional stress of the matrix were assumed to be 88.5 MPa and 10 MPa, respectively [88]. The fracture strain of the matrix was assumed to be 25%, which was also estimated from the mechanical behavior of the CFRP. Using these parameters, the mechanical behavior of our CFRP/steel hybrid laminate composites was predicted as described below.

Figure 3-11 shows the shear stress distribution of the matrix according to the axial strain of the CFRP in hybrid laminate composites. With a small axial strain (0.2%), the matrix polymer was subjected to elastic deformation, and there were no

differences in stress distribution as a function of the hybrid structure (Figure 3-11 (a)). The shear stress distribution changed with an intermediate axial strain (1%). In this case, some of the matrix polymer exceeded its yield stress and underwent plastic deformation (Figure 3-11 (b)). The modified yield stress of the polymer matrix was the largest (115.2 MPa) with a steel/CFRP/steel (SCS) sample and the length of the inelastic deformation zone was the narrowest. Figure 3-11 (c) shows the shear stress distribution of the matrix for a large axial strain (2%). This strain resulted in frictional stresses by fracturing the polymer matrix. Considering the frictional stress of pure CFRP (10 MPa), the calculated frictional stresses of CS, CSC, and SCS samples according to Equation (21) were 15.7, 17.8, and 19.0 MPa, respectively. Figure 3-12 shows the tensile stress distribution of carbon fibers near the fracture point, which was calculated using the results of Figure 3-11 and Equation (7). With an axial strain of 2%, the lengths of ineffective regions of SCS, CSC, CS, and pure CFRP samples were 176, 190, 214, and 391 μm, respectively. As the transverse compressive stress occurring in the CFRP increased, the ineffective region became shorter. The average stresses in the ineffective regions of SCS, CSC, CS, and pure CFRP samples were 1,304, 1,294, 1,242, and 1,169 MPa, respectively.

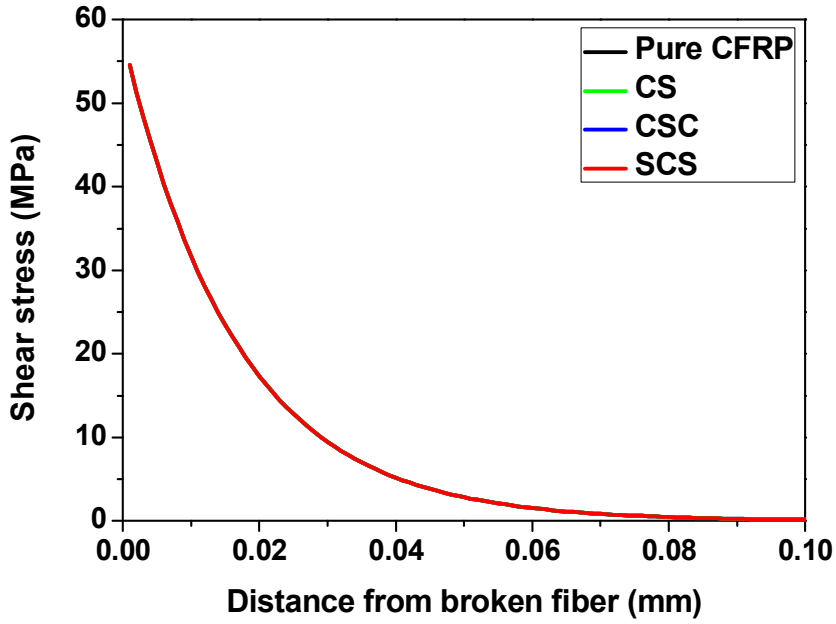
Pure CFRP
CS
CSC
SCS
Shear stress (MPa)
Distance from broken fiber (mm)
0
10
20
30
40
50
60
0.00
0.02
0.04
0.06
0.08
0.10

(a)

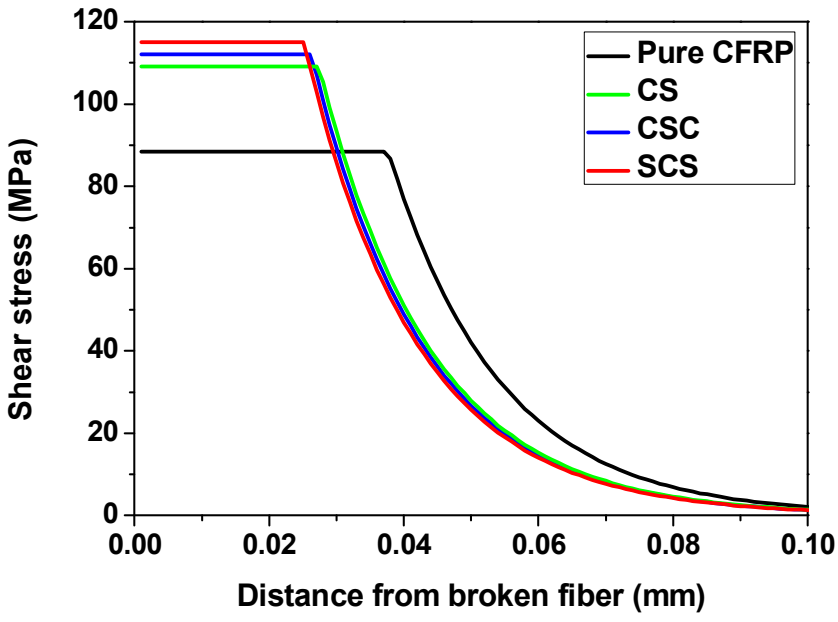
Pure CFRP
CS
CSC
SCS
Shear stress (MPa)
Distance from broken fiber (mm)
0
20
40
60
80
100
120
0.00
0.02
0.04
0.06
0.08
0.10

(b)

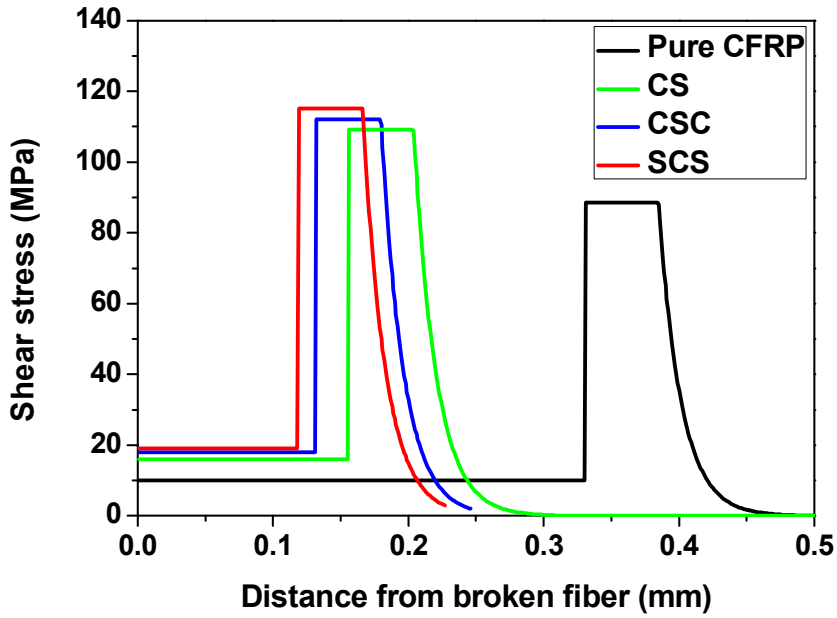

(c)

Figure 3-11 Shear stress distributions within the matrix of CFRPs within various hybrid laminate composites for axial strains of (a) 0.2%, (b) 1%, and (c) 2%.

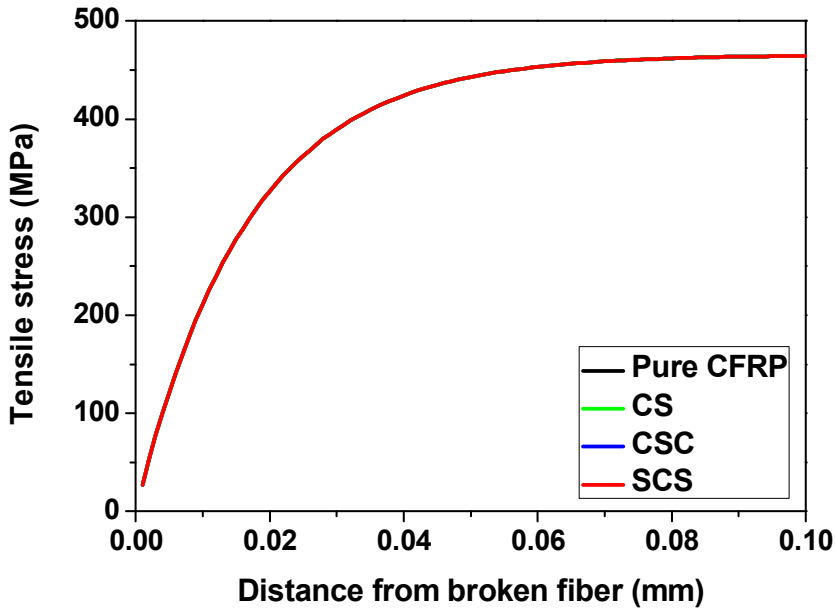
Tensile stress (MPa)
500
400
300
200
100
0
0.00
0.02
0.04
0.06
0.08
0.10
Distance from broken fiber (mm)
Pure CFRP
CS
CSC
SCS

(a)

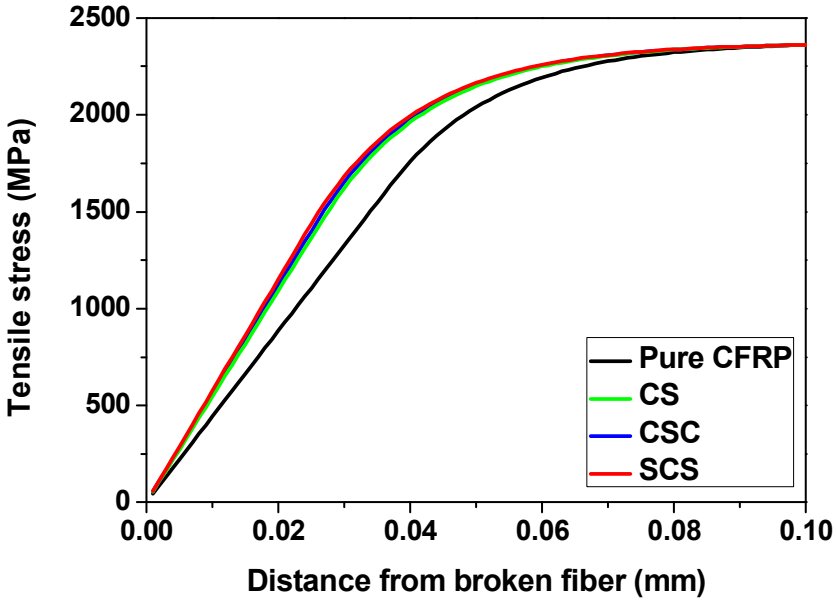
Tensile stress (MPa)
2500
2000
1500
1000
500
0
0.00
0.02
0.04
0.06
0.08
0.10
Distance from broken fiber (mm)
Pure CFRP
CS
CSC
SCS

(b)

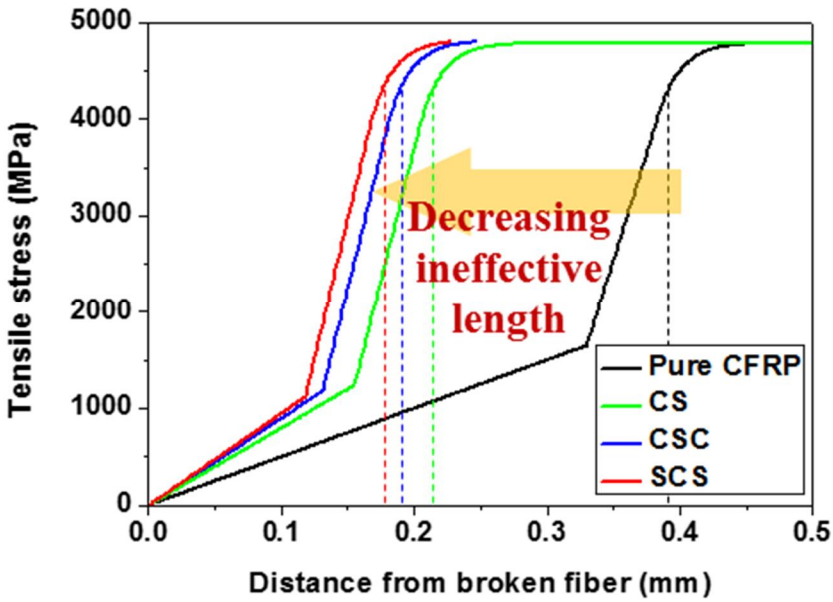

(c)

Figure 3-12 The tensile stress distributions of carbon fibers as a function of the structure of the hybrid composite for axial strains of (a) 0.2%, (b) 1%, and (c) 2%.

The predicted tensile behavior of the hybrid laminate composites is compared with experimental data in Figure 3-13. The predicted stress-strain curves accurately describe the dependence of the hybrid structure on the mechanical properties. Figure 3-13 (b) compares the fracture strains of various hybrid laminate composites. Note that fracture strain increased due to the increased breaking strain of the CFRP inside the hybrid laminate composites. This was ultimately due to transverse compressive stress induced by the steel. Considering the deviation in experimental results, we conclude that the current modeling approach is valid for predicting the tensile behaviors of hybrid laminate composites.

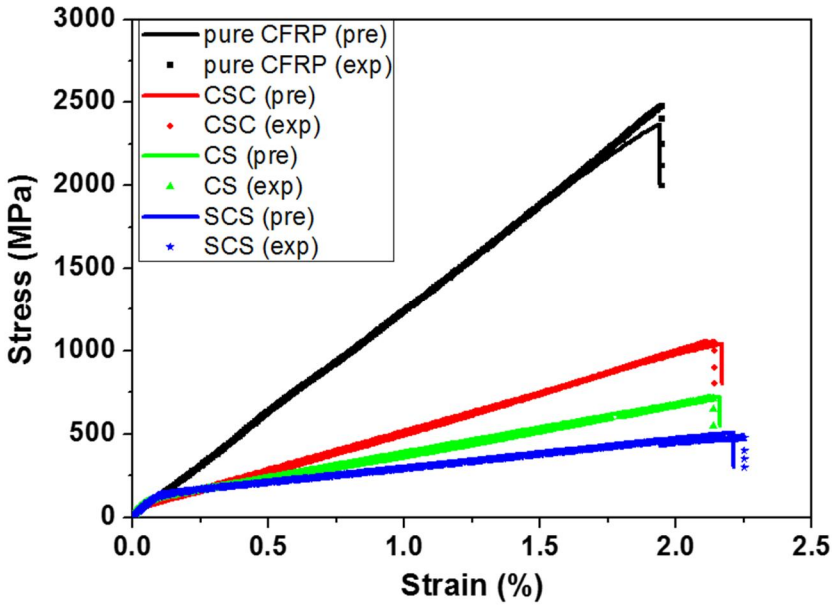

(a)

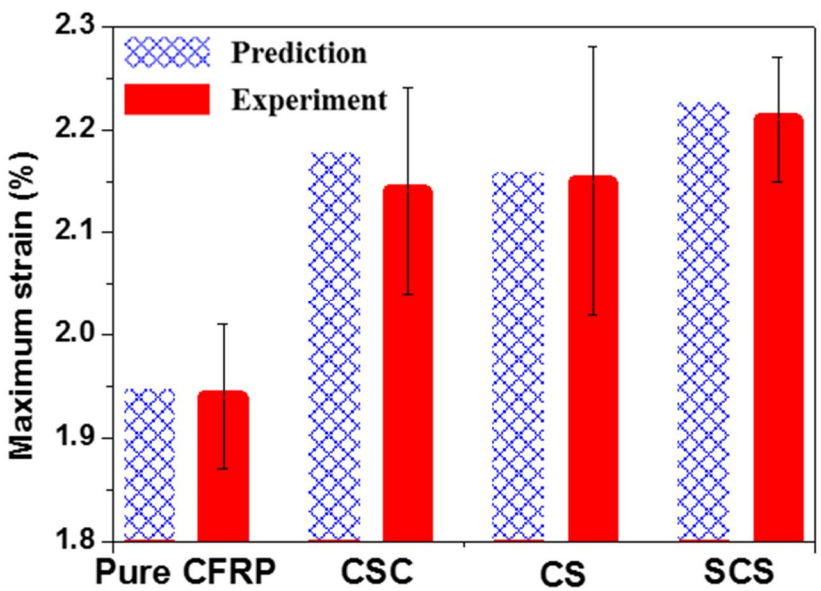

(b)

Figure 3-13 The predicted tensile behaviors of hybrid composites are compared with experimental results: (a) stress and strain curves and (b) breaking strain.

3.3. Analysis of compressive behavior

While the tensile properties of CFRP are influenced by the Weibull distribution of carbon fiber or the length of the ineffective region around the partially fractured fiber, the compression properties of CFRP are known to be most affected by longitudinal shear modulus [93]. When compressive deformation of CFRP occurs, microbuckling occurs in the inner fibers, resulting in local orientation. In the presence of local orientation, kinking of CFRP occurs due to compressive deformation, resulting in compressive failure of CFRP [94]. In order for kinking to occur, longitudinal shear strain must occur in the matrix, so it is known that the larger the shear modulus, the greater the compressive strength. Budiansky [95] proposed the following equation to predict the compressive strength (X_c).

$$X_c = \frac{G}{1+\Phi/\gamma_y} \quad (26)$$

Where G is longitudinal shear modulus, Φ is local orientation, and γ_y is CFRP longitudinal shear yield strain. According to this equation, the compressive strength of CFRP increases as the shear modulus or shear yield strain increases and the local orientation decreases.

In order to analyze the results obtained through the compressive test, it is necessary to analyze the transverse stress generated during axial compression. For this purpose, the transverse stress due to axial compression of laminate composites was calculated using the FEM software. From Figure 3-14, it can be seen that the

transverse tensile stress generated in CFRP occurs as the compressive strain increases. This is because the transverse expansion of steel is greater than that of CFRP when the compressive strain exceeds the yield strain of the steel, and this is the opposite of the axial tension case.

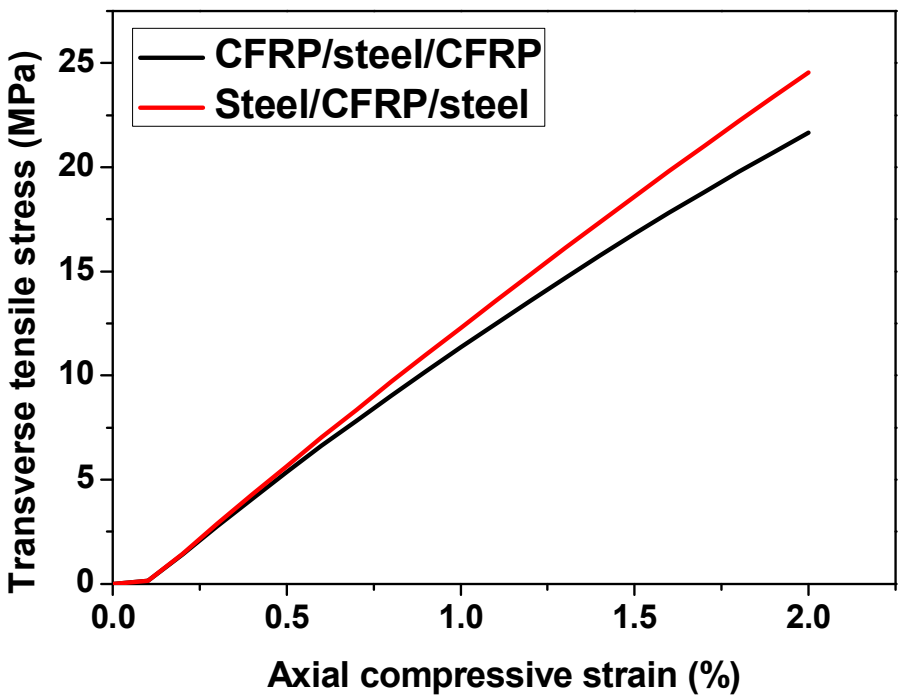

Figure 3-14 The transverse tensile stresses of CFRP layers within CFRP and steel laminates according to lay-up sequences.

Equation (26) was investigated to analyze the effects of transverse tensile stress of CFRP on compressive properties. The local orientation is not considered to be affected by transverse tensile stress. The analysis of the effect of transverse tensile

stress on longitudinal shear behavior were performed using FEM software. Figure 3-15 shows the longitudinal shear behavior of CFRP with transverse tensile stress. Increasing the magnitude of the transverse tensile stress has little effect on the longitudinal shear behavior. Unlike the tensile behavior, the transverse stress caused by steel during compressive deformation does not have a significant effect.

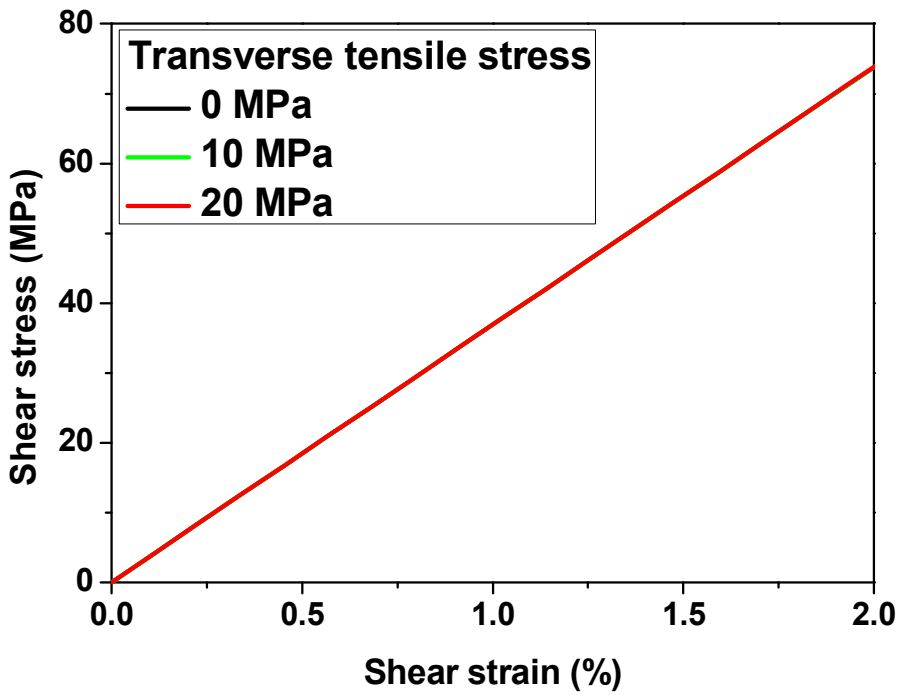

Figure 3-15 Longitudinal shear behavior of pure CFRP in the presence of transverse tensile stress.

Shear modulus of the steel was investigated to analyze the causes of the increased compressive fracture strain of the laminate composites. The tensile modulus of the

steel used in this study is 194 GPa, and the shear modulus in the isotropic condition is 65 GPa, which is larger than the CFRP longitudinal shear modulus (3.4 GPa). To calculate the shear modulus of the laminate composite, the harmonic mean using the mechanical properties and the volume fraction of each material was calculated. The modulus of CFRP/steel/CFRP and steel/CFRP/steel specimens is 6.1 and 8.7 GPa, respectively, 1.8 and 2.5 times the shear modulus of pure CFRP. That is, since the shear modulus of the laminate composite is larger than that of pure CFRP, the compressive fracture properties of the component CFRP are considered to be improved.

3.4. Summary

The CFRP layers within unidirectional CFRP/steel hybrid laminate composites exhibit fracture strain and maximum stress higher than those of pure CFRP. The main cause of this phenomenon is the transverse compressive stress due to differences in the Poisson's ratios of CFRP and steel and thermal residual stress. In this study, the mechanical behavior of hybrid laminate composites was predicted by considering the transverse compressive stress. The shear lag theory was invoked to predict the stress distributions of the matrix and the carbon fibers in the vicinity of partial fiber fractures in a CFRP. The mechanical properties of the CFRP were predicted using the average stress in the ineffective region and the Weibull parameters of the carbon fibers. The mechanical properties of the hybrid laminate composite were then predicted using the rule of mixture and compared with experimental results. The micromechanical model described herein showed that increased transverse compressive stress decreases the length of ineffective region in the vicinity of partially broken fibers, thereby increasing the fracture strain of the hybrid laminate composite. These predictions were confirmed with experimental data.

Chapter 4. New failure criterion of fiber-reinforced composites

4.1. Overview of failure criteria of the CFRP

Uniaxial testing confirmed that fracture behavior varied when CFRP deformation occurred under multiaxial stress conditions. Therefore, a study of failure criterion is needed to predict the failure of CFRP under multiaxial stress conditions. The failure criteria of FRPs under multiaxial stress conditions have been studied. Longitudinal fracture of an FRP is reportedly influenced only by axial stress [96]. However, Hashin [97] proposed that longitudinal fractures are also affected by shear stress. According to Puck's criteria [98], the longitudinal fracture of FRP is affected only by axial stress while inter-fiber fracture is determined by both transverse stress and shear stress. According to Hoffman's criteria [99], the axial, transverse and shear properties of the various materials interact with each other. For example, the axial strength of a material may be improved by the application of a certain amount of transverse compressive stress. This concept is consistent with the results of our previous research on hybrid laminate composites [80]. However, as discussed in Hoffman's paper [99], this concept lacks physical significance, necessitating a micromechanical model to analyze the effects of multiaxial stress on the fracture behavior of FRP while considering the fracture mechanism.

4.2. Development of new failure criterion based on micromechanics

4.2.1. Effect of multiaxial stress on the CFRP fracture

Previous studies have confirmed that axial tensile properties of CFRP can be improved when transverse compressive stress is present, while decreased when transverse tensile stress is present. However, transverse compressive stress does not always guarantee axial property improvement. According to Puck's study [98], axial properties are decreased when the tensile or compressive stress in the transverse direction increases beyond a certain level as shown Figure 4-1. This is because partial fracture of the carbon fiber generated during axial tension and the resulting fracture of the matrix or separation of the interface weaken the transverse properties of CFRP. The study did not discuss the conditions under which transverse stresses affect axial stresses, but related study [100] suggested that stresses in each direction can affect each other when it exceeds half of strength in each direction. However, the physical basis for this discussion is not available, and it is important to draw accurate failure criterion through a micromechanical approach.

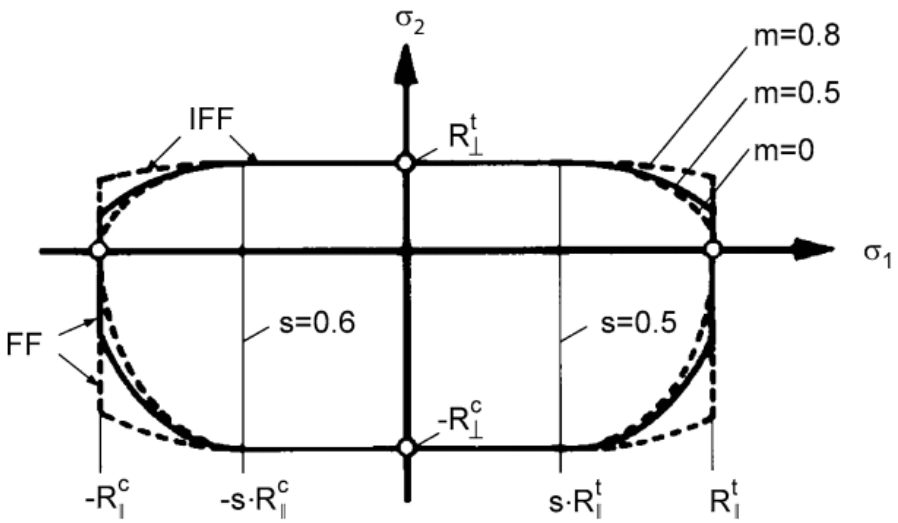

Figure 4-1 Relationship between axial strength and transverse strength, proposed in Puck's failure criterion [98].

4.2.2. Development of failure criterion based on the predictive model

In order to develop a failure criterion based on the micromechanical predictive model, it is necessary to distinguish between failure modes of CFRP in multiaxial stress situations. In this study, axial dominant fracture is named when axial stress is dominant in CFRP fracture, and transverse dominant fracture when transverse stress is dominant. To obtain the failure criterion determined by the axial dominant fracture, the predictive model can be used to predict the axial strength according to the transverse compressive stress, showing the results in Figure 4-2. Since the magnitude of transverse compressive stress of CFRP in the laminate composites is relatively small (below 40 MPa), axial dominant fracture is likely to occur.

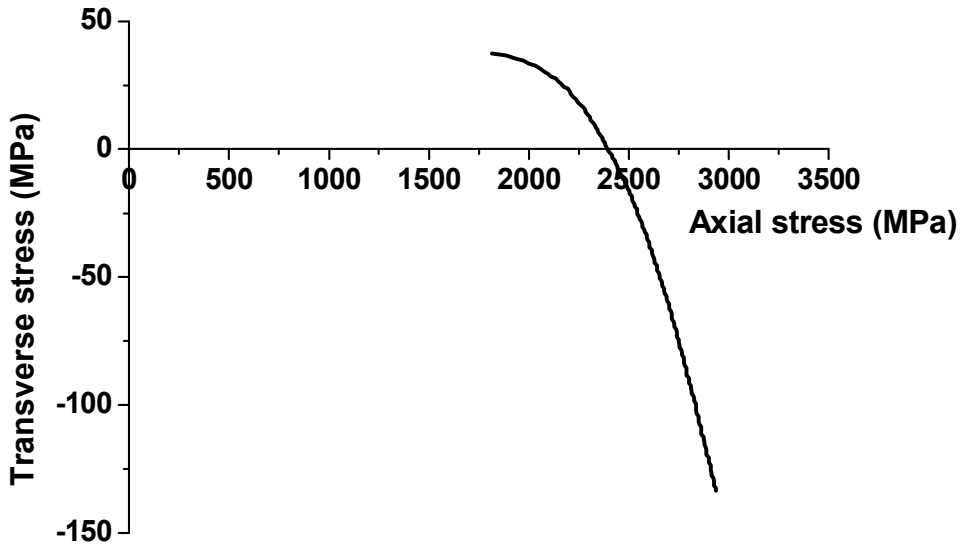

Figure 4-2 Axial dominant fracture criterion of CFRP developed through micromechanical predictive model.

As the transverse compressive stress increases, the situation changes when the CFRP failure mode changes to transverse dominant fracture. As can be seen in Figure 4-2, in case of failure only in axial dominant fracture mode, the axial strength only increases as the transverse compressive stress increases. However, this is not practical because the degradation of the transverse properties occurs as the transverse stress increases. In this study, it is assumed that axial dominant fracture is not involved in the transverse dominant fracture mode to describe the failure criterion when transverse stress is the main cause of failure. In other words, it is assumed that in transverse dominant fracture mode, axial deformation only

causes the matrix to break in the ineffective region and is not involved in axial failure. Internal defects, which occur during axial tension of CFRP, are represented by ineffective regions. As described in Section 3.1.3, when the axial tensile strain is small, there is only an elastic zone around the fracture fiber, but as the tensile strain increases, the inelastic and fracture zones of the matrix occur. Especially when the matrix is broken (fracture zone) and present as a crack, it can be a serious defect when the transverse stress is applied. If the axial tensile strain is very large and no axial fracture occurs (transverse dominant fracture assumption), then there will be numerous ineffective regions inside the CFRP as shown in Figure 4-3. The axial stress when the length of the ineffective region exceeds the threshold and can be destroyed by even a small amount of transverse compressive stress is named as critical axial stress ($R_{1T, crit}$).

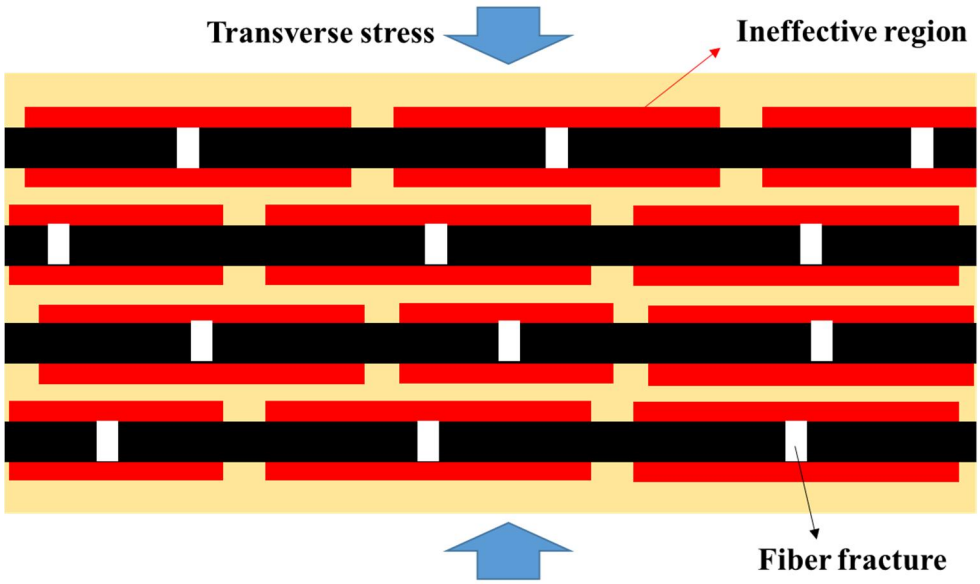

Figure 4-3 Ineffective region under critical axial strain assumed in transverse dominant fracture mode.

Critical axial stress is dominantly dependent on the Weibull distribution of carbon fiber. In order to determine critical axial stress, it is necessary to quantify the amount of broken matrix inside CFRP. In this study, the defect factor (D_f) was calculated to represent the amount of internal defects for axial deformation as follows.

$$D_f = \frac{the\ length\ of\ fracture\ zone}{the\ length\ of\ ineffective\ region} \qquad (27)$$

Increasing the defect factor implies an increase in the length of the fracture zone. If the fracture zone is very large, transverse fracture can occur under even small

transverse stress. As the defect factor decreases, the fracture zone length decreases, so the transverse stress required to break CFRP increases. It is necessary to determine the defect factor, which can cause the fracture of CFRP only by the length of the fracture zone, even if the transverse stress is very small. For this purpose, an axial strain was obtained to derive the corresponding defect factor, and the fracture probability of the carbon fiber at the axial strain was calculated. Figure 4-4 shows the failure probability of carbon fiber depending on the defect factor. When the defect factor is less than 0.8, that is, the fracture zone reaches 80% of the length of the ineffective region, the axial strain is relatively small, resulting in less than 5% probability of fiber breakage. If the axial strain increases further and the defect factor reaches 0.9, the probability of fiber fracture increases drastically. Therefore, the axial stress (3,276 MPa) of CFRP with a defect factor of 0.9 was determined as critical axial stress, which is the axial strength when the transverse stress converges to zero in transverse dominant fracture mode.

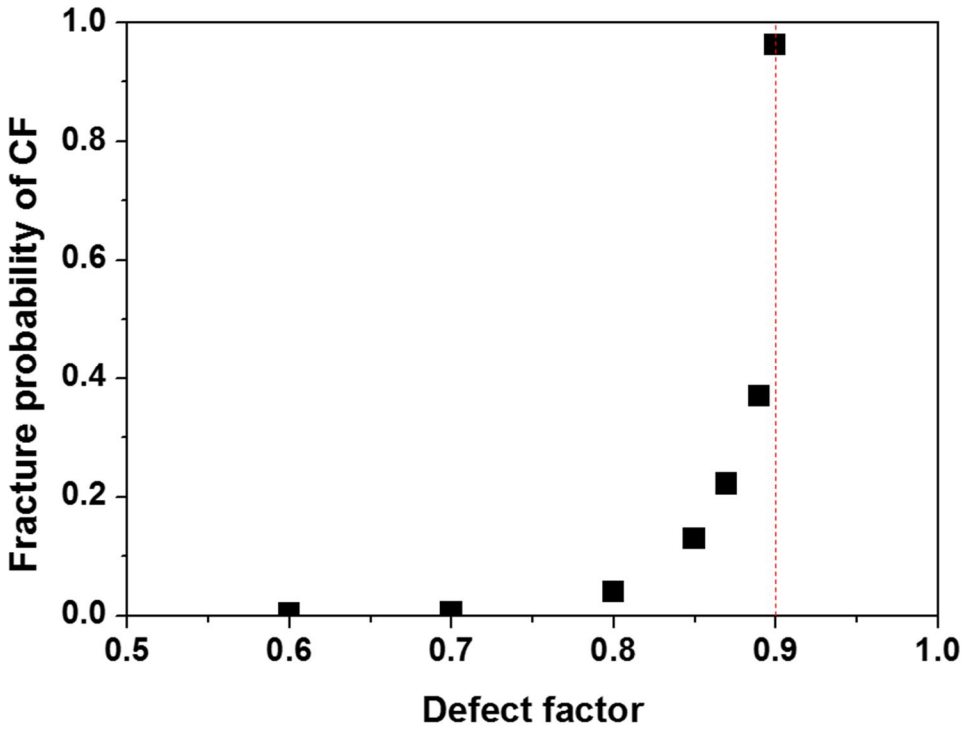

Figure 4-4 Fracture probability of carbon fiber depending on the defect factor to quantify the degree of fracture of matrix.

In order to develop failure criterion for transverse dominant fracture, the following equations are constructed using the fracture strength in each direction as follows.

$$\left(\frac{\sigma_1}{R_{1\mathrm{T,trans}}}\right)^{\alpha} + \left(\frac{\sigma_2}{R_{2T}}\right)^{\alpha} = 1 \quad (\sigma_2 \geq 0) \qquad (28)$$

$$\left(\frac{\sigma_1}{R_{1\mathrm{T,trans}}}\right)^{\alpha}+\left(\frac{\sigma_2}{R_{2C}}\right)^{\alpha}=1 \quad (\sigma_2<0) \qquad (29)$$

Using the equations, failure criterion for transverse dominant fracture can be obtained as shown in Figure 4-5. According to this criterion, if the stress state of CFRP exists inside the envelope, it is not destroyed by the transverse dominant fracture mode.

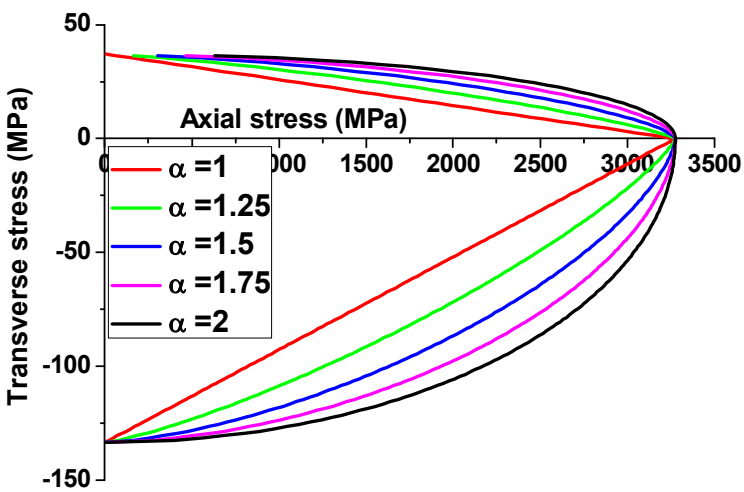

Figure 4-5 Transverse dominant fracture criterion of CFRP developed through micromechanical predictive model.

Now, it is necessary to draw failure criterion under multiaxial stress state, considering both failure modes. The axial dominant fracture and transverse

dominant fracture criteria are drawn simultaneously, as shown in Figure 4-6. In order to interpret this graph, it is necessary to determine the magnitude of the axial stress under a specific transverse stress. For example, if the transverse stress is -100 MPa and the axial stress is 2,500 MPa, it is in the safe state for axial dominant criterion, but in the fracture stats for transverse dominant criterion. In other words, when the absolute value of transverse compressive stress is large, transverse dominant criterion is applied. On the other hand, if the transverse stress is -50 MPa and the axial stress is 2,700 MPa, it is in the safe state for transverse dominant criterion but in the fracture state for axial dominant criterion. It can be seen that the axial dominant criterion is applied when the absolute value of the transverse stress is small.

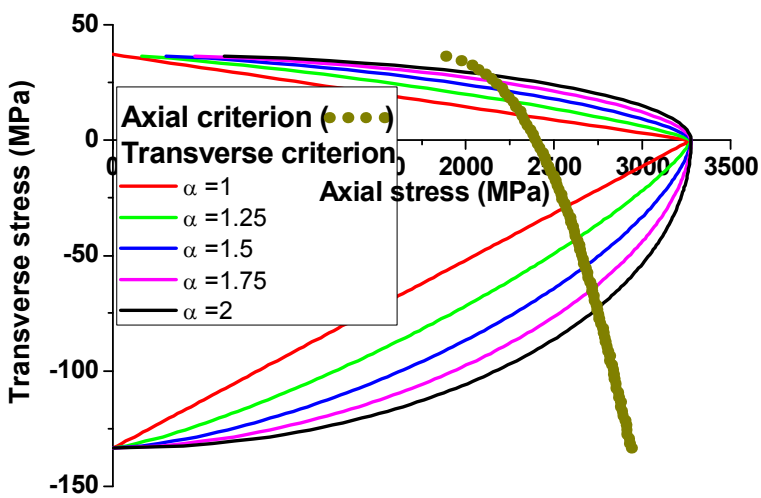

Figure 4-6 Combination of axial dominant criterion and transverse dominant criterion.

4.2.3. Validation examples

As described above, when the transverse stress is small, fracture is determined by the axial dominant criterion. Axial dominant criterion was experimentally verified in the micromechanical predictive model. Figure 4-7 shows the results of comparing the axial strength of CFRP estimated from the experimental results of the mechanical properties of laminate composite with the failure criterion. In CFRP/steel laminate composites, the CFRP's transverse compressive stress is less than 40 MPa, so the experimental results and failure criterion results are similar under the condition α is between 1 and 2.

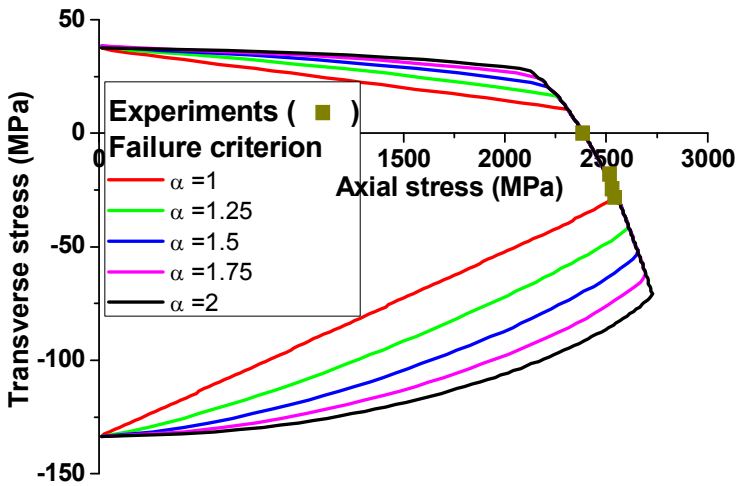

Figure 4-7 Comparison of developed criterion (micromechanical criterion) with experimental data from laminate composites.

When the transverse stress was large, the criterion was verified using experimental results of other research groups. In Gan's study, transverse compressive stress was applied to CFRP using an indenter, and axial strength was measured depending on the transverse stress [101]. In the study, The scale parameters, shape parameters and reference lengths of the carbon fibers used in the study are 8,270 MPa, 8.81, and 1.75 mm, respectively [102], and The axial tensile, transverse tensile and transverse compressive strengths of CFRP are 2,726, 64.1 and -1,200 MPa, respectively [103]. The shear yield stress, fracture strain and frictional stress of the matrix were assumed to be 40 MPa, 3% and 1 MPa, respectively, through the Weibull parameters of the carbon fiber and the mechanical properties of CFRP. The fracture criterion of CFRP was drawn using this parameters, and the graph compared with the experimental results is shown in Figure 4-8. The comparison shows the most similar result when α is 1.

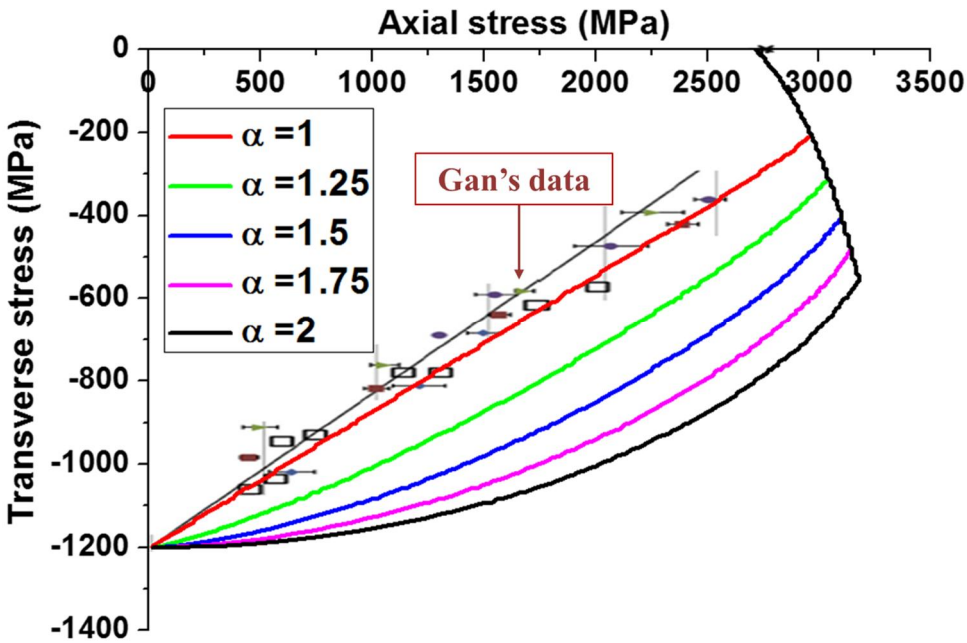

Figure 4-8 Comparison of developed criterion (micromechanical criterion) with Gan's experimental data.

4.2.4. Application to FEM analysis

In order to apply the developed failure criterion in various ways, it should be applicable to calculation using finite element method. FEM analysis software (ABAQUS, Simulia, USA) was used to calculate the axial strength of CFRP in the presence of transverse stress. The properties of each component (fiber and matrix) and CFRP used in the FEM analysis are the same as those used in Chapter 3. A user-defined subroutine UMAT (FORTRAN user-material subroutine) was written for applying the micromechanics in the developed failure criterion to the numerical

calculation. Figure 4-9 shows a graph comparing the results of FEM calculation of axial strength of CFRP with failure criterion. The similarity of the two results confirmed that the micromechanical model developed in this study was properly implemented in the UMAT subroutine code.

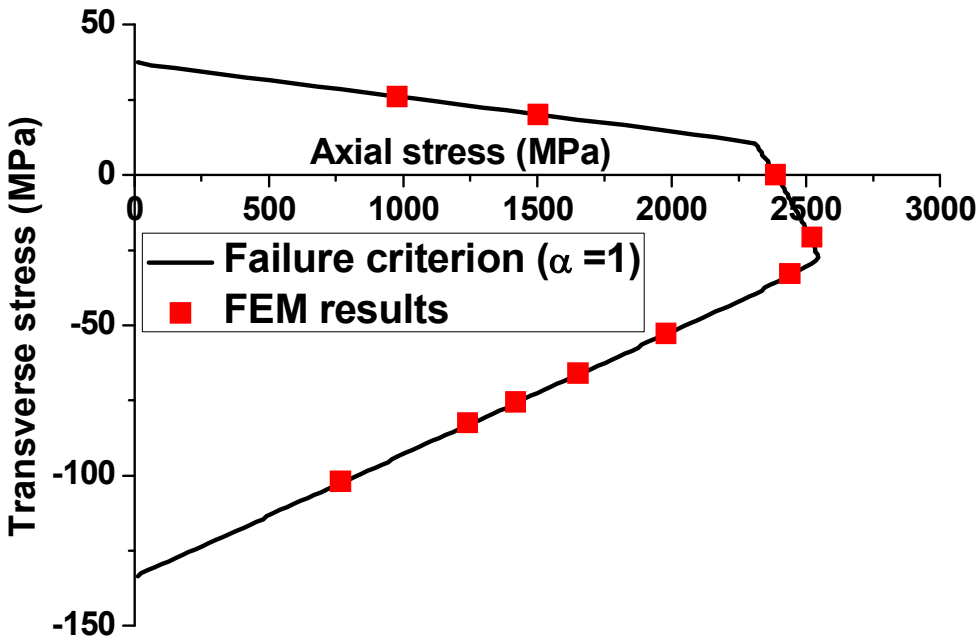

Figure 4-9 Comparison of developed criterion (micromechanical criterion) with FEM calculation results.

Figure 4-10 shows a graph predicting the deformation behavior of CFRP/steel laminate composites using FEM calculation. The UMAT subroutine code also includes the effects of thermal residual stresses during the fabrication of specimens. For example, For example, for CFRP/steel /CFRP specimens with the largest

volume fraction of CFRP (Figure 4-10 (b)), the yield strain at the beginning of deformation is the least compared to pure steel due to the effect of thermal residual stress. It was confirmed that the FEM calculation results were similar to the experimental results in each type of specimen, and this proved that the micromechanical model and implementation method are correct.

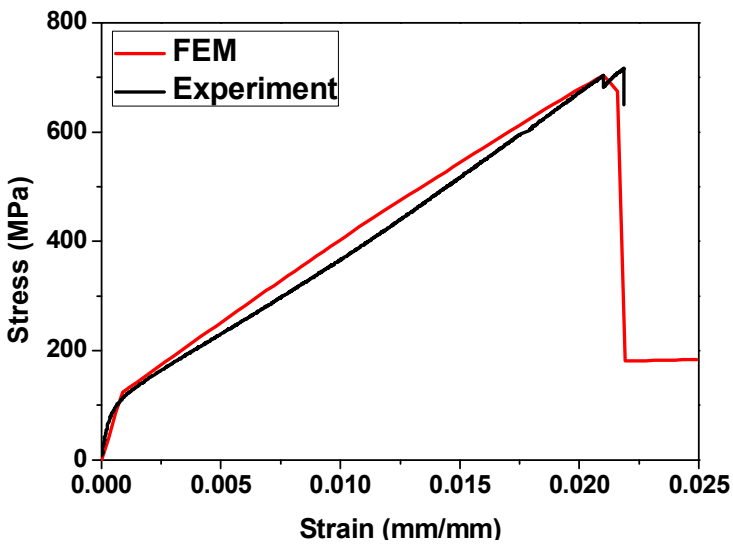

(a)

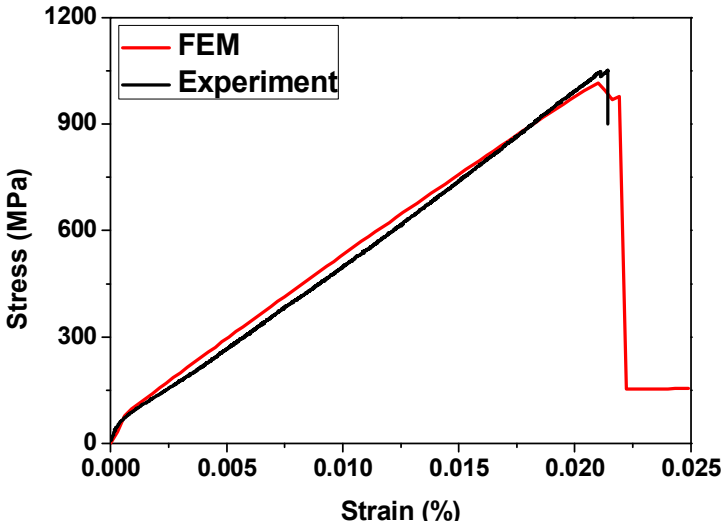

(b)

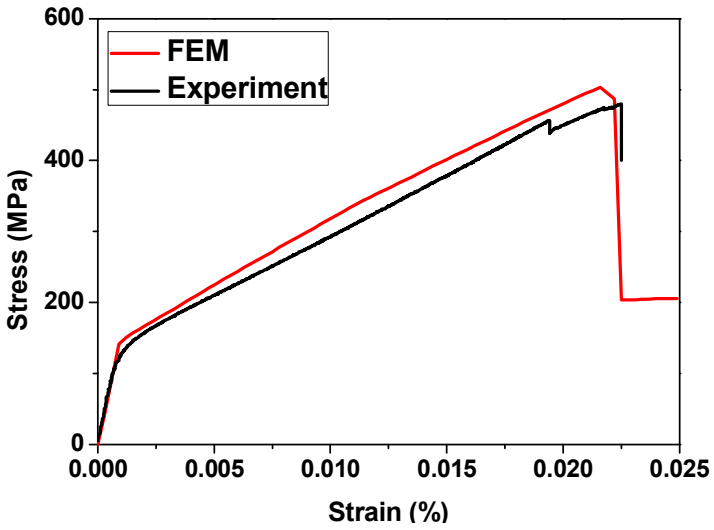

(c)

Figure 4-10 Comparison of FEM calculation results of (a) steel/CFRP, (b) CFRP/steel/CFRP and (c) steel/CFRP/steel laminate composites with each experimental result.

4.3. Summary

In addition to predicting the mechanical properties of laminate composites using a micromechanical approach, a failure criterion was developed to determine the failure of CFRP in multiaxial stress conditions. For this purpose, the failure criterion was developed by distinguishing between axial dominant fracture and transverse dominant fracture. Axial dominant fracture criterion can be obtained by calculating the axial strength depending on the transverse compressive stress using the micromechanical predictive model. The degree of fracture of the matrix due to axial deformation has a great influence on the transverse dominant fracture criterion, and the criterion is obtained using the critical axial stress, the virtual axial stress at the moment the matrix is mostly destroyed. In order for CFRP not to break, the stress state must be within the criteria of both failure modes. When the absolute value of transverse compressive stress is small, axial dominant fracture occurs. When the absolute value of transverse compressive stress is large, transverse dominant fracture occurs. In addition, the micromechanical failure criterion was determined to be appropriate by comparing it with previous experimental results.

Chapter 5. Concluding remarks

The purpose of this study was predicting the mechanical behavior of CFRP in multiaxial stress condition and applying the prediction method to CFRP and steel laminate composites.

Tensile test of CFRP and steel laminate composite showed that the failure strain of CFRP constituting the laminate composite was higher than that of pure CFRP. The interaction between the two materials was analyzed to determine the cause. After yielding, the Poisson's ratio of steel is larger than that of CFRP. Therefore, it is considered that transverse compressive stress will occur in CFRP under axial deformation of laminate composite. As a result of calculating the transverse compressive stress in CFRP through FEM software, it was confirmed that the transverse compressive stress increases when the laminate composite is symmetric in the thickness direction and when the volume fraction of steel is high. As a result of comparing with the tensile test results, it was confirmed that there is a tendency between the magnitude of the transverse compressive stress and the tensile properties, thereby confirming the cause of the phenomenon.

The fracture mechanism of CFRP was analyzed to quantitatively analyze and predict the effects of transverse compressive stress on the mechanical properties of CFRP. As the transverse compressive stress increases, the longitudinal splitting behavior of CFRP is considered to be suppressed. The possibility is verified by the

calculation of the internal stress distribution through shear lag theory. In the presence of transverse compressive stress, the yield stress of matrix increases, and the frictional stress increases even after the matrix fractures, reducing the length of the ineffective region. In CFRP, the ineffective region means the extent to which the partial fracture of internal fibers affects CFRP. In other words, reducing the length of the ineffective region means that the effects of carbon fiber fracture are localized and mechanical properties are improved. A predictive model was developed based on the micromechanical behavior, and the model was verified by comparison with the experimental results.

The predictive model was applied to the development of failure criterion to predict CFRP fracture in multiaxial stress condition. Previous studies on failure criterion have shown that increasing the magnitude of transverse stress decreases the axial strength of CFRP. This is because, under multiaxial stress conditions, as the major fracture mode changes, the failure criteria to be applied have to be varied. According to the micromechanical approach, axial dominant fracture occurs when the absolute value of transverse stress is small and transverse dominant fracture occurs when transverse stress exceeds the threshold. The validity was verified by comparing the developed micromechanical criterion with experimental results.

Reference

1. Tagawa, T. and T. Miyata, *Size effect on tensile strength of carbon fibers.* Materials Science and Engineering: A, 1997. **238**(2): p. 336-342.
2. Zhou, Y., et al., *Tensile behavior of carbon fiber bundles at different strain rates.* Materials Letters, 2010. **64**(3): p. 246-248.
3. Watanabe, J., et al., *Tensile strength distribution of carbon fibers at short gauge lengths.* Advanced Composite Materials, 2014. **23**(5-6): p. 535-550.
4. Drubetski, M., A. Siegmann, and M. Narkis, *Electrical properties of hybrid carbon black/carbon fiber polypropylene composites.* Journal of materials science, 2007. **42**(1): p. 1-8.
5. Jumahat, A., et al., *Fracture mechanisms and failure analysis of carbon fibre/toughened epoxy composites subjected to compressive loading.* Composite structures, 2010. **92**(2): p. 295-305.
6. Chen, J. and I. Harrison, *Modification of polyacrylonitrile (PAN) carbon fiber precursor via post-spinning plasticization and stretching in dimethyl formamide (DMF).* Carbon, 2002. **40**(1): p. 25-45.
7. Tan, L., et al., *Investigating the spinnability in the dry-jet wet spinning of PAN precursor fiber.* Journal of applied polymer science, 2008. **110**(4): p. 1997-2000.
8. Han, S.H., et al., *Study on high-speed RTM to reduce the impregnation time of carbon/epoxy composites.* Composite Structures, 2015. **119**: p. 50-58.
9. Kaynak, C. and Y.O. Kas, *Effects of injection pressure in resin transfer moulding (RTM) of woven carbon fibre/epoxy composites*. Polymers and Polymer Composites, 2006. **14**(1): p. 55-64.
10. Bruneau, M., C.-M. Uang, and A. Whittaker, *Ductile design of steel structures*. Vol. 389. 1998: McGraw-Hill New York.
11. Dey, A. and A.K. Mukhopadhyay, *Nanoindentation of brittle solids*. 2014: CRC Press.
12. Zhou, Y., et al., *Statistical analysis on the fatigue strength distribution of T700 carbon fiber.* Composites science and technology, 2006. **66**(13): p.

2100-2106.

13. Hill, R. and E. Okoroafor, *Weibull statistics of fibre bundle failure using mechanical and acoustic emission testing: the influence of interfibre friction.* Composites, 1995. **26**(10): p. 699-705.
14. Nedele, M. and M. Wisnom, *Stress concentration factors around a broken fibre in a unidirectional carbon fibre-reinforced epoxy.* Composites, 1994. **25**(7): p. 549-557.
15. Miyano, Y., et al., *Role of matrix resin on fracture strengths of unidirectional CFRP.* Journal of composite materials, 1986. **20**(6): p. 520-538.
16. Lee, H., I. Ohsawa, and J. Takahashi, *Effect of plasma surface treatment of recycled carbon fiber on carbon fiber-reinforced plastics (CFRP) interfacial properties.* Applied Surface Science, 2015. **328**: p. 241-246.
17. Na, W., et al., *Prediction of the tensile strength of unidirectional carbon fiber composites considering the interfacial shear strength.* Composite Structures, 2017. **168**: p. 92-103.
18. Sato, N., T. Kurauchi, and O. Kamigaito, *Fracture mechanism of unidirectional carbon-fibre reinforced epoxy resin composite.* Journal of materials science, 1986. **21**(3): p. 1005-1010.
19. Nairn, J.A., *Fracture mechanics of unidirectional composites using the shear-lag model I: theory.* Journal of composite materials, 1988. **22**(6): p. 561-588.
20. Ivens, J., M. Wevers, and I. Verpoest, *Influence of carbon fibre surface treatment on composite UD strength.* Composites, 1994. **25**(7): p. 722-728.
21. Na, W., D. Kwon, and W.-R. Yu, *X-ray computed tomography observation of multiple fiber fracture in unidirectional CFRP under tensile loading.* Composite Structures, 2018. **188**: p. 39-47.
22. Park, J.B., T. Okabe, and N. Takeda, *New concept for modeling the electromechanical behavior of unidirectional carbon-fiber-reinforced plastic under tensile loading.* Smart materials and structures, 2003. **12**(1): p. 105.

23. Park, J., et al., *Electromechanical modeling of unidirectional CFRP composites under tensile loading condition.* Composites Part A: Applied Science and Manufacturing, 2002. **33**(2): p. 267-275.
24. Odagiri, N., H. Kishi, and M. Yamashita, *Development of TORAYCA prepreg P2302 carbon fiber reinforced plastic for aircraft primary structural materials.* Advanced Composite Materials, 1996. **5**(3): p. 249-254.
25. Muto, N., et al., *Preventing Fatal Fractures in Carbon-Fiber–Glass-Fiber-Reinforced Plastic Composites by Monitoring Change in Electrical Resistance.* Journal of the American Ceramic Society, 1993. **76**(4): p. 875-879.
26. Swolfs, Y., et al., *Matrix cracks around fibre breaks and their effect on stress redistribution and failure development in unidirectional composites.* Composites Science and Technology, 2015. **108**: p. 16-22.
27. You, Y.-J., et al., *Hybrid effect on tensile properties of FRP rods with various material compositions.* Composite structures, 2007. **80**(1): p. 117-122.
28. McBride, A.K., et al., *Mechanical behavior of hybrid glass/steel fiber reinforced epoxy composites.* Polymers, 2017. **9**(4): p. 151.
29. Qi, L., et al., *Effect of fabrication parameters on carbon fibre reinforced magnesium matrix composite components.* Materials Science and Technology, 2017. **33**(1): p. 77-83.
30. Thakur, S.K., T.S. Srivatsan, and M. Gupta, *Synthesis and mechanical behavior of carbon nanotube–magnesium composites hybridized with nanoparticles of alumina.* Materials Science and Engineering: A, 2007. **466**(1-2): p. 32-37.
31. Uraiyer, F.A.J., *The new Steel-CFRP composite specimen (CFRP laminates sandwiched between two steel strips) and its behaviour under Uniaxial tension.* International Journal of Civil and Structural Engineering, 2012. **3**(1).
32. Cantwell, W., *The mechanical properties of fibre-metal laminates based on glass fibre reinforced polypropylene.* Composites Science and

Technology, 2000. **60**(7): p. 1085-1094.

33. da Costa, A.A., et al., *The effect of thermal cycles on the mechanical properties of fiber–metal laminates.* Materials & Design, 2012. **42**: p. 434-440.
34. Sadighi, M., R. Alderliesten, and R. Benedictus, *Impact resistance of fiber-metal laminates: a review.* International Journal of Impact Engineering, 2012. **49**: p. 77-90.
35. Hagenbeek, M., et al., *Static properties of fibre metal laminates.* Applied Composite Materials, 2003. **10**(4-5): p. 207-222.
36. Hannemann, B., et al., *Hybridisation of CFRP by the use of continuous metal fibres (MCFRP) for damage tolerant and electrically conductive lightweight structures.* Composite Structures, 2017. **172**: p. 374-382.
37. Vogelesang, L. and J. Gunnink, *ARALL: A materials challenge for the next generation of aircraft.* Materials & Design, 1986. **7**(6): p. 287-300.
38. Lin, C., P. Kao, and F. Yang, *Fatigue behaviour of carbon fibre-reinforced aluminium laminates.* Composites, 1991. **22**(2): p. 135-141.
39. Vogelesang, L.B. and A. Vlot, *Development of fibre metal laminates for advanced aerospace structures.* Journal of Materials Processing Technology, 2000. **103**(1): p. 1-5.
40. Cortes, P. and W. Cantwell, *The fracture properties of a fibre–metal laminate based on magnesium alloy.* Composites Part B: Engineering, 2005. **37**(2-3): p. 163-170.
41. Antipov, V., et al., *Investigation of a new fibre metal laminate (FML) family on the base of Al-Li-Alloy with lower density.* Materialwissenschaft und Werkstofftechnik, 2012. **43**(4): p. 350-355.
42. Sinmazçelik, T., et al., *A review: Fibre metal laminates, background, bonding types and applied test methods.* Materials & Design, 2011. **32**(7): p. 3671-3685.
43. Guillen, F. and W. Cantwell, *The fracture properties of fibre-metal laminates based on glass fibre reinforced polyamide.* Advanced Composites Letters, 2000. **9**(3): p. 096369350000900305.
44. Abdullah, M. and W. Cantwell, *The impact resistance of polypropylene-*

based fibre–metal laminates. Composites Science and Technology, 2006. **66**(11-12): p. 1682-1693.

45. Castrodeza, E., F. Bastian, and J.P. Ipiña, *Critical fracture toughness, JC and δ5C, of unidirectional fibre–metal laminates.* Thin-walled structures, 2003. **41**(12): p. 1089-1101.
46. Moussavi-Torshizi, S.E., et al., *A study on tensile properties of a novel fiber/metal laminates.* Materials Science and Engineering: A, 2010. **527**(18-19): p. 4920-4925.
47. Wu, H.F., et al., *Use of rule of mixtures and metal volume fraction for mechanical property predictions of fibre-reinforced aluminium laminates.* Journal of Materials Science, 1994. **29**(17): p. 4583-4591.
48. Agarwal, A., S.J. Foster, and E. Hamed, *Testing of new adhesive and CFRP laminate for steel-CFRP joints under sustained loading and temperature cycles.* Composites Part B: Engineering, 2016. **99**: p. 235-247.
49. Teng, J., et al., *Treatment of steel surfaces for effective adhesive bonding*, in *Advances in FRP composites in civil engineering*. 2011, Springer. p. 865-868.
50. Lawcock, G., et al., *The effect of adhesive bonding between aluminum and composite prepreg on the mechanical properties of carbon-fiber-reinforced metal laminates.* Composites Science and Technology, 1997. **57**(1): p. 35-45.
51. Kim, J., et al., *Improved adhesion of metal–polymer sandwich composites using a spontaneous polymer grafting process.* Functional Composites and Structures, 2019.
52. Bhat, S., et al. *A Theoretical Model for Estimation of Yield Strength of Fiber Metal Laminate*. in *IOP Conference Series: Materials Science and Engineering*. 2017. IOP Publishing.
53. Hausmann, J., P. Naghipour, and K. Schulze, *Analytical and numerical residual stress models for fiber metal laminates–comparison and application.* Procedia Materials Science, 2013. **2**: p. 68-73.
54. Lu, Y., et al., *Study of the tensile properties of CFRP strengthened steel plates.* Polymers, 2015. **7**(12): p. 2595-2610.

55. Sharma, A.P., S.H. Khan, and V. Parameswaran, *Experimental and numerical investigation on the uni-axial tensile response and failure of fiber metal laminates.* Composites Part B: Engineering, 2017. **125**: p. 259-274.
56. Botelho, E.C., et al., *A review on the development and properties of continuous fiber/epoxy/aluminum hybrid composites for aircraft structures.* Materials Research, 2006. **9**(3): p. 247-256.
57. Cortes, P. and W. Cantwell, *The prediction of tensile failure in titanium-based thermoplastic fibre–metal laminates.* Composites Science and Technology, 2006. **66**(13): p. 2306-2316.
58. Guangquan, Y., Z. Jiazhen, and M. Songhe, *Study on Cure-Induced Residual Stresses for Fibre Metal Laminate.* Polymers and Polymer Composites, 2013. **21**(9): p. 561-564.
59. Mittal, K.L., *Silanes and other coupling agents*. Vol. 4. 2007: CRC Press.
60. Callens, M.G., et al., *Tensile behaviour of stainless steel fibre/epoxy composites with modified adhesion.* Composites Part A: Applied Science and Manufacturing, 2015. **69**: p. 208-218.
61. International, A., *Standard test method for apparent shear strength of single-lap-joint adhesively bonded metal specimens by tension loading (metal-to-metal)*. 2010: ASTM international.
62. Standard, A., *Standard test method for tensile properties of polymer matrix composite materials.* ASTM D3039/D M, 2008. **3039**: p. 2008.
63. Hong, S.-T., et al., *Dynamic crush behaviors of aluminum honeycomb specimens under compression dominant inclined loads.* International journal of plasticity, 2008. **24**(1): p. 89-117.
64. *Standard Test Method for Compressive Properties of Polymer Matrix Composite Materials Using a Combined Loading Compression (CLC) Test Fixture*.
65. Amacher, R., et al., *Thin ply composites: experimental characterization and modeling of size-effects.* Composites Science and Technology, 2014. **101**: p. 121-132.
66. Wisnom, M., *Size effects in the testing of fibre-composite materials.*

Composites Science and Technology, 1999. **59**(13): p. 1937-1957.

67. Wisnom, M., B. Khan, and S. Hallett, *Size effects in unnotched tensile strength of unidirectional and quasi-isotropic carbon/epoxy composites.* Composite Structures, 2008. **84**(1): p. 21-28.
68. Lee, J. and C. Soutis, *A study on the compressive strength of thick carbon fibre–epoxy laminates.* Composites science and technology, 2007. **67**(10): p. 2015-2026.
69. Lee, J. and C. Soutis, *Measuring the notched compressive strength of composite laminates: Specimen size effects.* Composites Science and Technology, 2008. **68**(12): p. 2359-2366.
70. Taniguchi, N., T. Nishiwaki, and H. Kawada, *Tensile strength of unidirectional CFRP laminate under high strain rate.* Advanced Composite Materials, 2007. **16**(2): p. 167-180.
71. Wang, W., et al., *Strain rate effect on tensile behavior for a high specific strength steel: from quasi-static to intermediate strain rates.* Metals, 2017. **8**(1): p. 11.
72. Cartié, D., et al., *The influence of hydrostatic pressure on the interlaminar fracture toughness of carbon/epoxy composites.* Composites Part B: Engineering, 2006. **37**(4-5): p. 292-300.
73. Parry, T. and A. Wronski, *Kinking and compressive failure in uniaxially aligned carbon fibre composite tested under superposed hydrostatic pressure.* Journal of materials Science, 1982. **17**(3): p. 893-900.
74. Zinoviev, P.A., et al., *The behavior of high-strength unidirectional composites under tension with superposed hydrostatic pressure.* Composites science and technology, 2001. **61**(8): p. 1151-1161.
75. De Strycker, M., et al., *Measuring the thermal expansion coefficient of tubular steel specimens with digital image correlation techniques.* Optics and Lasers in Engineering, 2010. **48**(10): p. 978-986.
76. Ahmed, A., et al. *STUDY OF THERMAL EXPANSION IN CARBON FIBER-REINFORCED POLYMER COMPOSITES*. in *SAMPE International Symposium Proceedings*. 2012.
77. Pickering, K. and T. Murray, *Weak link scaling analysis of high-strength*

carbon fibre. Composites Part A: Applied Science and Manufacturing, 1999. **30**(8): p. 1017-1021.

78. Melanitis, N., et al., *Interfacial shear stress distribution in model composites Part 2: Fragmentation studies on carbon fibre/epoxy systems.* Journal of composite materials, 1992. **26**(4): p. 574-610.
79. Puchkov, L. and S. Bazhenov, *Effect of longitudinal splitting on tensile strength of unidirectional aramid fiber reinforced plastics.* Journal of composite materials, 1992. **26**(10): p. 1402-1426.
80. Sung, M., et al., *Increased breaking strains of carbon fiber-reinforced plastic and steel hybrid laminate composites: experimental study.* Manuscript submitted for publication, 2019.
81. Swolfs, Y., et al., *Global load-sharing model for unidirectional hybrid fibre-reinforced composites.* Journal of the Mechanics and Physics of Solids, 2015. **84**: p. 380-394.
82. Padgett, W., S. Durham, and A. Mason, *Weibull analysis of the strength of carbon fibers using linear and power law models for the length effect.* Journal of Composite Materials, 1995. **29**(14): p. 1873-1884.
83. Landis, C.M. and R.M. McMeeking, *A shear-lag model for a broken fiber embedded in a composite with a ductile matrix.* Composites Science and Technology, 1999. **59**(3): p. 447-457.
84. Yang, W., *A generalized von Mises criterion for yield and fracture.* Journal of Applied Mechanics, 1980. **47**(2): p. 297-300.
85. Hosford, W., *A generalized isotropic yield criterion.* Journal of Applied Mechanics, 1972. **39**(2): p. 607-609.
86. Ward, I. *The yield behavior of polymers*. in *Journal of Polymer Science Part C: Polymer Symposia*. 1971. Wiley Online Library.
87. Sørensen, E.S., *Elasto-Plastic Strain Hardening Mohr-Coulomb Model: Derivation and Implementation into the Finite Element Model using Principal Stress Space.* AALBORG UNIVERSITY, STUDENT STUDYREPORT (Master Thesis), 2012.
88. Bullegas, G., S.T. Pinho, and S. Pimenta, *Engineering the translaminar fracture behaviour of thin-ply composites.* Composites Science and

Technology, 2016. **131**: p. 110-122.
89. Kim, M., et al., *Property enhancement of a carbon fiber/epoxy composite by using carbon nanotubes.* Composites Part B: Engineering, 2011. **42**(5): p. 1257-1261.
90. Karapappas, P., et al., *Enhanced fracture properties of carbon reinforced composites by the addition of multi-wall carbon nanotubes.* Journal of Composite Materials, 2009. **43**(9): p. 977-985.
91. Joshi, S.C. and V. Dikshit, *Enhancing interlaminar fracture characteristics of woven CFRP prepreg composites through CNT dispersion.* Journal of Composite Materials, 2012. **46**(6): p. 665-675.
92. Naito, K., et al., *The effect of gauge length on tensile strength and Weibull modulus of polyacrylonitrile (PAN)-and pitch-based carbon fibers.* Journal of Materials Science, 2012. **47**(2): p. 632-642.
93. Prabhakar, P. and A.M. Waas, *Interaction between kinking and splitting in the compressive failure of unidirectional fiber reinforced laminated composites.* Composite Structures, 2013. **98**: p. 85-92.
94. Naik, N. and R.S. Kumar, *Compressive strength of unidirectional composites: evaluation and comparison of prediction models.* Composite structures, 1999. **46**(3): p. 299-308.
95. Budiansky, B. and N.A. Fleck, *Compressive kinking of fiber composites: a topical review.* 1994.
96. Davila, C.G., P.P. Camanho, and C.A. Rose, *Failure criteria for FRP laminates.* Journal of Composite materials, 2005. **39**(4): p. 323-345.
97. Hashin, Z., *Failure criteria for unidirectional fiber composites.* Journal of applied mechanics, 1980. **47**(2): p. 329-334.
98. Puck, A., J. Kopp, and M. Knops, *Guidelines for the determination of the parameters in Puck's action plane strength criterion.* Composites Science and Technology, 2002. **62**(3): p. 371-378.
99. Hoffman, O., *The brittle strength of orthotropic materials.* Journal of Composite Materials, 1967. **1**(2): p. 200-206.
100. Kaiser, C., E. Kuhnel, and A. Obst. *Failure Criteria for Non-metallic Materials. Part I: Fibre Reinforced Plastics*. in *11th European conference*

on composite materials, Rhodes, May. 2004.

101. Gan, K.W., M.R. Wisnom, and S.R. Hallett, *Effect of high through-thickness compressive stress on fibre direction tensile strength of carbon/epoxy composite laminates.* Composites Science and Technology, 2014. **90**: p. 1-8.

102. Qian, H., et al., *Carbon nanotube grafted carbon fibres: a study of wetting and fibre fragmentation.* Composites Part A: Applied science and manufacturing, 2010. **41**(9): p. 1107-1114.

103. *HexTow IM7 Carbon Fiber, Product Data Sheet, HEXCEL*. 2018.

Korean abstract

탄소섬유 복합재료(CFRP)는 고강도 및 가벼운 특성으로 인해 구조재료 분야에서 큰 주목을 받았지만 부족한 내충격성과 취성 파괴거동으로 인해 더 많은 적용분야로의 확장에는 한계점으로 작용하고 있다. 금속은 연성 및 내충격성과 같은 우수한 기계적 물성을 갖지만 비중이 크다는 점이 단점으로 작용한다. 두 재료의 장점을 동시에 발현할 수 있는 재료를 얻기 위해 두 재료를 혼합함으로써 라미네이트 복합재료를 제조하는 연구가 수행되어 왔다. 본 연구에서는 CFRP/스틸 라미네이트 복합재료의 기계적 물성을 예측하기 위해 실험적, 이론적 연구를 수행하였다.

우선 CFRP/스틸 라미네이트 복합재료의 시너지 효과에 대해 정적 및 동적 시험을 통해 체계적으로 분석하였다. 다양한 조건(CFRP와 스틸 사이의 접착력, 적층 순서, 각 재료의 부피분율에서 시편을 제조하고 기계적 물성을 평가하였다. 순수한 CFRP의 파괴변형율은 1.94%로 측정되었으며, 라미네이트 복합재료를 구성하는 CFRP의 파괴변형율은 2.21%로 증가한 것을 확인하였다. 원인을 분석하기 위해 유한요소해석 및 파단면 분석을 진행하였으며, 그 결과 라미네이트 복합재료 내의 CFRP에 발생한 횡방향 압축응력이 주 원인이라고 판단했다. CFRP에 발생한 횡방향 압축응력은 스틸과의 푸아송비 차이에서 기인하며, 이 응력이 CFRP 내부의 섬유 파괴의 영향을 국소화 시킴으로써 CFRP의 기계적 물성을 향상시킨다.

더불어 앞서 발견한 라미네이트 복합재료 내 CFRP의 파괴변형률 증가 현상을 정량적으로 분석함으로써 기계적 물성을 예측하기 위한 연구를 진행하였다. 첫 번째로, CFRP와 스틸 사이의 상호작용인 횡방향 응력의

크기를 상용 유한요소해석 소프트웨어를 이용하여 계산하였다. 두 번째로, 라미네이트 복합재료의 축방향 변형에 따라 CFRP에 발생하는 횡방향 압축응력이 CFRP의 longitudinal splitting 거동에 미치는 영향에 대해 분석하였다. 이 과정에서 CFRP 내부의 파괴섬유 주변의 응력분포를 계산하기 위해 shear lag theory를 사용하였으며, 비효율 구간에서의 응력분포와 global load sharing model을 통해 CFRP의 변형거동을 예측하였다. 최종적으로 제조과정에서 발생하는 열적잔류응력을 고려하였으며, 혼합 법칙을 통해 CFRP/스틸 라미네이트 복합재료의 기계적 물성을 예측하는 모델을 개발했다.

마지막으로 다축 응력 조건에서 CFRP의 파괴 여부를 예측하기 위한 파손 기준을 개발된 예측 모델을 이용하여 정립했다. 이를 위해 CFRP의 횡방향 응력이 횡방향 파괴에 미치는 영향을 분석하였다. 또한 CFRP의 횡방향 파괴는 횡방향 응력뿐만 아니라 축방향 응력의 영향도 받는데, 이 영향을 반영하기 위해 예측 모델에서 얻은 비효율 구간에 대한 정보를 이용하여 횡방향 파단에 대한 기준을 정립했다. 최종적으로 주어진 응력 조건에서 적합한 CFRP의 파괴 모드를 분석하고 미소 역학적 접근법에 기반한 파손 기준을 개발하고 검증하였다.

핵심어: CFRP/스틸 하이브리드, 파괴변형률, 하이브리드 효과, 다축 응력, 파손 기준

학번: 2014-21474

감사의 글

졸업 논문을 마무리하며 마치 대단한 여정을 끝낸 것 마냥 들떠 있었지만 감사의 글을 작성하려고 보니 이상할 정도로 마음이 차분해지는 것을 느낀다. 대학원에 들어온 이후로 지난 시간을 차근차근 떠올려보니 많은 사람들을 만나고 그 분들로부터 참 많은 도움을 받았다는 것을 깨닫게 되었다. 이 글은 그 분들께 전하는 편지라는 생각으로 작성하고 있으며, 글재주는 없지만 진실된 마음이 전달되기를 바란다.

처음 대학원 진학을 위해 지도 교수님을 찾아 뵀던 날부터 지금까지 힘든 날도 있었지만 확실한 것은 그 때의 컨택이 무조건 옳았다는 것이다. 다양한 이유가 있겠지만 큰 이유는 지도 교수님이신 유웅열 교수님이다. 교수님께는 두서가 없더라도 다음과 같이 말씀드리고 싶다. 처음 연구실에 받아주셔서 감사합니다. 연구 방향을 이끌어 주셔서 감사합니다. 대학원을 그만 두겠다고 말씀드렸을 때 세 번씩이나 만류해 주셔서 감사합니다. 맷집이 있다는 확신을 주셔서 감사합니다. 주눅들지 않게 챙겨주시고 저를 자신감 있는 모습으로 만들어 주셔서 감사합니다. 어떤 상황에서도 인간적인 교감이 느껴지게 대해 주신 점에 대해 항상 감사드립니다. 저의 앞으로의 길에 있어서 최소한 교수님께 실망시켜 드리지 않겠다는 마음가짐은 잊지 않도록 하겠습니다.

연구실 생활이 길지 않다고 정신차려야 한다고 말씀해주신 전승렬 박사님 감사드립니다. 형과 집이 가까운 덕분에 퇴근을 같이 자주 하면서 연구실 생활에 쉽게 적응을 한 것 같습니다. 솔직히 그 때는 형이 좀 더 일찍 퇴근하시기를 바라긴 했었지만 그게 나빴다는 것은 아니고 덕분에 즐거운 시간이 많았다는 그런 의미로 오해 없으시면 좋겠습니다. 신입생 때 지켜봤던 형의 졸업 준비과정을 제가 지금 진행하면서 형과의 추억을

특히 많이 떠올렸던 것 같습니다. 건강하세요 승렬이 형.

연구실 선배님들에 대해서 감사함을 표현하자면 끝이 없을 것 같다. 뭐든지 다 알고 계시고 뭐든 다 해결해주시는 현철이 형, 어떤 상황에서도 차분함과 침착함을 유지해야 멋있다는 것을 깨닫게 해주신 원진이 형, 노력과 꾸준함에 대해 느끼게 해 주신 호성이 형, 정도를 지키고 올바른 생각에 대해 배울 점이 많은 태형이까지 선배 복은 좋았다고 늘 생각하고 있다.

적지 않은 나이에 연구실 생활을 시작하다 보니 선배님들 중에 친구가 많았던 것은 행운이었다고 생각한다. 근성이와 석빈이는 보낸 시간도 많지만 같이 먹은 밥과 술도 많아서 연구실 생활에 있어서 아주 큰 부분으로 자리잡고 있다. 많이 놀아줘서 고맙기도 한데, 그게 다는 아니고 연구적 마인드의 기준점이랄까, 그런 것을 정해준 것 같아서 고맙다는 생각이 많이 든다. 특히 근성이는 나 신입생 때 자료도 많이 수정해주고 그래서 내가 박살낸 충전기와 더불어 큰 빚이라고 생각하고 있다. 재호와 진용이도 재미있게 놀아줘서 너무 고마웠다. 나도 이제 졸업했으니 너희가 놀 때 나도 불러주면 참 고맙겠다.

또 다른 친구이자 선배인 사랑이와 유빈이에게도 고마운 점이 많다. 그렇지만 두 사람은 나에게 너무도 큰 배신감을 느끼게 해 주었기 때문에 지금도 손이 부들거려 글이 잘 써지지 않는다. 그렇지만 최대한 억누르고 표현해 보도록 하겠다. 사랑이는 사실 친구로 지내고 있지만 늘 누나 같은 느낌이 강했다. 우리 친 누나가 나를 챙겨줄 때의 느낌이 강하게 느껴진다. 너한테는 도움을 받은 것이 너무 많아서 일일이 쓰기엔 너무 길고 밥 먹을 때 생각나면 하나씩 얘기하는게 좋을 것 같다. 굳이 진짜 하나만 얘기하자면 나 방장 할 때 많이 도와줘서 진짜 고마웠다. 유빈이도 도와준 부분이 엄청 많지만 그 중에서도 가장 최근에 졸업 관련해서 내가 밤낮으로 문의하는 것에 대해 친절히 답을 주어 너무 고맙다. 사실

두 사람 없었으면 졸업 준비과정이 훨씬 더디고 힘들었을 거라고 확신한다.

연구실 생활에서 빼놓을 수 없는 든든한 버팀목은 동기라고 생각한다. 운이 좋게 두 명의 동기와 함께 연구실 생활을 시작하게 되었으며, 그 덕분에 힘든 일 있을 때마다 크게 의지를 할 수 있었던 것 같다. 가장 학회를 같이 많이 갔던 성진이는 추억도 많고 미안한 것도 몇 개 있긴 하다. 그래도 너랑 같이 있으면 내 성격과 달리 몸을 사리는 일도 줄어들고 진짜 신나게 뭔가를 할 수 있다는 점이 참 좋았다. 앞으로 기회가 될지 모르겠지만 여행이나 캠핑 같은데 가서 지난 날의 기억을 되새기는 것도 꽤 괜찮을 것 같다. 물론 과거의 실수들은 반복하지 않을 예정이다. 항상 막내 같은 귀여운 원보도 너무 고맙다. 함께한 추억이 많다고는 할 수 없지만 동기로서 너가 많이 든든하고 고마웠다는 건 알아주길 바란다.

훌륭하신 선배님들 만큼이나 똑똑한 후배들이 많아서 가끔 미안할 정도로 든든했다는 점도 후배님들이 꼭 알아줬으면 좋겠다. 진혁이는 내가 연구적으로 많은 도움을 받은 것 같아서 항상 고맙고, 지현이도 내가 방장할 때 여러모로 도움을 줘서 고마웠다. 용산이는 방장이라 내가 요청하는 것도 많은데 늘 묵묵히 처리해줘서 고맙고, 준혁이는 항상 밝은 모습이 보기 좋고 정이 많이 간다. 가영이는 어떻게 보면 나와 일적으로 많이 겹쳤던 것 같은데 힘든 스케줄에도 연구비 처리나 행정적인 부분까지 빠짐없이 잘 해주어 고맙다. 연송이는 연송투어 덕분에 내가 더 즐거운 학회 및 여행을 하게 된 것 같아서 참 고마웠다. 진수는 연구실에서 항상 궂은일을 도맡아 하는 것 같아 신경이 쓰일 때가 많았다. 진수의 역할이 연구실에서 정말 핵심적이란 것을 잘 알고 항상 고마움을 느끼고 있다. 생각해보니까 용민이는 내가 좀 편하게 생각해서 그런지 알게 모르게 이것저것 많이 부탁한 것 같은데 다음부터는 조금 자제해보도록 하겠지만 장담은 못하겠다. 제욱이와 재혁이는 실험적으로 내가 도움을 많이 받아서 항상 고마웠는데 제대로 고마움을 표현한 적은 없었던 것 같

다. 이 글을 통해서라도 고마움이 전달되었으면 좋겠다. 준호도 업적관련해서 내가 이것저것 자주 요청하는데, 늘 도움을 줘서 고맙다. 현준이도 짧은 시간이지만 같이 섬유도 짜고 이것저것 내가 많이 시켰는데 묵묵히 잘 해줘서 너무 고맙다. 현우랑 용이는 만난 시간이 짧은 것 치고는 기억에 많이 남을 것 같은데, 너희들의 성격이 좋아서 그런 것 같다. 내기 잘 못하는 용이는 선배들 커피도 많이 사주고 그래서 특히 고맙다.

사실 고마운 분들을 언급하자면 끝도 없을 것 같다. 재료, 장비, 가공 등의 필요한 부분을 채워주신 업체 관계자 분들부터 분석 관련 담당자 분들까지 생각해보면 일일이 감사를 표하지 못하는 점 너무도 송구스럽다. 그 밖에도 나의 정신건강을 지켜준 소중한 친구들에게도 감사를 표하고 싶다. 특히 나약한 정신력과 외로움을 많이 타는 성격 탓에 종종 찾아오는 우울증과 무기력함으로 내가 힘들어 할 때 무너지지 않도록 곁을 지켜준 존재에 가장 큰 감사함을 표하고 싶다. 혼자였다면 절대 쉽지 않은 길이었다는 것을 잘 알고 있습니다. 항상 고마움 잊지 않고 보답하면서 살도록 하겠습니다.

끝으로 제가 어떤 모습을 보이더라도 항상 묵묵히 응원하고 지원해주시는 아버지, 어머니, 누나에게 감사드립니다. 효도라고 할만한 것은 아직 멀게만 느껴지지만 최소한 실망하실만한 아들이 되지 않도록 노력하겠습니다. 글을 마무리 하려고 보니 혹시라도 마음과 달리 언급하지 못한 분이 있을 까봐 두려움이 앞섭니다. 제가 정말 감사드리는 것에 비해 글은 아주 작은 부분이라는 점 잘 이해해주실 것이라고 생각하겠습니다. 다시 한번 모든 분들께 감사드리며, 모두 행복 가득하시길 바라겠습니다.

성 민 창 드림